Boron-selective membranes by surface functionalization with affinity hydrogel

Dissertation

zur Erlangung des akademischen Grades eines Doktors der Naturwissenschaften

- Dr. rer. nat.-

vorgelegt von

Qirong Ke

geboren in Fujian, China

Fakultät für Chemie

der

Universität Duisburg-Essen

Essen 2021

DOI: 10.17185/duepublico/75006
URN: urn:nbn:de:hbz:464-20211125-070710-4

Approved by the examining committee on: 4th Nov. 2021

Chair: Prof. Dr. Oliver J. Schmitz

Advisor: Prof. Dr. Mathias Ulbricht

Reviewer: Prof. Dr. Christian Mayer

The work presented here was performed from June 2016 till June 2020 at the Lehrstuhl für Technische Chemie II of the University of Duisburg-Essen and supervised by Prof. Dr. Mathias Ulbricht.

I declare that this dissertation represents my own work, except where due acknowledgement is made.

.....

ABSTRACT

The conventional reverse osmosis (RO) membranes in the one-pass RO configuration have limited competence to remove boron efficiently from seawater. They have only around 80 % of boron rejection, while the projected boron rejection should exceed 90 % in order to meet the requirements for using the water in irrigation. One promising approach is to diminish the boron concentration before the RO stage, which can be achieved in the RO pretreatment step. Upon this context, a membrane adsorber that integrated membrane-based separation with selective boron adsorption can be used in the pretreatment step for boron polishing.

In this work, commercial ultrafiltration (UF) and microfiltration (MF) polyethersulfone (PES) membranes have been modified to integrate specific boron binding property. First, an active coating can be formed in the support layer of the UF membrane by infiltrating a reactive polymer and a cross-linker, and a subsequent post-functionalization endows the active coating with boron affinity. In the other alternative strategies, the commercial UF or MF membranes can be pre-modified by a tertiary amine containing layer via macromolecular adsorption or a two-step surface treatment. And the polymeric boron affinity coating can be constructed on such premodified surface via a graft-from approach or an integrated initiation system of combining graft-from and graft-through approaches. The modified membranes show specific boron binding and a trade-off between water permeability and boron binding capacity.

Furthermore, the parameters that affect the final filtration performance and boron binding performance have been systematically studied. And the parameter optimization has been done to screen for the membrane adsorber with good potential for practical application. Finally, the cost estimation has been done to evaluate the feasibility of using the tailored membrane adsorber in the pretreatment step considering aspects of modification cost and regeneration cost.

ACKNOWLEDGMENT

With the completion of this dissertation, I would like to express my sincere appreciation to those who have accompanied and supported me during my Ph.D. study in Germany. Very special thanks go to my Doktorvater, Herrn Prof. Dr. Mathias Ulbricht. It is of great honor and best luck for me to pursue Ph.D. work in this group. I always enjoy the fruitful discussions with Prof. Dr. Mathias Ulbricht. I have learned that the importance of critical and scientific thinking to problem-solving; how to find out valuable information from the negative result; how to filter useless information and focus on the real important aspect; how to solve the scientific problem by doing proper analysis on existing data, instead of bypassing the issue. I appreciate his willingness to generously share his time with students and the enlightening comments on my Ph.D. work.

I would like to thank China Scholarship Council (CSC) for providing financial support for my 4 years' Ph.D. study in Germany and the extension for another two years for my postdoc. work.

I Also want to thank Prof. Dr. Christian Mayer for kindly reviewing this thesis.

I would like to appreciate the continuous support provided by Dipl.-Ing highly. Inge Danielzik, Dipl.-Ing. Tobias Kallweit, Claudia Schenk, Mrs. Roswitha Nordmann, M.Eng. Pascale Wünscher, and Dr. Christina Kamp-Meltzer. Furthermore, I would like to thank Duc Hoa Tran, Inga Frost, Marcel Matthias, Mohamed Elleithy, Philipp Jahn, Sebastian Buchholz, Vanessa Schnecke, Dr. Patrick May, Dr. Sarah Verena Walter, and other colleagues who have directly contributed to the success of this work. I am glad that we have many creative and motivating conversations in the past few years. With all your contribution, this work could eventually come to this current stage.

Special thanks to my friend, Dr. Ibrahim Mohamed Ahmed ElSherbiny, for his endless support during my Ph.D. study. I wish you good luck with your new proposal. Additionally, I would like to acknowledge another friend, Dr. Huibin He, for his constructive advice on organic synthesis. I do miss our coffee time in the cafeteria. I wish you very success in your research work in Shang Hai.

Moreover, I would like to thank my student Peiwen Huang for her excellent and hard work. Also, many thanks to my student assistants Daria Belous, Maximilian Franiel, for their helpful assistance on lab work that I could spend more time correcting my thesis.

And Last but not least, I would like to thank my parents and my dogs for the overseas support from China. Most of all, I would like to show my greatest respect and love to my wife, Hua Yifan. Without her company, the life would be boring. I wish my wife gets her Ph.D. degree smoothly.

All the best to all of you!

CONTENT

1. Introduction

1.1 Problem definition

With the increasing demand for potable and irrigation water, it requires another pathway to get alternative water resources instead of simply rely on the limited water source from the mainland. The desalination of seawater was introduced to solve this problem, and it shows great potential as an alternative water source for human usage and irrigation consumption. Among several desalination methods, the reverse osmosis (RO) has been widely used because of the outstanding salt rejection and good energy efficiency.

Boron is one of the trace elements in seawater majorly present as a form of boric acid with a boron concentration of approximately 5 mg/L. For drinking water, the European Union (EU) set a limit of 1 mg/L boron, where the World Health Organization (WHO) recommends limits of 2.4 mg/L base on the perspective of human health [1,2]. A significant issue is boron tolerance of plants, although boron seems to be one of the essential micro-nutrient [3]. Thus more rigorous boron concentration limits in terms of irrigation have been set as low as 0.5 mg/L [4,5]. However, the boron rejection of single-stage commercial RO membrane still relatively low, which only reduces the boron concentration to about 0.9-1.8 mg/L [6]. To address this problem, various methods such as ion exchange, nanofiltration (NF), electrodialysis (ED), Donnan dialysis (DD), sorption–membrane filtration hybrid processes have been applied [7–10]. Boron removal by ion exchange or adsorption has been developed to couple with RO desalination to eliminate the boron from seawater. And the estimated cost of boron removal via ion exchange method is 3.7-10.1 cent €/m^3 (2011) out of 0.3-1.4 €/m^3 of total expenditure in seawater reverse osmosis (SWRO) [11].

One of the promising approaches for boron removal in SWRO is via a hybrid process of adsorption-membrane filtration, which can simplify the SWRO configuration to compress chemicals, energy, construction, and human power cost. The utilization of microfiltration (MF) and ultrafiltration (UF) in seawater pretreatment is of great interest and showing good potential to reduce RO membrane fouling [12]. For this, a new type of membrane is needed that could integrate the adsorption process with MF or UF step. On the other hand, to

develop entirely new materials for membrane manufacture is unfavourable in terms of capital and time aspects. Thus, it would be more reasonable and attractive to modify existing materials instead of fabricating new materials. Such in situ modification technique should be easily tunable, environmentally friendly, and ready to upscale.

Under this context, a new modification strategy should be explored to endow MF or UF membrane with selective boron binding performance while maintaining a certain level of filtration performance that can adapt to the seawater pretreatment.

1.2 Aim of the work

In seawater, the major species of boron presents as boric acid at the pH = 8.0. Molecules with two or more hydroxyl groups (di- or polyols) have high affinity and selectivity to boron over a wide range of pH values, and this binding is pH-dependent (cf. Fig. 1.1). In order to endow membranes with selective boron binding capacity, the substance containing di- or polyols functional groups should be introduced to the membrane for specific boron binding. Polyethersulfone (PES) membranes can be used as the based membrane materials since it is widely used as a substrate for surface modification via graft-to, graft-through, and graft-from strategy without obvious damage to its membrane structure. Besides, it has an increasing tendency toward using UF and MF membrane in the pretreatment step of SWRO configuration. Therefore, either UF or MF PES membranes can be taken as an ideal start material for modification, and graft PES membrane by a cross-linked coating containing boron ligand groups is thought to be an ideal strategy. Under such context, the first aim of this project is to figure out an in situ membrane modification strategy to graft boron affinity coating onto the PES membrane surface and/or pore wall. Two kinds of membrane modification approaches are thought to be fit on this topic: 1) pre-forming an active coating of cross-linked polyethylenimine (PEI) inside the isotropic UF membrane via infiltration process, and later post-hydroxyl functionalization this precursor coating to endow membrane with boron binding capacity; 2) introduce surface-initiated polymerization approach on membrane outer and inner surface thus to form boron affinity hydrogel from tailored monomers, such as glucosamine derivatives monomers.

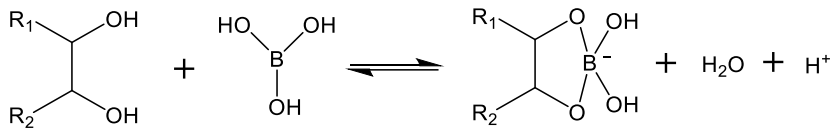

Fig. 1.1 boron chelating mechanism with polyols.

Certain throughput and boron binding capacity should be achieved to adapt the modified membrane to SWRO pretreatment step. Generally, the required throughput in the SWRO pretreatment step should around 30-150 LMH with a recovery of 88-94 % [13–16]. The MF membrane with the pore size of 0.1-0.35 μm and the UF membrane with the pore size of 0.01-0.05 μm are commonly used in the pretreatment step [12]. Trans-membrane pressure (TMP) is another aspect that should be taken into consideration when targeting the required flux. The TMP fluctuates in the practical case, and the typical TMP is 0.1-0.5 bar for MF pretreatment and 1.0 bar for UF pretreatment [17]. Consider the practical operation conditions and the typical membrane type, the targeting pure water permeability for modified MF membrane should be in the range of 5,000-20,000 LMH bar, while for modified UF membrane it should be in the range of 30-150 LMH bar. Another criterion is boron binding capacity. The boron rejection for common RO membrane is around 80%. Hereof, the boron break-through should not exceed 50% in the pretreatment step, thus achieving a final boron concentration of 0.5 mg/L. However, there is thought to be a trade-off between final flux and boron binding capacity in the aspect of membrane functionalization degree. Such trade-off relation can be altered by: 1) applying different modification approaches; 2) conditioning various modification parameters. For such, the second aim would focus on screening different modification approaches and optimizing modification parameters to fabricate suitable lab-scale modified flat sheet membrane for the practical scenario.

As foregoing described, the modification approaches should be ready to upscale. Thus, the third aim of this work is to figure out the optimal modification condition from the flat sheet membrane modification and transfer this optimal modification condition to commercial membrane modules. The modified membrane modules should have comparable performance in terms of flux and boron binding capacity.

1.3 Scope of the work

This work focuses on the modification of commercial MF and UF membranes/modules for boron removal. The following tasks should be done:

i. Explore suitable modification approaches

- Pre-modify commercial UF membrane with PEI active coating via infiltration method and later exact post-hydroxyl functionalization to endow this coating with boron affinity.
- Modify commercial UF or MF membrane with boron affinity coating via graft-from approach: 1) Pre-modifying the MF membrane with macro-initiator or relevant chemical that carries co-initiate groups on the membrane surface; 2) surface functionalization via surface-initiated polymerization of glucosamine derivatives monomers.
- Modify commercial MF membrane with boron affinity coating via a method integrating graft-through and graft-from approaches: 1) pre-modifying membrane with macro-initiator; 2) applying surface-initiated polymerization together with bulk polymerization for the sake of higher grafting degree.

ii. Optimize modification parameters and characterize membrane performance.

- Characterize the final modified MF membrane to reveal the change of the membrane structure and surface chemistry.
- Optimize modification parameters to better trade-off between flux and boron binding capacity, and investigate the influence of each parameter on flux and boron binding capacity.
- Study the boron adsorption isotherm and kinetics.
- Study the flow-through adsorption and the regeneration performance of the modified membrane.

iii. Transfer optimal modification parameter from flat sheet membrane to lab-scale module.

- Adapt the optimal modification parameters to the lab-scale membrane module and investigate the membrane performance in terms of flux and boron binding capacity.
- Attempt to calculate the boron removal cost of the modified membrane.

2. State of the art

2.1 Introduction of boron

2.1.1 Chemistry of boron in aqueous solutions

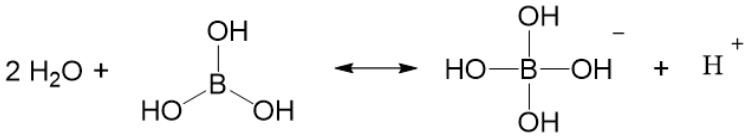

Fig. 2.1 boron dissociation in aqueous media.

Boron behaves as a Lewis acid in the aqueous solution (Fig. 2.1). At low boron concentration (≤ 22 mg/L), boron only presents as the mononuclear species of $B(OH)_3$ or $B(OH)_4^-$. The dissociation of boric acid can occur by accepting a hydroxyl ion to form a tetra-hydroxyborate ion [18–20].

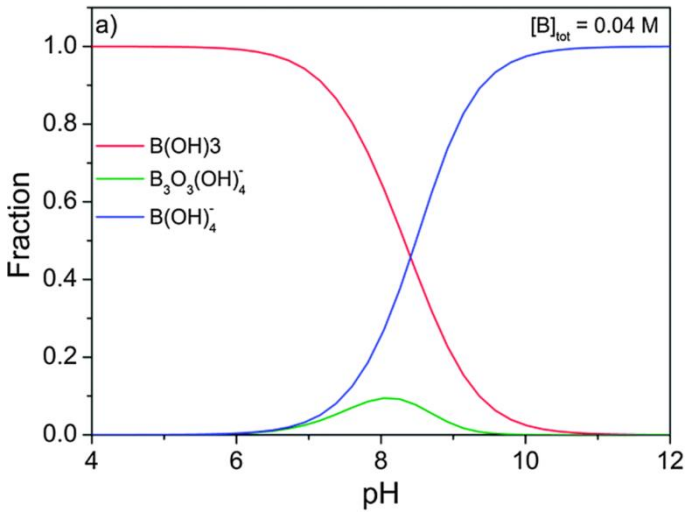

Fig. 2.2 Fraction diagram of aqueous boron species within the pH range of 4-12 at a total boron concentration of 0.4 M [18–20].

Boron acid is a weak acid, and the apparent pKa value can be affected by ionic strength, temperature, and pressure [21]. The intrinsic pKa of this dissociation is 9.23 (at 25°C and atmospheric pressure). One proton is released in this dissociation leading to a pH-dependent distribution of these two boron species (cf. Fig.2.2). At high boron concentration,

especially with high pH value, boron can also present as poly-nuclear ions $B_3O_3(OH)_4^-$, $B_3O_3(OH)_5^{2-}$, $B_5O_6(OH)_4^-$, and $B_4O_5(OH)_4^{2-}$ [19,20]. However, boron is usually present as the form of boric acid ($B(OH)_3$) in seawater (pH ≈ 8.0). Because of the poor hydration capacity of $B(OH)_3$, the hydration size of $B(OH)_3$ molecular is less pronounced and be expected to have a similar size with water molecule. While for the $B(OH)_4^-$, it can be fully hydrated because of the charge, which has a larger hydration size of 0.230 nm [22]. Thus, the hydration size and charge difference results in different rejection of $B(OH)_3$ and $B(OH)_4^-$ species in the RO membrane.

2.1.2 Importance and toxicity of boron

Boron is a ubiquitous element in the natural environment, and it's vital micronutrients for humans, plants, and animals. However, an excessive level of boron is harmful to humans causing nausea, vomiting, diarrhea, and blood clotting. The boron issue is more problematic in agriculture, where the uncharged form of boron ($B(OH)_3$) can pass the lipid bilayers out of control [23]. The plants affected by excess boron exhibit chlorosis and browning at the tips and margins of older leaves; some plants present as stunted growth, and some fruit trees will have less yield. It should be noticed that the boron toxicity depends on specific plants of which having various boron tolerance (cf. Table 2.1). Thus the standard and the guideline values of boron in irrigation utilization seem to be followed with the most sensitive plants, below 0.5 mg/L.

Table 2.1 Boron sensitivity of specific agricultural crops [24].

Boron sensitivity	C_{Boron} (mg/L)	Agricultural crop
Very sensitive	< 0.5	Blackberry
Sensitive	0.5 -1.0	Peach, cherry, plum, grape, cowpea, onion, garlic, sweet potato, wheat, barley, sunflower, sesame, strawberry
Less sensitive	1.0 – 2.0	Red pepper, pea, carrot, radish, potato, cucumber
Moderately tolerance	2.0 – 4.0	Lettuce, cabbage, celery, turnip, oat, corn, artichoke, tobacco, mustard, squash

2.1.3 Boron complexation with diols or polyols

A chemical compound that contains two or more hydroxyl groups as ligands located in the cis position has higher affinity and selectivity to boron. Over a wide range of pH, a relatively stable complex between diols groups and boron can be formed via either a mono-chelate or bi-chelate complexes according to Fig. 2.3. It generates one proton according to this chelation mechanism. Thus the higher proton concentration, i.e., lower pH value, gives an unfavorable environment for this chelation, and only a small amount of these complex exist.

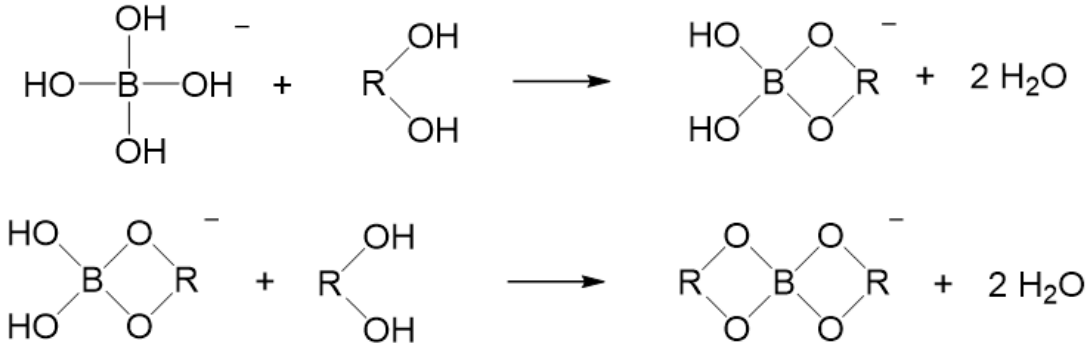

Fig. 2.3 Boron complexation via mono-chelate and bi-chelate.

The stability of the chelation between diols and boric acid mainly depends on the different types of diol compounds. Table 2.2 illustrates the reaction constant of mono-chelate (*K1)*

and bi-chelate (*K2)* of different types of boron ligands. N-methyl-D-glucamine (NMDG) group, a glucose derivative, gains lots of interest as the boron ligands because of its amino moiety, which can be protonated during the boric acid chelation [25]. NMDG can form monochelate, tetradentate, and bischelate complex with boric acid at the pH range of 8-10.

Table 2.2 The reaction equilibrium constant of mono-chelate formation (K1) and bi-chelate formation (K2) in each boron ligands [17].

Diols or polyols	***K1***	***K2***
Glycerol	16.0	41.2
Catechol	7.80×10^3	1.42×10^4
D-Mannitol	1.10×10^2	1.37×10^5
D-Glucose	1.50×10^3	7.60×10^3
D-Sorbitol	-	4.44×10^5
D-Ribose	-	1.57×10^7
N-methyl-D-glucamine	$\sim 10^5$	$\sim 10^6$
1,3-propanediol	1.27	0.11
1,2-ethanediol	2.15	1.15

As previously mentioned, boron prefers to present as polyborates at high boron concentration (> 25 mM) in the pH range of 4-13, thus a more complicated chelation mechanism should be taken into consideration [26,27]. In the scenario of high boron concentration, one boron ligand will chelate with polyborates instead of single boron chelation as shown in Fig. 2.4 [28].

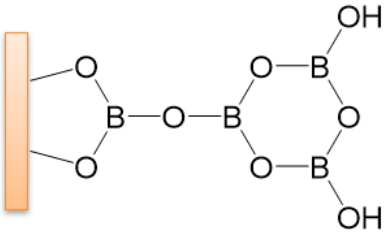

Fig. 2.4 The chemical structure of chelation between polyols and polyborates.

2.2 Boron removal methods

2.2.1 Ion exchange

Ion-exchange is the most extensively used method for boron removal in the water treatment field. In the ion-exchange process, the boron exchange with solute ions having a lower affinity with the immobile functional group in resin [29]. Different ion-exchange resins containing NMDG or other polyols groups have been commercialized for boron removal via the ion-exchange method such as Dowex, Purolite S108, Diaion CRB 01, Diaion CRB 02, Purolite 108, Amberlite IRA 743, etc. [30–33]. The commercial resin has an excellent binding capacity within a wide range of boron concentrations in different application scenarios (cf. Table 2.3). In the established boron removal via the ion-exchange method, operating capacity and kinetic capacity are the two most important parameters to determine the size and ion-exchange unit cost. The operation capacity describes the regeneration frequency and chemical usage, while the kinetic capacity will have a major influence on flow velocity, i.e., the throughput of the adsorption bed. Other factors, such as temperature, pH value, feed solution condition, also impact the boron removal efficiency.

Table 2.3 The boron adsorption capacity of various commercial boron removal resin.

Resin name	Resin type	Resin form	Initial C_{boron} (mg/L)	q_e (mg/g)
Dowex 2X8	Microporous benzyl dimethylethanolamine	Cl	600	16.98
Purolite S 108	Macroporous NMDG-type	OH	18-20	2.44
Diaion CRB 01	Highly porous NMDG-type	OH	18-20	3.43
Diaion CRB 02	Highly porous NMDG-type	OH	18-20	3.23
Amberlite IRA 743	Macroporous NMDG-type	OH	10	3.17
Purolite S 108	Macroporous NMDG-type	Cl	400	9.31

Kabay et al. studied the boron removal from wastewater of geothermal plant by using NMDG type resins Diaion CRB 01, Diaion CRB 02, Purolite S108 [34]. They applied batch-mode sorption test and column-mode sorption-elution test to obtain the optimum operation parameter for boron removal. A resin concentration of 3 g-resin/L-wastewater is enough to eliminate 90% of boron in batch-mode sorption. In column-mode operation, Diaion CRB 01 shows higher break-through capacity at both 10 and 15 h^{-1} space velocities (SV, defined as bed volume per hour compared with Diaion CRB 02 and Purolite S108. In the elution process, 15-20 bed volume (BV) of 5% H_2SO_4 is required to recover the adsorption column with a 96-100% elution efficiency.

Apart from the commercial products, a series of new ion-exchange resins have been prepared. A chitosan/$Fe(OH)_3$ based sorbent was synthesized by Demey et al. [35]. The chitosan/$Fe(OH)_3$ based sorbent shows good stability in a continuous treatment system, and the resin can be later regenerated by an alkaline solution at pH=12. One of the interesting research is done by Kumar et al.; they used synthesized glucaminium-based ionic liquid for boron removal in which the boron species can be extracted by in-situ liquid-liquid micro-extraction with this synthesized ionic liquid [36].

2.2.2 Reverse osmosis

RO process can be used to reduce boron concentration in the desalinization. The feed water condition and other operation parameters directly affect boron removal efficiency via the RO process, such as temperature, salinity, pH, pressure, feed boron concentration and recovery, fouling, etc. [37,38]. As previously mentioned in Section 2.1.1., at low boron concentration, boron presents as mononuclear species of either $B(OH)_3$ or $B(OH)_4^-$ depending on the specific pH surrounding. And pH becomes the dominant factor because of this pH-dependent effect. At the pH value of 8, which is the typical pH in seawater, the uncharged form of $B(OH)_3$ species take dominates and results in a boron rejection level of 60-96% in the single-pass RO process; in contrast, the salt rejection is 99.6% [1,39,40]. For the commercial desalination membrane, FILMTEC^{TM} BW30, the boron rejection increases from ~50% at pH = 7 to ~93% at pH = 11 [41]. However, improved boron rejection via elevating pH would create undesired cost because of the aggravation of scaling propensity, salt precipitation, and chemical consumption [11,42].

Higher operation pressure also could improve boron rejection in the RO process. It has been found out that the FILMTEC^{TM} SW30XHR has a higher boron rejection of 92-97% at 48.3 bar in comparison with the rejection of 74-84% at 15.5 bar [43]. It's well known that the water and salt transport through RO membrane via solution-diffusion models, and the water flux increase as the function of different trans-membrane pressure, while the boron flux does not [41,44,45]. On the other hand, the increase of water flux would lead to more dramatic concentration polarization, and the boron back diffusion will be promoted because of the higher boron concentration at the membrane surface. However, under the given high operation pressure, the higher water flux increase is more prominent than the boron flux increase. Thus the boron rejection tends to increase overall.

With respect to the influence of salinity, higher salinity leads to low boron rejection because the surface potential of the membrane will be neutralized at a high ion-strength environment, therefore, this effect would increase the boron passage [46]. An opposite phenomenon has been observed under low salinity feed solution that higher boron rejection can be achieved when increasing the salinity from 0 to 5000 μS/cm [47]. At such

salinity range, the increasing salinity will not result in a significant increase of concentration polarization, instead, the boron will be ionized, leading to the boron rejection decline. However, the influence of salinity on boron rejection still remains lots of discussions.

Interestingly the membrane fouling and scaling have been reported to interfere with the boron rejection. The membrane fouling caused by sodium alginate, colloidal silica, or $CaSO_4$ will lead to cake-enhanced concentration polarization, which will neutralize the charge at the membrane surface, thus increasing boron passage. While the fouling of humic acid will improve boron rejection because the negatively charged fouling layer is formed, thus creating electrostatic repulsion to boron [48].

The temperature also influences boron rejection upon a trade-off between boron permeability change or pKa value change. In most cases, it will promote boron permeability at a higher temperature, but the pKa valve will decrease. However, the increase of boron permeability is more prominent, therefore, the boron rejection decrease with the increase of operation temperature.

Overall, the single-pass RO membrane still has limited capacity to reduce boron to the desired concentration, although the new commercial RO membrane has shown much better boron rejection compared to the first generation of RO membrane prepared by cellulose acetate. Owning to the insufficient boron removal capacity in the single-pass RO process, using a hybrid system to remove boron is preferable and promising.

Table 2.4 Boron rejection of various commercial RO membranes at the corresponding feed water condition.

Membrane type	Manufacturer	Flux (GPD)	Feed water condition	pH	Boron rejection (%)
FILMTEC™ SEAMAXX™	DOW chemical	9050 (600 psi)	32 g/L NaCl, 600 psi, 8% recovery	8	81.8
FILMTEC™ SW30ULE™-400i	DOW chemical	7500 (600 psi)	32 g/L NaCl, 700 psi, 8% recovery	8	86.4
FILMTEC™ SW30XHR™-400i	DOW chemical	6600 (600 psi)	32 g/L NaCl, 800 psi, 8% recovery	8	93
FILMTEC™ SW30XLE™-400i	DOW chemical	9900 (600 psi)	32 g/L NaCl, 5 ppm boron, 800 psi, 8% recovery	8	91.5
TM820E	Toray	6000 (800 psi)	32 g/L NaCl, 5 ppm boron, 800 psi, 8% recovery	8	91
TM820V	Toray	7500 (800 psi)	32 g/L NaCl, 5 ppm boron, 800 psi, 8% recovery	8	92
TM820K	Toray	4600 (800 psi)	32 g/L NaCl, 5 ppm boron, 800 psi, 8% recovery	8	96
TM820M	Toray	5600 (800 psi)	32 g/L NaCl, 5 ppm boron, 800 psi, 8% recovery	8	95
TM820C	Toray	4800 (800 psi)	32 g/L NaCl, 5 ppm boron, 800 psi, 8% recovery	8	93
TM820R	Toray	6750 (800 psi)	32 g/L NaCl, 5 ppm boron, 800 psi, 8% recovery	8	95
SWC4 MAX	Hydranautics	6750 (1200 psi)	32 g/L NaCl, 5 ppm boron, 800 psi, 10% recovery	7	93
SWC5 MAX	Hydranautics	9900 (1200 psi)	32 g/L NaCl, 5 ppm boron, 800 psi, 10% recovery	7	92

2.2.3 Hybrid system

To compensate for the insufficient boron removal in the single-pass RO stage, various hybrid systems have been designed, such as the NF-RO hybrid system [49], RO-adsorption hybrid system [50], polyol-assisted filtration system [51,52], etc. In this section, we only focus on the RO-adsorption hybrid system and polyol-assisted filtration system.

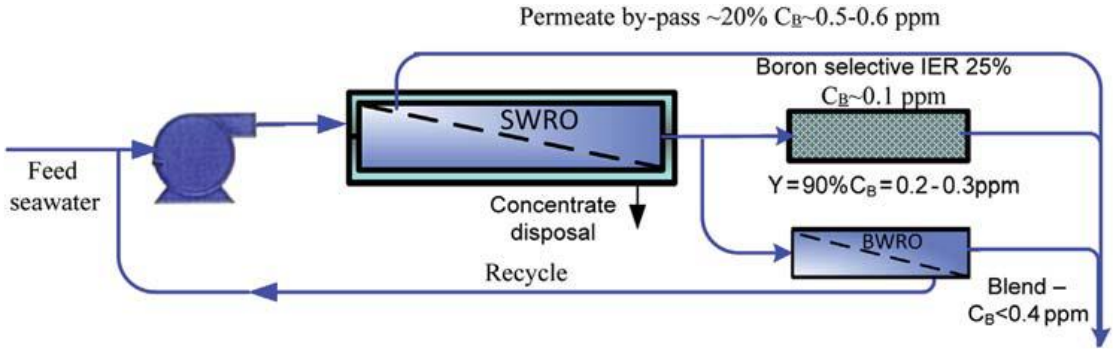

Fig. 2.5 Schematic presentation of boron removal design via hybrid system contains ion-exchange and BWRO unit [6].

RO-adsorption hybrid system refers to a combination of RO stage, ion-exchange stage, and resins regeneration stage [6]. After single-pass SWRO process, the permeate still contains 0.5 - 0.6 mg/L of boron depending on feed solution condition, operation parameters, and the membrane used. The first common approach to maintaining a stable boron concentration is to adapt the permeate split, which split the permeate to the boron ion-exchange stage and the BWRO stage (Fig.2.5). The ion-exchange stage can efficiently remove the boron from the upstream RO stage and eliminate boron down to 0.1 mg/L. The rest of permeate from the upstream RO stage is treated by a second RO process at lower pressure, and a high pH of 10 comes out with a recovery of 90 % and boron concentration of 0.2 - 0.3 mg/L. The total boron concentration in the combined permeate can be maintained at < 0.4 mg/L. In the second method, the ion-exchange resin is introduced as a fixed or fluidized bed, and the saturated resins are frequently replaced by the regenerated resins for subsequent boron adsorption (Fig. 2.6). In the regeneration process, the spent resins are collected by UF or MF membrane [53,54].

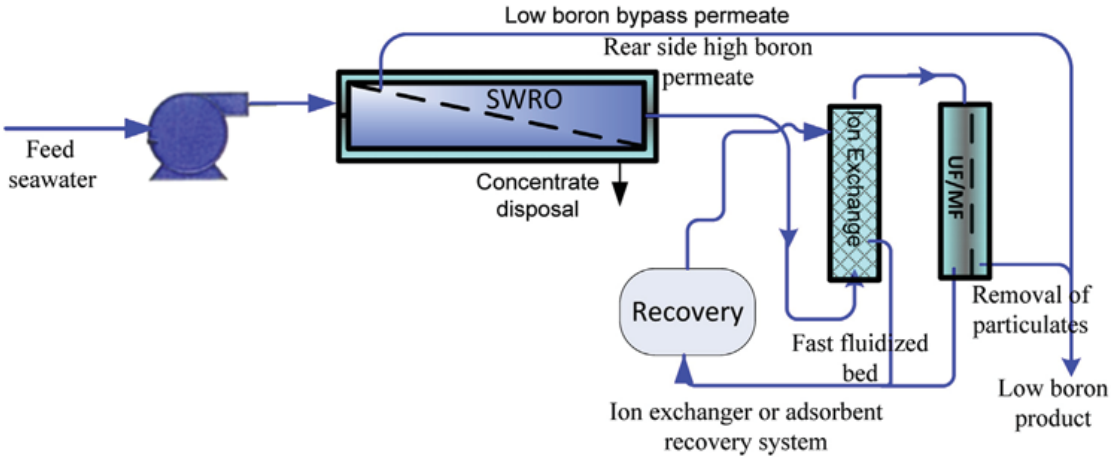

Fig. 2.6 Schematic presentation of boron removal design via hybrid system contains ion-exchange and UF/MF unit [6].

Polyols-assisted filtration seems to be an interesting alternative for the boron removal method that can easily be applied to the existing RO configuration without new construction. Polyols compounds, including small molecular like sorbitol, mannitol, glycerol, NMDG, or macromolecules, contains multi-hydroxyl groups like polyvinyl alcohol, hyper-branched polyglycidol and etc., can be integrated into NF or UF process to enhance boron rejection [49,52,55–58]. The polyols compounds can chelate with boric acid or borate ions forming a large anionic complex, thus significantly increasing boron retention in the NF and UF step is because of the size exclusion and charge repulsion effects. After adding polyols compounds into the feed solution, the boron rejection can go beyond 90 % at the pH condition of 10 in the NF process [55]. The self-synthesized 2,3-dihydroxypropyl-functionalized hyper-branched polyethyleneimine can achieve 91 % of boron rejection in the UF process at the optimal operation condition [59]. However, the boron rejection in these kinds of designs strongly depends on the affinity of selected polyols compounds and the final size of the boron complex. The drawback of this boron removal method is obvious, i.e., extra chemicals are sued in this system, either for boron complexation or the regeneration of polyols compounds, and both of which would enhance the operation and materials cost.

2.2.4 Other methods

Apart from the techniques above-mentioned, electrodialysis (ED), membrane distillation (MD), forward osmosis (FO) has been advanced with certain competitive edges as boron removal method [60–65]. This section only gives a basic introduction of the boron removal mechanism of each technique. ED can be used for brackish water desalination and consists of a stack of anion-exchange membrane (AEM) and cation exchange membrane (CEM) shown in Fig. 2.7. The applied voltage between the membrane stacks causes the anions moving through AEM toward the anode, and the cations are moving through CEM toward the cathode, respectively. As such, boron can be removed when it presents as borate ions at higher pH value [65].

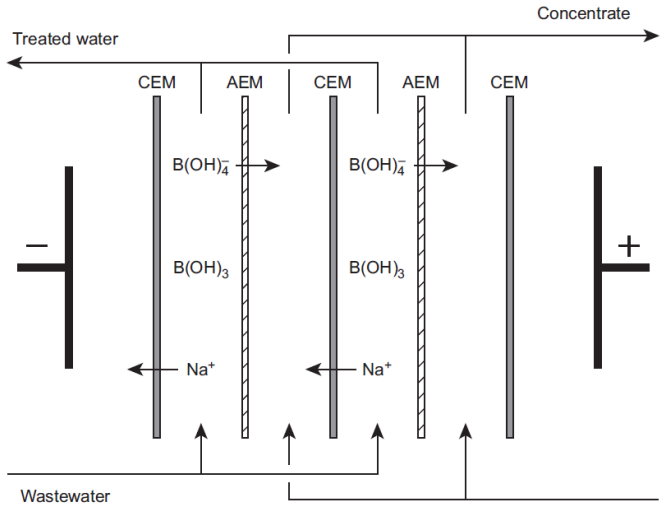

Fig. 2.7 Schematic presentation of boron removal mechanism via electrodialysis [65].

The water from the dilute phase can pass through the semi-permeable membrane to the concentrated draw via the osmotic pressure difference across the membrane, which is called FO process. At neutral pH, boron presents as an un-dissociated form, and the permeation of this un-dissociated boron species is able to transport through the selective layer via a solution-diffusion mechanism, while transportation of un-dissociated boron in the support layer follows with convection-diffusion mechanism [66,67]. The main influence on boron transport in the FO process is the reverse salt diffusion and internal concentration polarization inside the FO membrane. Therefore, the membrane operation orientation,

water flux, membrane structure, types of draws solution directly determine the final boron rejection [66,67]. According to the literature, the boron rejection is within 10% - 90% under different operation conditions in terms of membrane structure, pH value, and water flux [63,68,69]. However, extra energy input and treatment steps are required to concentrate the draw phase and produce pure water.

MD is a separation process able to separate water across a porous hydrophobic membrane from non-volatile solutes. This thermally driven separation process has several advantages out of other boron removal methods regarding its higher boron rejection over 99.5% and less sensitivity to boron feed concentration [61,62,70]. Still, compared to other boron removal methods, removing boron by MD has several drawbacks, such as sever membrane scaling and intensive energy consumption.

2.2.5 Cost of boron removal in seawater desalination

It is difficult to give a simple estimation on the cost of boron removal by membrane process because the total boron cost depends on feed boron concentration, feed condition, and the required boron level in the final produced water. In addition, the cost of construction, human power, chemicals, energy, amortization, and maintenance should be taken into consideration, and all these expenditures are regional dependent [71]. Table 2.5 gives a certain concept of the overall capital cost of boron removal from seawater. It should be noticed that target boron concentration brings a great difference to boron removal cost. Generally, the lower the boron concentration required, the higher capitals cost. However, it still remains lots of space to cut the cost of boron removal by: 1) figuring out a better hybrid system in the specific scenario; 2) applying better RO membrane; 3) using cheaper resins or the resins with better adsorption performance; 4) used chemicals more efficient; 5) using alternative energy such as solar energy, or improving energy recovery efficiency for lower energy consumption.

Table 2.5 Capital cost of different boron removal methods.

Target C_{boron} (mg/L)	Method	Cost (€ cent/m^3)	Ref.
> 0.5	RO	< 1	74
< 0.5	Single RO stage	5-8	74
0 - 0.5	2-pass RO	2.8 - 12.6	11
0 - 0.5	IE + RO	3.7 - 10.1	11
0.5	IE + BWRO	7 - 9	75
0.8	ED	18.5	76

2.3 Surface modification of polyethersulfone (PES) membrane

2.3.1 General background of surface modification on PES membrane

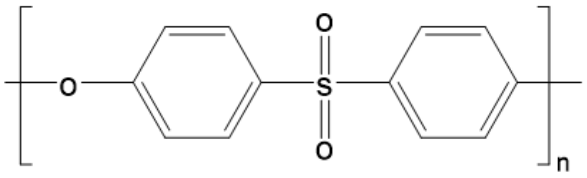

Fig. 2.8 The chemical structure of PES.

Polymeric membranes are now developed and widely used for sterile filtration, hemodialysis, desalination, water purification, gas separation, food and beverage processing, energy recovery, biomedical field, and other industrial applications. PES is one of the most widely used polymeric materials in the membrane-based separation field (cf. Fig. 2.8). The presence of the aromatic part in PES endows the PES with good thermal, oxidative, and hydrolytic stability [72]. However, owing to the nature of the polymer, the established polymeric membrane cannot meet all the required performance to a particular application [73,74]. For example, due to the relatively hydrophobic nature of PES, it has a severe fouling tendency on pure PES membrane [75,76]. Membrane modification is of increasing importance to improve membrane performance (e.g. retard membrane fouling), broadening its application (e.g. organic solvent filtration), or introduce/integrate new separation function (e.g., membrane adsorption or responsive sieving membrane) [77–80]. Regarding the membrane shape, flat-sheet and hollow fiber membrane are the most common membrane type in the industry. However, the hollow fiber membrane is thought to be more efficient than the flat sheet membrane in terms of operation and economic points of view. Such advantage is mainly due to the higher surface/volume ratio in hollow fiber membrane. The hollow fiber membrane can be assembled to a module with higher packing density than the flat sheet module because the flat sheet module should integrate with spacer, which leads to relatively lower packing density. On the other hand, the hollow fiber membrane or module has more complex morphology and membrane structure, which

may impede accessibility of membrane modification, for example, to modify the inner surface of hollow fiber membrane homogenously [81].

Three approaches toward PES membrane modification can be distinguished: 1) bulk modification on polymer for the subsequent membrane fabrication; 2) blending of functional polymers or additives during the membrane fabrication; 3) surface modification of the pre-formed membrane. Here we will have a further detailed discussion on surface modification of the pre-formed PES membrane, i.e., post-modification, in the following context. Various techniques were carried out for the surface modification on the pre-formed membrane, either via physical or chemical modification. The surface modification via physical approaches can be performed via adsorption or adhesion between membrane surface and adsorbent under secondary interactions such as van der Waals force or electrostatic force [82,83]. Interpenetration is another physical modification under solvent curing or heat curing, making added functional polymer partially mixes with the membrane polymer in an interphase level [84]. The last physical approach can be categorized in macroscopic entanglement of the added polymer and the porous structure of membrane [85]. Both of these three methods have no covalent binding between added functional polymer and based membrane matrix, nevertheless, the interpenetration and macroscopic entanglement approaches are able to give relative stable modification comparing to the adsorption/adhesion method.

To achieve modification durability, chemical modification is always preferable over the physical approach because of the stable covalent binding between the functional coating/polymer and membrane surface. Chemical surface modification can be done via: 1) graft-to method in which the functional polymer can be grafted to the membrane surface [86]; 2) graft-from method in which functional coating or polymer is prepared via surface-initiated polymerization, e.g., surface-initiated atom transfer radical polymerization (SI-ATRP), photo-induced surface grafting [87–90]; 3) heterogeneous reaction of membrane polymer such as plasma treatment, gamma-ray treatment [91]; 4) reactive coating that utilizes simultaneous cross-linker and polymerization attachment onto the membrane surface [78,92]. It should be noticed that in the chemical grafting approach for surface modification, the controlled degree of functionalization is of extreme importance to

balance additional functions and the change of membrane geometry (e.g., pore size, pore structure).

2.3.2 Surface-initiated polymerization for coating preparation.

There are several techniques to initiate polymerization starting from the membrane surface. Photo-induced surface initiation is a controllable grafting-from method to produce stable and homogeneous coating onto the membrane surface. Photo-induced surface initiation can proceed in two approaches: 1) for membrane material already intrinsically photoactive without using photo initiator; 2) adding photo-initiator to assist surface initiation [93,94]. PSF and PES are well known for their photoreactivity and generate free radicals upon UV irradiation (Fig 2.9), and the PES membrane can be successfully modified by 2-hydroxyethyl methacrylat (HEMA), glycidyl methacrylate (GMA), or methacrylic acid (MA). For photo-initiator assist surface grating, commonly it is preferable to using type II photo initiator, in which this photo initiator can abstract proton from substrate materials thus generate free radical from substrate materials upon UV irradiation. Hydrophobic benzophenone and hydrophilic Irgacure 2959 are the most commonly used type II photo initiators.

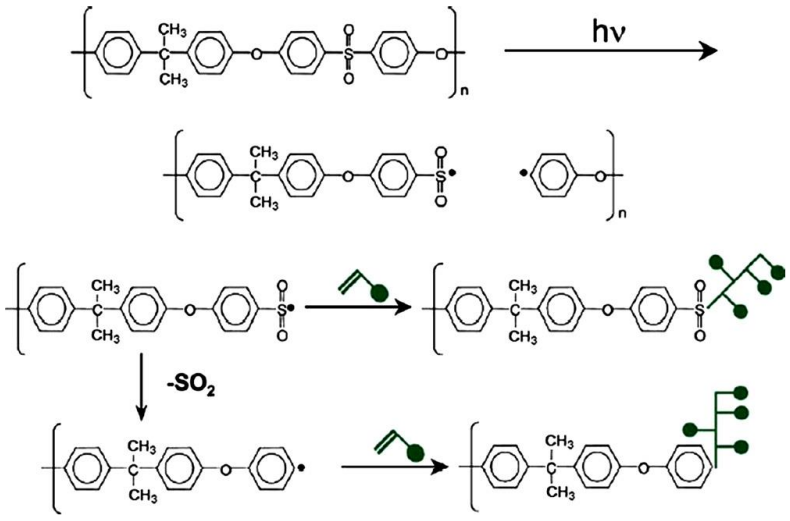

Fig. 2.9 Free radical generation mechanism of photoreactive PES membrane under UV irradiation in surface initiation polymerization.

Redox initiation is one of the most effective methods to generate free radicals under mild conditions with much lower activation energy compared with thermal initiation, and it has

been implemented for initiating polymerization and industrials process, e.g., emulsion polymerization at low temperature. Persulfate/tertiary amine, e.g., ammonium persulphate (APS) and N,N,N',N'-tetramethylethylenediamine (TEMED), is a well-studied redox initiation system that produces free radicals [95]. The mechanism of the APS/TEMED system is shown in Fig 2.10. Three kinds of free radicals can initiate the polymerization: TEMED radicals, bisulfate radicals, and hydroxyl radicals. Like TEMED, the molecular or polymer containing tertiary amine moiety can decompose APS generating free radicals under the same mechanism. Thus, this kind of macroinitiator can initiate polymerization for membrane modification. It has been reported that a co-polymer that contains tertiary amine moieties can play the role as part of a macro-initiator system for free radical generation [78,96]. The self-prepared tertiary amine included macro-initiator can be absorbed by a pristine PES membrane. Thus the tertiary amine moieties at the membrane surface can decompose APS and generating proper free radicals to initiate polymerization for surface coating grafting. The grafting coating is durable because of the covalently binding with the membrane surface, and the modified membrane shows good anti-fouling property [78,96].

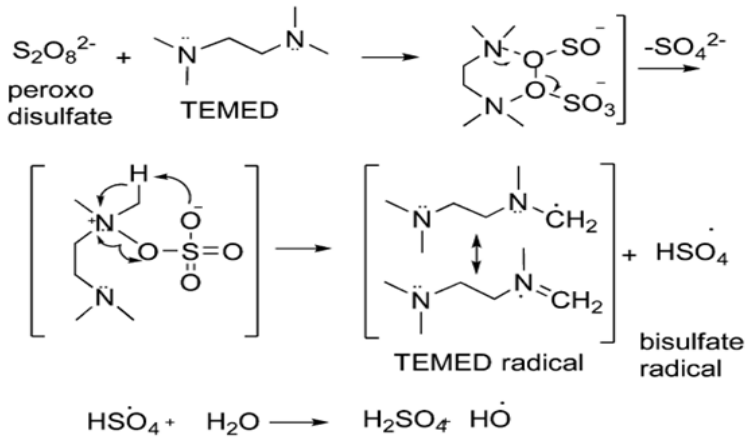

Fig. 2.10 Mechanism of redox initiation system of persulfate/TEMED

2.4 Membrane adsorption techniques in water treatment

2.4.1 The general concept of membrane adsorption

Membrane adsorption is an integrated membrane process comprise filtration and a simultaneous adsorption. When considering the membrane adsorption process as a separation tool, then it can be further classified into two directions: either for enrichment to collect the desired compound out of the mobile phase or to get rid of the undesired compound for mobile phase purification. It has been intensively studied and widely used in water treatment such as heavy metal removal and trace organic pollutant removal. Adsorption is a mass transfer process in which the adsorbate transfer from the liquid phase to the solid phase, i.e., adsorbent, and bound via physical and/or chemical interaction. The interaction between adsorbent and adsorbate can be classified into three types: ion-exchange, affinity, and hydrophobic interaction [96]. However, chemical adsorption is preferable because of the stronger interaction and higher adsorption capacity towards adsorbate. Generally, the main steps in the chemical's membrane adsorption process include: 1) the adsorbate transport from the bulk solution to the boundary layer at the membrane surface; 2) the film diffusion from the boundary layer to membrane surface; 3) adsorbate chemically bind to active sites.

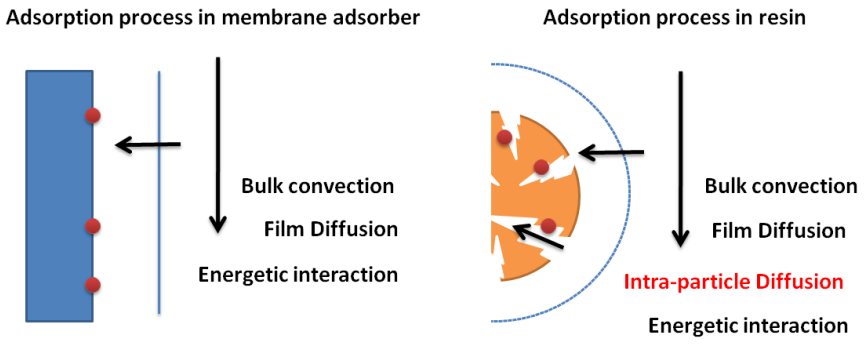

Fig. 2.11 The schematic presentation of adsorption processes in porous membrane adsorption and resin adsorption.

Membrane adsorption apparatus outperforms traditional column adsorption in terms of operational and economic aspects. The main advantage is the significant improvement of mass transfer efficiency, comparing to column adsorption. The adsorption site in

membrane absorber are located evenly on the pore surface. Due to the relatively large pore size compared to column adsorption, the mass transfer of adsorbate can be largely facilitated by means of convection flow (cf. Fig. 2.11). Conversely, in traditional column adsorption, due to the smaller pore size in adsorption resin, it has huge mass transfer resistance, i.e., intra-particle diffusion. Other benefits of using membrane adsorber are less energy and chemical consumption because of less pressure drop during operation and the lower void volume. Additionally, the membrane adsorber can be operated in a disposable way, thus, simplifying the operation.

Nevertheless, the membrane adsorber still remains several drawbacks. The main disadvantage of membrane adsorber is its poor binding capacity associated with its lower specific area compared with adsorption resin. A less specific area leads to a low adsorption site per filtration area. This drawback can be compensated by increasing the thickness of adsorbent materials on the membrane surface. However, a thicker adsorption layer normally may decrease the pore size, thus increasing the mass transfer resistance in the membrane pore, which will alleviate the advantage of fast mass transfer. From the above discussion, the way to tackle the trade-off between binding capacity and mass transfer is to adapt to the specific application scenario by well designing of the membrane module, structure, and operation condition.

2.4.2 The influence of membrane structure and membrane module design

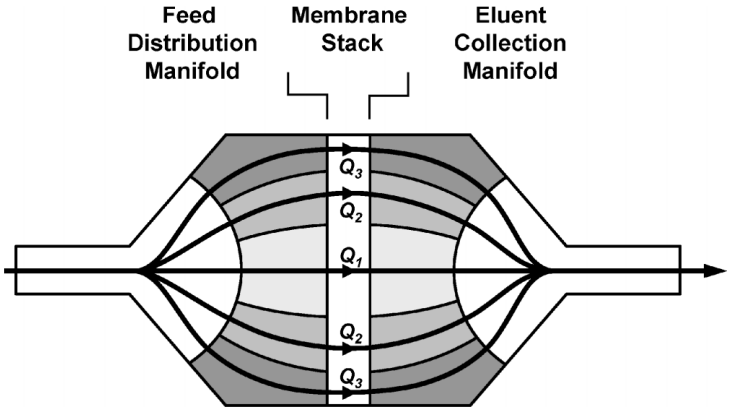

Fig. 2.12 The flow rate distribution profile across the syringe membrane filter [101,102].

The membrane modules can be classified into the dead-end flow, cross-flow, and radial flow based on the processing type. In the mode of dead-end flow and radial flow, similar to traditional adsorption columns, the membrane adsorber is usually assembled as multiple stacked membrane discs. The cross-flow mode can be adapted by using a cross-flow sheet cassette, spiral wound, and pleated sheet, giving the membrane adsorber module high throughput. However, the stacked discs form, such as syringe membrane filter, is the most common membrane module design for membrane adsorber. Membrane module design also influences the binding capacity as well as permeability [97–100]. For efficient utilization of overall membrane adsorber, the adsorption process should follow with two scenarios: firstly, the solute in front of the feed flow (inlet) should ideally attach to the membrane surface simultaneously, and secondly, the permeate should be collected in a uniform mixing (outlet). However, such an ideal flow condition is almost impossible to achieve, while an uneven dispersion of adsorbate is commonly observed during the membrane processing. The common membrane cell, both inlet and outlet, have a shape of a circular channel resulting in maldistribution of flow condition (cf. Fig 2.12). And the uneven flow distribution in both inlet and outlet leads to uneven utilization of membrane, namely the break-through of adsorbate from the center are of membrane adsorber is prior to the outer radial position [101,102]. And such radial flow distribution results in various residence times distributed at the radial direction in the membrane. Therefore, the adsorbate break-through from the central area of the membrane prior to the outer radial

positions. With a proper membrane unit design, e.g., applying porous supporting discs in both inlet and outlet sides, offering high mass transfer while maintaining high binding capacity and resolving energy [102].

Moreover, the selection of support matrix and the geometry of membrane critically affect the separation performance in the membrane adsorption process. Binding capacity and membrane permeability are the two main parameters to evaluate the performance of membrane adsorber. However, the conventional approaches to improve the binding capacity of the membrane, such as increasing binding site density, will decrease pore size and further deteriorate membrane permeability. The pore size, membrane structure, porosity, membrane specific area should be carefully designed for the specific application, e.g., larger pore size is preferable to separate large bimolecules while smaller pore size is preferable to bind small molecules because of the higher specific area. Sometimes harsh conditions such as high temperature, high ionic strength, a wide range of pH, external force during membrane assemble, etc., may be introduced into the operation procedures. Thus the membrane should be capable to withstand this harsh or corrosive operation condition, naming the membrane should chemical and physical stable [90]. The distribution of pore size in the membrane adsorber, the uneven pore size will lead to the diverse axial flow rate in the membrane porous structure.

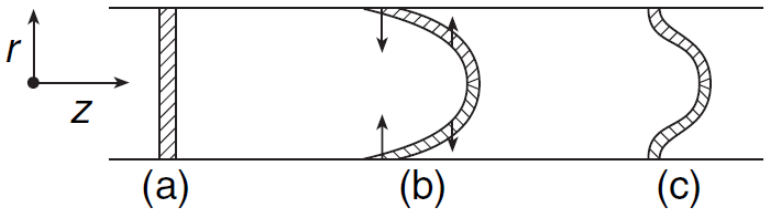

Fig. 2.13 Schematic presentation of occurrence of Taylor dispersion [103,104].

To a laminar flow, which is the typical flow condition in MF and UF membrane, the Taylor dispersion results in uneven solute or adsorbate dispersion along with the flow direction because of the lacking sudden concentration or velocity fluctuation in laminar flow [103,104]. Under the stationary laminar flow condition, the initial solute or adsorbate pulse enters the channel (a) and is deformed by the flow in the z-direction (b), as shown in

Fig. 2.13. The solute or adsorbate at the fast-flowing region would diffuse towards the channel wall (r direction), while the solute or adsorbate in the slow-flowing region diffuses toward the bulk phase. Such solute or adsorbate diffusion retard the dispersion caused by the bulk convective flow (c), leading to the complicated solute or adsorbate concentration profile. In the practical scenario, the adsorption and desorption process is coupling with the Taylor dispersion effect, thus leading to even more complicated adsorbate mass transfer.

2.4.3 Boron removal via membrane adsorption process

Membrane adsorber has been prepared and adapt to the application of boron removal from seawater [105–109]. UF and MF membranes are the most common platforms to prepare membrane adsorber. However, most of the UF adsorber only includes a boron affinity coating at the selective layer, while the MF membrane adsorber is able to include affinity coating on its overall surface [107,108]. Regarding the ligands groups, polyols chemicals, especially NMDG derivatives (cf. Fig. 2.14), are commonly introduced in membrane modification for the sake of specific boron binding. Several techniques have been applied to integrate specific boron binding with the membrane filtration process, and some of the membrane adsorbers for boron removal are summarized in Table 2.6.

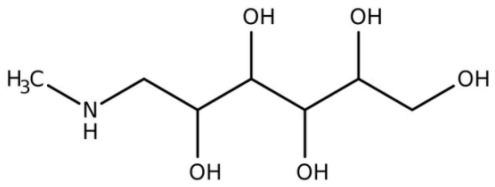

Fig. 2.14 The chemical structure of NMDG.

A chloromethylated PSF is used as additives during UF membrane preparation via non-solvent induced phase separation (NIPS) process, and the chloromethylated PSF faction in membrane matrix acts as active sites for post grafting of NMDG derivates monomer via surface-initiated ATRP [105]. This modified membrane has a functionalization degree of 1.8-5.9 mg/cm^2, depending on polymerization time. The boron binding capacity is proportional to the functionalization degree, where it has a binding capacity of 26.6 mg/g

when the functionalization degree is 4.7 mg/cm^2. The boron adsorption process fits well with the Langmuir model and the Pseudo-second order model in terms of adsorption isotherm and adsorption kinetics, respectively [105]. Similar work has been done by Shi et al., where the chloromethylated PSF included membrane was first modified by poly(glycidyl methacrylate) (PGMA) and later post-functionalize PGMA with NMDG endowing a UF membrane with specific boron binding [108]. The modified membrane show 0.8 - 2.2 mg/g of boron binding capacity at pH of 9.0, and the boron adsorption process follows with Langmuir model and Pseudo-second order model. Another surface-initiated ATRP is use to grafted regenerated cellulose MF membrane with NMDG derivative polymers giving a membrane with 7.7 mg/g of boron binding capacity [108]. This modified RC membrane follows with Freundlich model in terms of adsorption isotherm. Apart from the NMDG derivates, other polyols or diols moiety can also be grafted onto the membrane via post-modification. For example, 2,3-dihydroxypropyl methacrylate (HPMA), 3-(N-glycidol-N-methyl) amino-2-hydroxypropyl methacrylate (GMHP), 2-(bis(2,3-dihydroxypropyl)amino) ethyl methacrylate (HAEM) have been used in the post-modification of PSF membrane, and showing various boron binding capacity [110].

Table 2.6 Capital cost of different boron removal methods.

Based polymer	Membrane type	Ligand	Adsorption isotherm	Adsorption kinetics	q_e (mg/g)	Ref.
PSF	UF	NMDG	Langmuir	pesudo-2nd-order	26.6	105
PSF	UF	NMDG	Langmuir	pesudo-2nd-order	0.8-2.2	108
RC	MF	NMDG	Freundlich	/	7.7	108
PSF	UF	HPMA	Langmuir	pesudo-2nd-order	3.9	110
PSF	UF	GMHP	Langmuir	pesudo-2nd-order	5.5	110
PSF	UF	HAEM	Langmuir	pesudo-2nd-order	6.8	110
Cellulose	UF	NMDG	/	/	/	106
PSF	Mixed matrix UF membrane	NMDG	S-type	pseudo-2nd-order	/	109

Mixed matrix membrane is considered a new-generation membrane with a heterogeneous matrix in which contains membrane matrix and functional 'fillers'. Such well combination is of great interest due to the integration of inherent characteristics of polymer matrix and functional fillers. This concept has also been adapted to prepare membrane adsorber for boron binding [109]. A commercial boron selective resin (BSR) with NMDG as chelation groups is mixed with PSF casting solution, and later a mixed matrix membrane can be prepared via the NIPS process. The BSR fillers provide the boron adsorption property, while the PSF matrix provides a membrane sieving property. This mixed matrix membrane has S-type boron adsorption isotherm, which may indicate different boron binding mechanisms under different initial boron concentrations. When speaking of the adsorption process, either via membrane adsorber or commercial adsorption resin, the regeneration of membrane adsorber shouldn't be ignored. This mixed matrix membrane adsorber shows 97.6% of binding capacity remains after 10 runs of regeneration-adsorption cycles using a 0.1 N HCl and a 0.1 N NaOH [109]. However, only very few researchers perform the membrane adsorber regeneration step.

3. Experiments

3.1 Materials

3.1.1 Membranes

The commercial membranes used for modification are listed in Table 3.1.

Table 3.1 Information of used commercial membrane

Name	MWCO or pore size	Permeability (LMH bar)	Company
PES-50	50 kDa	210	Sartorius
PES-100	100 kDa	500	Sartorius
Multibore® module	300 kDa	900-1000	Inge GmbH
MicroPES 2F	0.2 µm	10000	3M
MicroPES 6F	0.6µm	40300	3M

3.1.2 Chemicals

All the chemicals that were used in this work are listed in Table 3.2.

Table 3.2 The chemicals used in this work

Name	Abr.	CAS No.
37% Hydrochloric acid	-	7647-01-0
2-(Dimethylamino)ethyl methacrylate	DMAEMA	2867-47-2
2,2'-Azobis(2-methylpropionitrile)	AIBN	78-67-1
Acetone	-	67-64-1
Ammonium persulphate	APS	7727-54-0
Ammonium thiocyanate	NH_4SCN	1762-95-4
Boric acid	-	10043-35-3
Butyl methacrylate	BMA	97-88-1
CalciumchloridDihydrat	CaCl2·2H2O	10035-04-8
Curcumin	-	458-37-7
Dichloromethane	DCM	51325-91-8

Dipentaerythritol penta-/hexa-acrylate	5-Acl	60506-81-2
Di-tert-butyl dicarbonate	Boc_2O	24424-99-5
Ethyl acetate	EA	141-78-6
Ethyl alcohol	EtOH	64-17-5
Ethylenediamine	EDA	107-15-3
Ferrous ammonium sulfate	FAS	7783-85-9
Gluconolactone	GA	90-80-2
Glycidol	-	556-52-5
Hexane	-	110-54-3
Hydroquinone	HQ	123-31-9
Hyperbranched Poly(ethyleneimine)	PEI-750	9002-98-6
Isopropanol	-	67-63-0
Magnesium chloride hexahydrate	$MgCl_2·6H2O$	7791-18-6
Methacryloyl chloride	-	920-46-7
Methanol	MeOH	67-56-1
Methyl Orange	-	547-58-0
N,N,N',N'-tetramethylethylenediamine	TEMED	110-18-9
N,N-dimethylformamide	DMF	1968/12/2
N,N'-methylene-bis-acrylamide	MBA	110-26-9
Oxalic acid dihydrate	-	144-62-7
Potassium bromide	KBr	7758/2/3
Potassium chloride	KCl	7447-40-7
Silica gel 60	-	-
Sodium carbonate	Na_2CO_3	497-19-8
Sodium chloride	NaCl	7647-14-5
Sodium hydrogen carbonate	NaHCO3	144-55-8
Sodium sulfate	Na_2SO_4	7757-82-6
Triethylamine	TEA	121-44-8
Urea	-	57-13-6
Water	-	-

3.1.3 Artificial seawater (ASW) preparation

The ASW is used in the specific adsorption experiment to mimic the boron removal process in seawater. The composition of self-prepared ASW according to literature can be found in Table 3.3 [111].

Table 3.3 The composition of self-prepared artificial seawater

Chemicals	Amount (g)
NaCl	23.92
Na_2SO_4	4
KCl	0.677
$NaHCO_3$	0.196
KBr	0.098
$MgCl_2{\cdot}6H_2O$	10.81
$CaCl_2{\cdot}2H_2O$	1.52
Boron solution (5 mg/L)	958.8

3.2 Monomer and polymer synthesis.

3.2.1 GAMEM monomer synthesis

1) Synthesis of N-(tert-butoxycarbonyl)-1,2-diaminoethane (Boc-EDA).

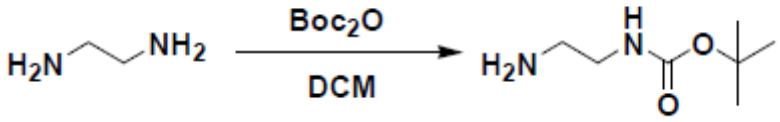

Fig. 3.1 Synthesis route of Boc-EDA.

The synthesis of Boc-EDA was performed according to literature [112, 113]. Boc_2O (11.6 g) in DCM (200 mL) was added dropwise into a solution of EDA (20 mL) in DCM (200 mL) over 4 h with vigorous stirring in ice-bath, and the reaction carries out for another 16 h. After concentrating the solution by the evaporator, 20% of $NaCO_3$ (60 mL) was added, and the mixture was extracted with DCM. After drying over by Na_2SO_4, remove the DCM via evaporator, affording the product Boc-EDA with the yield of ~99 %. The NMR spectra of Boc-EDA can be found in Appendix A, Fig. A1.

2) Synthesis of N-2-[(tert-butoxycarbonyl)amino] ethyl methacrylamide (Boc-AEMA)

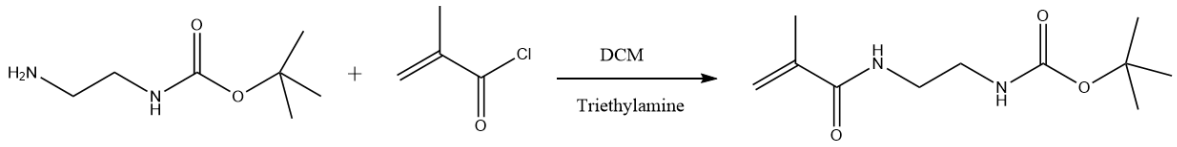

Fig. 3.2 Synthesis route of Boc-AEMA.

The synthesis of Boc-AEMA was performed according to literature [112]. To a solution of Boc-EDA (8 g) in DCM (80 mL) was added TEA (7.2 g) then cool down this mixture in ice-bath. To this cooled mixture, a solution of methacryloyl chloride (6.24 g) in DCM (50 mL) was added dropwise with vigorous stirring; then, this reaction was carried out overnight. The next day, the reaction mixture was washed by 4 X 80 brine solution, and the organic phase was dried over Na_2SO_4. The dried concentrated organic phase was purified by column

chromatography using silica gel as stationary phase and a mixture of EA/hexane as eluent. After removing the solvent, Boc-AEMA can be obtained with a yield of ~82 %. The NMR spectra of Boc-AEMA can be found in Appendix A, Fig. A2.

3) Synthesis of N-(2-aminoethyl) methacrylamide hydrochloride (AEMA)

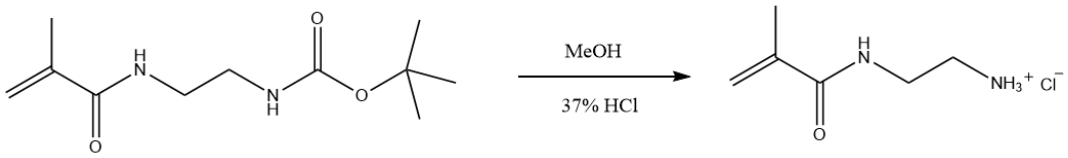

Fig. 3.3 De-protection of AEMA.

The synthesis of AEMA was performed according to literature [112,114]. To a solution of Boc-AEMA (9.35 g) in MeOH (80 mL) was added HCl/MeOH mixture (70 mL MeOH + 30 mL 37% HCl) dropwise with vigorous stirring, the reaction was carried out for overnight. The next day, remove the solvent via evaporator affording the products AEMA with the yield > 99 %. The NMR spectra of AEMA can be found in Appendix A, Fig. A3.

4) Synthesis of 2-gluconamidoethyl methacrylamide (GAEMA)

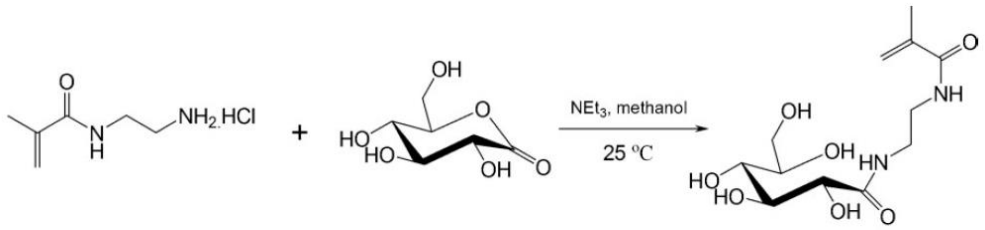

Fig. 3.4 Synthesis route of GAEMA monomer.

The synthesis of GAEMA was performed according to literature [115–117]. Dissolving GA (5.7 g) and hydroquinone (few particles) in MeOH (250 mL) at 50 °C and then cooled down to room temperature obtaining a transparent GA solution. This mixture was added by a solution of AEMA (6.5 g) and TEA (20 mL) in MeOH (250 mL) dropwise with vigorous stirring. The reaction was carried out overnight with vigorous stirring. The next day, the mixture was concentrated by the evaporator and then precipitated into iso-propanol. Filtrate the mixture and washed the white solid with iso-propanol and acetone, respectively.

Afterwards, the white product was dried under vacuum overnight, and the GAEMA can be obtained with a yield of ~ 92%. The NMR spectra of GAEMA can be found in Appendix A, Fig. A4.

3.2.2 Macro-initiator synthesis

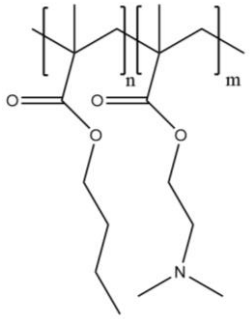

Fig. 3.5 The chemical structure of macroinitiator PBD.

The self-synthesized poly(BMA-co-DMAEMA) with a designed molecular weight was used as the macro-initiator in membrane surface modification (cf. Fig. 3.5). The inhibitor in the fresh BMA and DMAEMA should be removed by inhibitor remover before use. To a monomer solution of BMA and DEMEMA in DMF, the dissolved oxygen was removed by bubbling argon for 30 min while heating the mixture to desired reaction temperature. After reaching the target temperature, a solution of AIBN in DMF was added to initiate polymerization while keeping the whole reaction system under the argon atmosphere. After the desired reaction time, the mixture was precipitated in water and drying. After performing two cycles of dissolution-precipitation procedures, the final product is dried under vacuum at 60 °C. Table 3.4 shows two different PBD, PBD-300 and PBD-74, prepared at the specific conditions.

Table 3.4 Information of self-prepared macroinitiator PBD-300 (cf. Appendix A, Fig. A 7) and PBD-74 (cf. Appendix A, Fig. A 8)

Name	DMAEMA (mL)	BMA (mL)	DMF (mL)	AIBN (mg)	T. (°C)	Time (h)	Mw (kDa)	PDI
PBD-300	4.56	8.41	30	22	65	36	300	2.79
PBD-74	4.56	8.41	40	32.8	80	3	74	3.3

3.2.3 Preparation of hydroxyl functionalized PEI (PEI-OH)

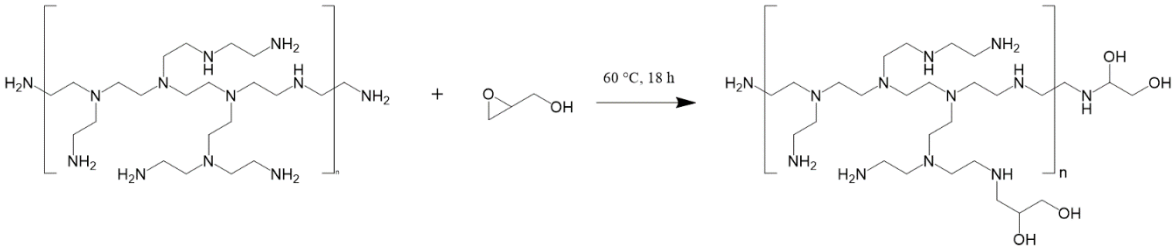

Fig. 3.6 Synthesis and chemical structure of partial hydroxyl functionalized PEI (PEI-OH).

The PEI-OH (cf. Fig. 3.6) can be synthesized via epoxy-amine nucleophilic addition. Adding water into hyperbranched PEI solution (50 wt%), affording a final solid concentration of 10 wt%, then remove the oxygen by bubbling argon for 30 min. Afterward, adding glycidol into the mixture with vigorous stirring. The reaction is carried out at 60°C for 18 h. After the reaction, the mixture was purified by dialysis tube (MWCO = 4000 Da). The purified solution was subsequently dried via lyophilization to obtain the final product. By altering the amount of glycidol, the PEI-OH with a different functionalized degree can be obtained (cf. Table 3.5).

Table 3.5 Reaction condition of preparing PEI-OH with different hydroxyl functionalization degrees.

Name	PEI solution (g)	Glycidol (mL)	T (°C)	T (h)
PEI-OH-0.35	5.376	1.551	60	18
PEI-OH-0.56	5.376	2.418	60	18
PEI-OH-0.7	5.376	3.023	60	18

3.3 Membrane modification

3.3.1 Membrane functionalization via infiltration of active coating

3.3.1.1 Modification UF flat sheet membrane via PEI-OH/5-Acl infiltration

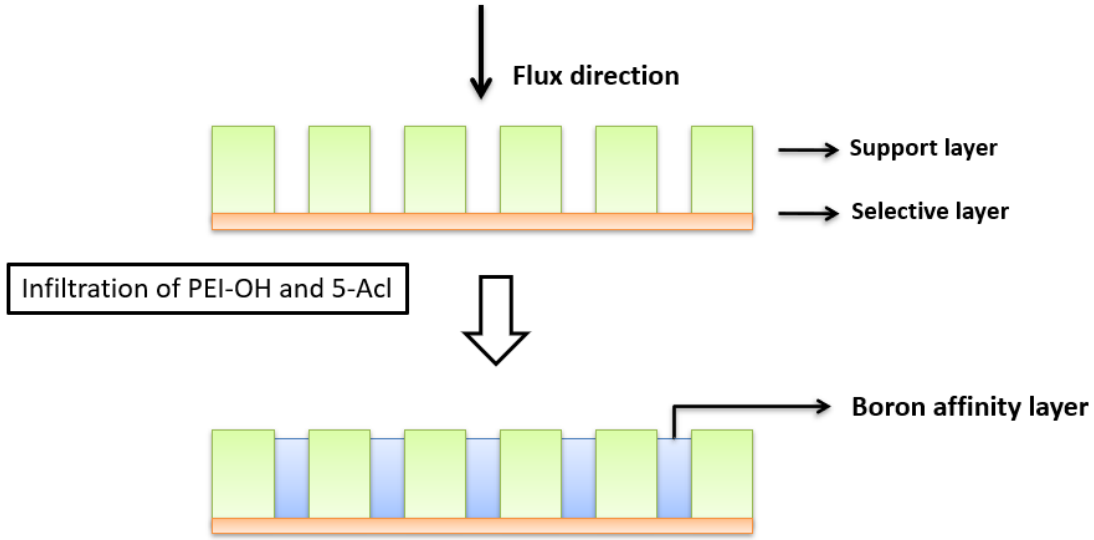

Fig. 3.7 The schematic presentation of modification procedures via infiltration of PEI-OH and the cross-linker 5-Acl.

Before the modification, the pristine membrane was thoroughly washed by Milli-Q water and EtOH and later stored in 95% EtOH overnight. For the modification solutions, firstly, dissolve PEI-OH in EtOH with a concentration of 0.3 mg/L. Afterward, different amounts of cross-linker, 5-Acl, were added to achieve three cross-linker degrees (DC) of 25 wt%, 10 wt%, and 2 wt%. During the infiltration process, 10 mL of modification solution was filtrated out of 30 mL in the dead-end filtration setup with an effective membrane diameter of 33 mm. The infiltration is carried out at three operation pressures (OP) of 0.5, 1.0, and 1.5 bar. In total, nine different modifications have been done (cf. Table 3.6) during the infiltration process. The permeate was collected and weighted automatically via electronic balance with a fixed time interval. After the modification, switch the filtration direction to normal orientation where the selective layer faces to feed. The modified membrane was washed by Milli-Q water and stored in Milli-Q water for later use.

Table 3.6 Different modification conditions in infiltration modification using PEI-OH/5-Acl

OP / DC	0.5 bar	1.0 bar	1.5 bar
25 wt%	PEI-OH-25-0.5	PEI-OH-25-1.0	PEI-OH-25-1.5
10 wt%	PEI-OH-10-0.5	PEI-OH-10-1.0	PEI-OH-10-1.5
2 wt%	PEI-OH-2-0.5	PEI-OH-2-1.0	PEI-OH-2-1.5

3.3.1.2 Modification of UF flat sheet membrane via PEI/5-Acl infiltration followed by post functionalization with hydroxyl groups

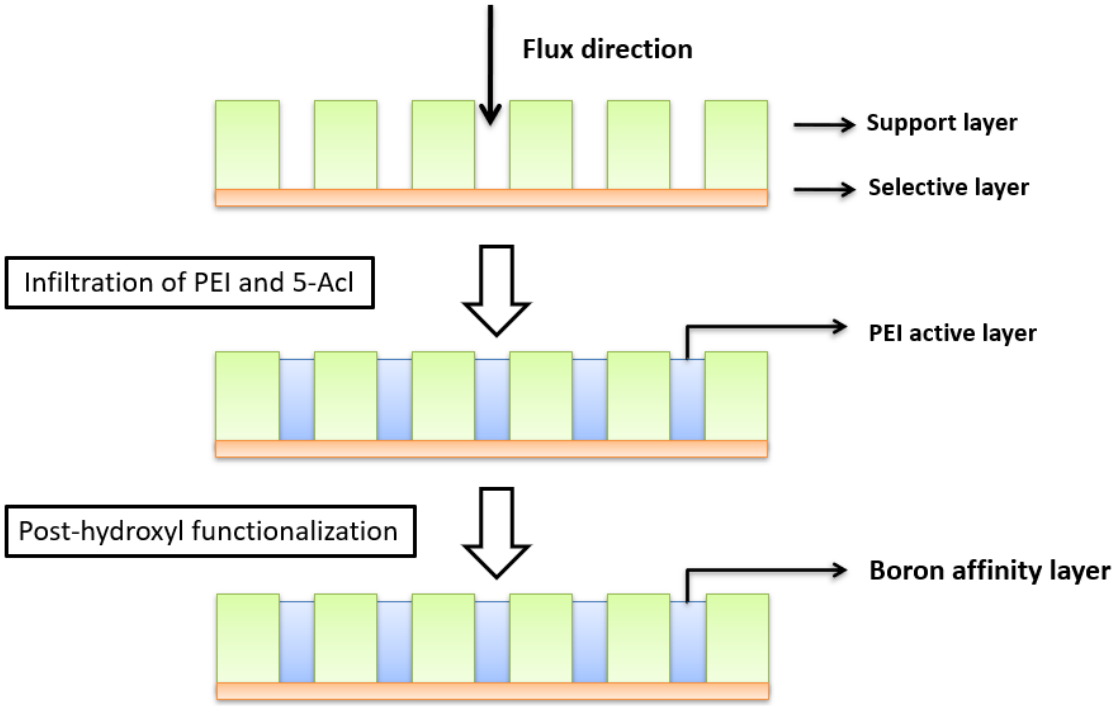

Fig. 3.8 The schematic presentation of modification procedure: first prepare the PEI active coating and later perform the post-hydroxyl functionalization.

The infiltration protocol in the pre-modification step here is analogous to the modification protocol mentioned in Section 3.3.1.1. Briefly, a modification solution of PEI and 5-Acl in EtOH was infiltrated into the support layer of PES50 under three operation pressures (cf. Table 3.7). The modification was ceased when filtrated 10 mL out of 30 mL modification solution and the modified membrane was washed thoroughly by Milli-Q water. After that, the premodified membrane was soaked in 22 mL of 9% glycidol aqueous solution at 50 °C

for 48 hours. In the end, the final modified membranes were thoroughly washed by Milli-Q to remove the residual glycidol and store in Milli-Q water for later use.

Table 3.7 Different modification conditions in infiltration modification using PEI/5-Acl

OP / DC	0.5 bar	1.0 bar	1.5 bar
25 wt%	PEI-25-0.5	PEI-25-1.0	PEI-25-1.5
10 wt%	PEI-10-0.5	PEI-10-1.0	PEI-10-1.5
5wt%	PEI-5-0.5	PEI-5-1.0	PEI-5-1.5
2 wt%	PEI-2-0.5	PEI-2-1.0	PEI-2-1.5

3.3.1.3 In-situ modification of Multibore® module

The modification on the Multibore® module is analogous to the modification protocol mentioned in section 3.3.1.2. Briefly, PEI/5-Acl solution was infiltrated into the support layer of the Multibore® module of which has an effective membrane area of 5165.7 mm^3. In the dead-end mode, the modification was ceased when 60.4 mL permeate is collected out of 241.6 mL at the operation pressure of 1.5 bar. After that, the hydroxyl-functionalization is performed by recirculation of 9% glycidol aqueous solution (132 mL) through the pre-modified Multibore® module. During the recirculation of glycidol solution, the membrane module is immersed in the 50 °C water bath. After 48 h, the hydroxyl-functionalization is done, and wash the Multibore® module thoroughly with Milli-Q water.

3.3.2 Membrane functionalization via surface-initiated polymerization

3.3.2.1 MF modification via macro-initiator meditated redox initiated polymerization (graft-from method)

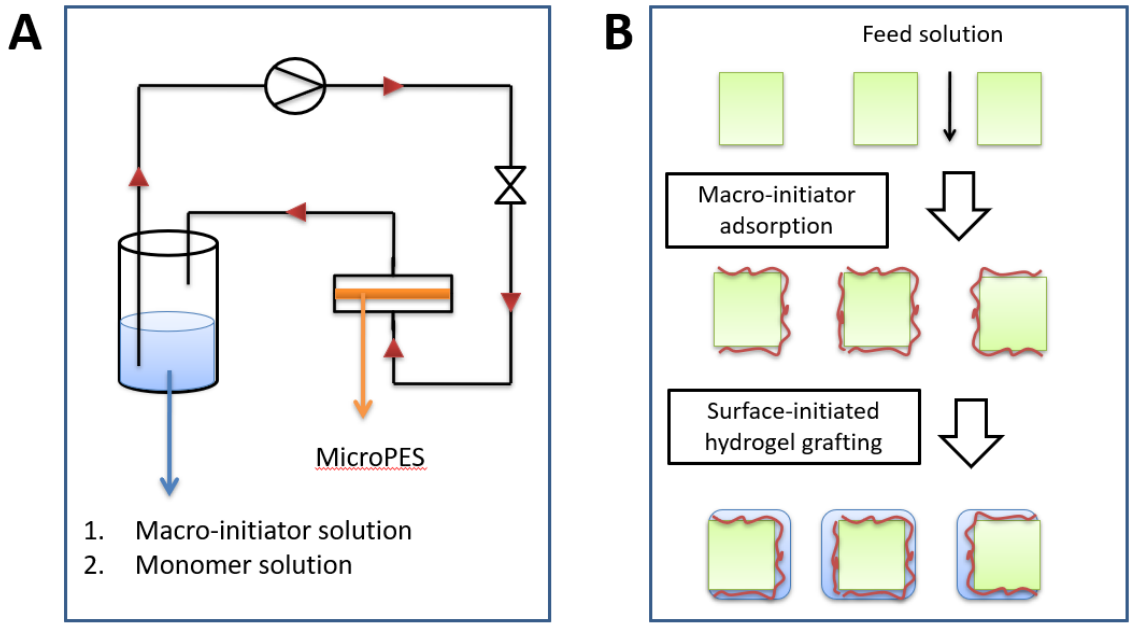

Fig. 3.9 The schematic presentation of modification apparatus (A) and modification procedures (B).

A commercial MF membrane, MicroPES, has been selected as the base membrane for boron affinity layer grafting. The modification was carried out in a close recirculation system, as shown in Fig. 3.9. Firstly, dissolve the self-prepared macro-initiator (0.25 g), PBD, into isopropanol (50 mL). After completely dissolve the PBD, 1 N HCl (2.5 mL) was added, then Milli-Q water was filled up to 250 mL. And macro-initiator solution with a concentration of 1 g/L is ready for use. The commercial MF membrane MicroPES should be washed by Milli-Q water and isopropanol thoroughly before the modification. Load the washed 2.5 cm MicroPES membrane into the reusable syringe filter holder with an effective modification area of 3.46 cm^2 (effective diameter of 1.05 cm). Recirculate 25 mL of fresh prepared macro-initiator solution (1 g/L) through the membrane via a peristaltic pump. The modification was carried out at the flow rate of 3 mL/min for 6 hours. After the pre-modification, the membrane was washed by Milli-Q water at the flow rate of 3 mL/min for 30 min and ready for the subsequent modification.

Table 3.8 Different monomer solution conditions used to modify MF membrane via surface-initiated grafting.

No.	Membrane	PBD	C_{GAEMA} (wt%)	C_{MBA} (wt%)	C_{APS} (wt‰)
1	2F	PBD-300	10	5	0.5
2	2F	PBD-300	10	5	2
3	2F	PBD-300	10	5	3
4	2F	PBD-300	10	10	2
5	2F	PBD-300	15	5	0.5
6	2F	PBD-300	15	5	2
9	6F	PBD-300	10	5	2
10	6F	PBD-300	10	10	2
11	6F	PBD-300	15	5	2

The monomer solution was freshly prepared. Dissolve GAEMA and MBA in 10 wt% urea solution at 50 °C, and cool down this mixture when the GAEMA completely dissolved obtaining a transparent monomer solution. The dissolved oxygen in the monomer solution is removed by bubbling argon for 15 min. To the degassed monomer solution, APS solution was added and keep degassing for another 5 min. After that, the degassed monomer solution was carefully transferred to the recirculation system and pumped through the pre-modified membrane. The hydrogel grafting via surface-initiation polymerization is carried out under recirculation with a 3 mL/min flow rate for 2 hours. Finally, the modified membrane was washed with Milli-Q water for 30 min and later recirculate Milli-Q water with a 3 mL/min flow rate overnight to eliminate non-adherent polymer. The final degree of grafting can be tolerated by altering monomer concentration, cross-linker concentration, APS concentration. Table 3.8 presents different monomer solution conditions used in this work.

3.3.2.2 Modification of commercial MF membrane with boron affinity coating via an integrated initiation system: macro-initiator meditated surface initiation integrated with bulk initiation

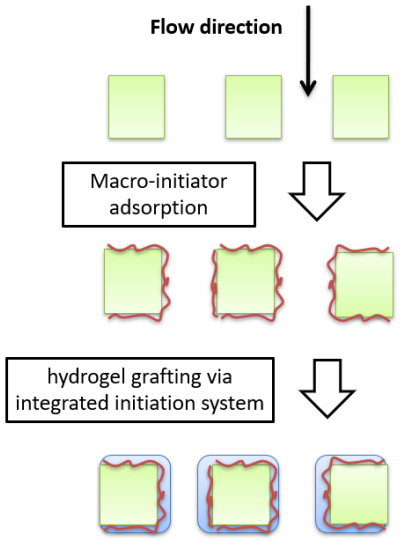

Fig. 3.10 The schematic presentation of applied integrated initiation system to modify MF membrane.

The MF membrane was pre-modified via macro-initiator adsorption akin to the modification procedures in Section 3.3.2.1. To coat the premodified membrane, a designed amount of TEMED was added to the degassed monomer solution containing GAEMA, MBA, and APS. After that, the monomer solution was carefully transferred to the recirculation system and started recirculation under the same operation parameters as mentioned in section 3.3.2.1. (flow rate and recirculation time). The membrane was washed by Milli-Q water overnight to get rid of the unstable fraction of the coating material. The degree of grafting can be tailored by altering GAEMA, MBA, APS, and the ratio of APS/TEMED ratio. However, the monomer solution condition should be carefully controlled to prevent bulk gelation, leading to permanent membrane pore blocking. Table 3.9 presents the various monomer solution conditions used in this modification.

Table 3.9 Different monomer condition used to modify MF membrane via integrated initiation system

No.	Membrane	PBD	C_{GAEMA} (wt%)	C_{MBA} (wt%)	C_{APS} (wt‰)	APS/TEMED
1	6F	PBD-74	15	2	2	1
2	6F	PBD-74	15	2	2	0.5
3	6F	PBD-74	15	1	2	1
4	6F	PBD-74	15	1	2	0.5
5	6F	PBD-74	10	2	2	0.5
6	6F	PBD-74	10	2	2	1
7	6F	PBD-74	10	1	2	1
8	6F	PBD-74	10	1	2	0.5
9	6F	PBD-74	12.5	1.5	2	1
10	6F	PBD-74	12.5	2	2	1
11	6F	PBD-74	12.5	2	2	1
12	6F	PBD-74	12.5	4	2	1
13	6F	PBD-74	13.5	2	2	1
14	6F	PBD-74	13.5	2.5	2	1
15	6F	PBD-74	14	2	2	1
16	2F	No	15	1	2	1
17	2F	PBD-74	15	1	2	0.5
18	2F	PBD-74	15	1	2	1
19	6F	PBD-300	15	2	2	1
20	6F	PBD-300	15	1	2	1
21	6F	PBD-300	15	1	2	0.5

3.3.2.3 UF membrane modification via integrated initiation system

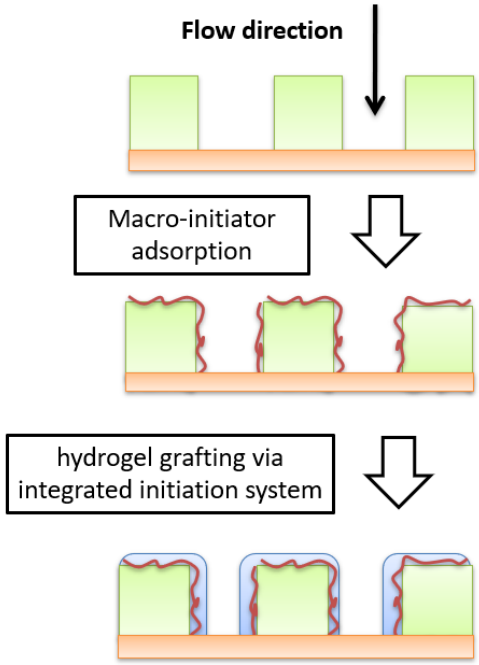

Fig. 3.11 The schematic presentation for applying integrated initiation system to modify UF membrane

PES-100 was used as the base membrane here, and it has been washed thoroughly with Milli-Q water and isopropanol before used. The boron hydrogel coating was grafted in the support layer of PES-100 (Fig 3.11). Akin to the modification procedures in Section 3.3.2.2, a macroinitiator solution, PBD-300 or PBB-74, was infiltrated into the support layer of PES-100 for 5 min at a flow rate of 3 mL/min. The adsorption takes place for 6 hours before washed thoroughly by Milli-Q water. A monomer solution containing a certain concentration of monomer, cross-linker, APS, and TEMED was pump into the membrane with a flow rate of 3 mL/min. After 30 min recirculation of monomer solution, suspend the recirculation and incubate for another 90 min. Finally, the membrane was washed with Milli-Q water at the low rate of 3 mL/min overnight to remove unstable hydrogel coating.

3.3.2.4 Precoating of the MF membrane with a layer containing tertiary amine groups and subsequent graft coating via surface initiation.

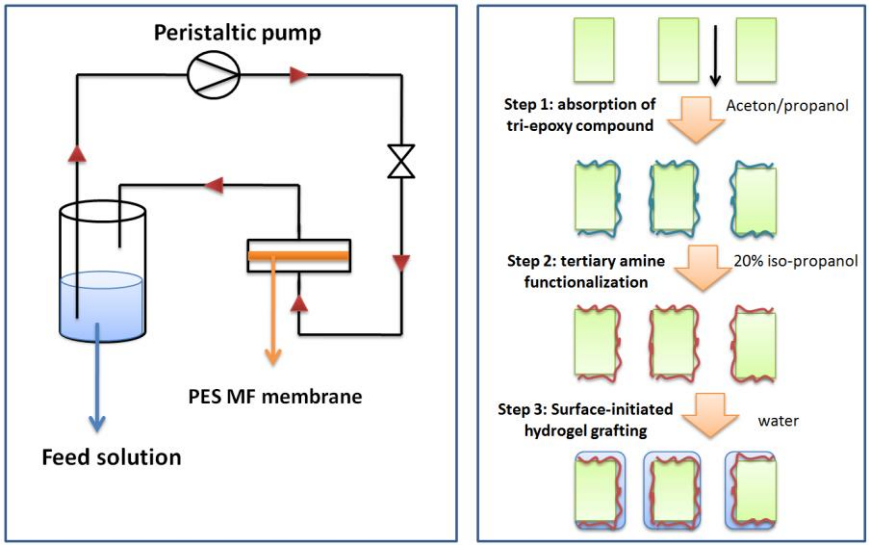

Fig. 3.12 Schematic presentation of modification procedures of modifying MF membrane via tri-epoxy/DMA coating and the subsequent hydrogel grafting.

The base MF membrane was washed thoroughly prior to performing modification. Tris (4-hydroxyphenyl) methane triglycidyl ether (tri-epoxy) was dissolved in the acetone/isopropanol mixture (2:8), affording a tri-epoxy concentration of 10 wt%. Afterwards, a washed based membrane (d = 25 mm) was immersed into 5 mL of 10 wt% tri-epoxy solution and then incubating for 12 h for the sake of saturated adsorption of tri-epoxy compound on the based membrane. After that, the membrane was washed with Milli-Q water and isopropanol thoroughly and adding 5 mL of 10 wt % N, N-dimethylethylenediamine aqueous solution. The tertiary amine functionalization was carried out in the incubator at 45 °C for 24 h. Finally, the premodified membrane can be obtained after thoroughly washing. The premodified membrane has tertiary amine groups at the membrane surface and ready for later hydrogel grafting step. The hydrogel grafting was performed under analogous operation conditions in section 3.3.2.1 and section 3.3.2.1; thus, the detail will not describe here for the sake of simplicity.

3.4 Characterization for the synthesized monomer and polymer

3.4.1 Gel permeation chromatography (GPC)

GPC is a type of size exclusion chromatography used to determine polydispersity index (PDI) and the molecular weight of polymer (M_n, $M_{w,}$ and M_v). Also, the GPC can determine the molecular weight cut off (MWCO) of the pristine modified membrane (the details can be found in Section 3.6.3.3).

For polymer characterization, a Gram column (PSS, 10 µm, Germany) integrated with a refractive index detector (Shodex Showa Denko K.K., Tokyo, Japan) and differential viscosity detector (ETA-2020, WGE Dr. Bures, Germany) were used.

In Mw determination, the polymer was first dissolved in DMAc with a concentration of 4 g/L, then 200 µL of the prepared polymer solution was injected for measurement. The measurement is carried out under the flow rate of 1 mL/min at 60 °C. And the PMMA was used for calibration.

In MWCO measurement, RI-101 differential refractive index detector was used to determine the molecular weight distribution of two dextran mixture solutions, feed dextran mixture (1 g/L), and the dextran mixture from permeate. The measurement is carried out under the flow rate of 1 mL/min at 45 °C. Later on, the MWCO can be defined as the molecular weight where the membrane has 90 % rejection.

3.4.2 NMR spectroscopy

The ^{1}H-NMR spectra of self-prepared GAEMA and macro-initiator PBD were recorded by DMX300 (Bruker, USA) 300 MHz NMR. Two kinds of deuterium solvents, D^6-DMSO and D_2O, were used depends on the measured object.

For the monomer preparation, GAEMA and its precursors have been measure, proofing a successful synthesis (cf. Appendix A1-A4). For macro-initiator, the molar ratio of BMA segments and DMAEMA segments can be verified by ^{1}H-NMR, which is 1:2 (cf. Appendix A6).

3.4.3 Gelation point determination via rheometer.

The point where gelation occurs and a cross-linking network is formed, is called gelation point or sol/gel transition point. Gelation point is defined when storage modulus (G'') equal to loss modulus (G'), i.e., damping factor = 1. In this work, prior to the membrane modification, the gelation point measurement should be done to investigate proper modification parameters in terms of monomer concentration, polymer concentration, etc. The rheological measurement is done by MCR-300 (Anton Paar, Austria), equipped with a cone-plate measuring upper plate (0.1°,25 mm). In PEI/5-Acl and PEI-OH/5-Acl modification system, a solution of 5-Acl in EtOH was added to a PEI or PEI-OH in EtOH to reach the desired cross-linker and polymer concentration, then 200 µL of this mixture was transferred onto the measuring platform. For the redox initiation system, a degassed monomer solution of GAMEA, MBA, and APS in Milli-Q water was first prepared. An initiator solution of TEMED in Milli-Q water was added and mixed for 30 s before transferring 200 µL of this mixture onto the measuring platform. All the measurements were carried out via oscillatory mode, and the measuring parameters were: angular frequency of 10 rad/s; strain amplitude of 0.01%; the measuring temperature of 20 °C. The G'' and G' were recorded along with time, and the gelation point is defined as the time where G' crossover G''.

3.4.4 Bulk hydrogel test refers to boron adsorption capacity

Before doing the membrane adsorption test, the boron adsorption of the respective bulk hydrogel should be characterized. To a solution of 10 mL PEI in EtOH solution (150 mg/L), a 5-Acl solution was added to achieve different cross-linker degrees of 2, 5, and 25 wt%. After well mixing for 30 s, the mixture was incubated for 2 hours. The final PEI/5-Acl gel was washed thoroughly with Milli-Q water, then immersing the washed PEI/5-Acl gel into 30 mL of 9 % glycidol aqueous for 48 hours at 50 °C. Afterward, the hydroxyl functionalized PEI/5-Acl gel was washed by Milli-Q water and dried via lyophilization.

PEI-OH-0.35 was used to prepare PEI-OH/5-Acl gel. Akin to the PEI/5-Acl gel, PEI-OH/5-Acl gel was prepared under the same protocol but without post-hydroxyl functionalization, because the PEI-OH already contains polyols moiety for boron binding. The final prepared

PEI-OH/5-Acl gel was dried via lyophilization.

The GAMEA bulk hydrogel was prepared via the redox initiation system of APS/TEMED. The monomer condition is 10-10-2, in which the monomer, cross-linker, and APS concentration is 10 wt%, 10 wt%, and 2 wt‰, respectively. 10 mL of this monomer solution was first degassed by argon for 15 min before adding a designed amount of TEMED, making a mass ratio of TEMED/APS as 1. The polymerization was carried out overnight to achieve complete conversion. Afterward, the hydrogel is immersed into the Milli-Q water to remove unreacted residuals. The bulk hydrogel was dried via lyophilization.

Towards the different bulk hydrogel, the boron adsorption experiment was carried out at the same condition: 1) initial boron concentration of 5 mg/L; 2) adsorbent (hydrogel) dosage of 10 g/L; 3) adsorption temperature of ~ 20°C; 4) the initial pH value of boron solution of ~8.0; 5) adsorption time of 48 hours. After 48 hours, the remaining boron concentration in the bulk solution was measured via the curcumin method.

3.5 Characterization of initiation efficiency in the macro-initiator meditated initiation

3.5.1 Persulfate determination

The macro-initiator initiation system's initiation efficiency can be evaluated by qualitatively determining the decomposition efficiency of APS. The based membrane first adsorbs PBD in the pre-modification step. The tertiary amine groups of the adsorbed PBD can accelerate the decomposition of persulfate to generate free radicals for polymerization (cf. section 3.3.1.4, 3.3.2.1, and 3.3.2.2). Thus, the change of persulfate concentration along with the recirculation time should be measured.

Firstly, a premodified membrane was assembled in a syringe filter holder with an effective area of 3.46 cm^2. Then 4 mL of degassed APS solution (2 g/L) was pumped through the pre-modification membrane with a flow rate of 3 mL/min for 2 hours. The APS solution was sampled (0.08 mL) every 30 min and measuring the remaining persulfate concentration; thus, the persulfate concentration variation against recirculation time can be determined.

The persulfate concentration can be determined via UV/Vis method [118]. 0.08 mL of the

persulfate solution was first placed into a container containing 0.9 mL of Milli-Q, 0.2 mL of 0.2N FAS, 10 mL of 2.5N H_2SO_4, and then a well mixing this mixture and incubate for 45 min at room temperature (~20 °C). Afterward, a 0.2 mL of 0.6N NH_4SCN solution was added, and measure the absorbance at a wavelength of 450 nm. The final persulfate concentration can be obtained according to the calibration (cf. Fig. 3.13).

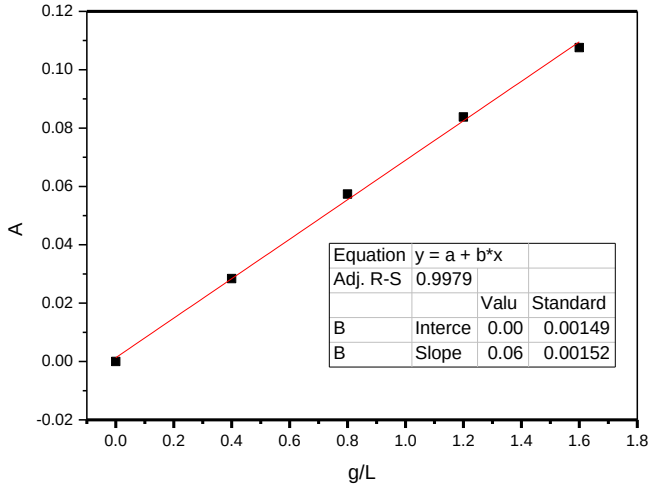

Fig. 3.13 The calibration curve for APS determination via UV-Vis method.

3.6 Membrane characterization

3.6.1 Characterization of membrane morphology

3.6.1.1 Scanning electron microscopy (SEM)

The surface and cross-section morphology can be observed via SEM image taken from ESEM Quanta 400 FEG scanning electron microscope (FEI, USA). Before the SEM picture is taken, the membrane was dried via lyophilization to maintain the coating and membrane morphology. The membrane was cooled with liquid nitrogen and broken to get intact cross-section morphology. Both the surface and the cross-section need to be sputtered with a conductive layer of Au/Pt (80:20) by a K550 sputter coater from Emitech Ltd. (Ashford, UK).

3.6.1.2 Gas flow / liquid displacement permporometry

The pore geometry of pristine and modified membrane, such as pore size distribution, largest pore size, mean pore size, can be determined by Capillary Flow Porometer, CFP-34RTG8A-X-6-L4, (PMI Inc., Ithaca, NY, USA) by means of “wet-up/dry-up” mode. Before measuring the sample, the membrane was dried via lyophilization. The dry-up program runs first to measure the dry-up curve of the dry membrane sample, later immerse the exact same dry membrane into a wetting liquid called “Galwick” (1,1,2,3,3,3-hexafluoro propene, γ = 16 dyne/cm), making sure the pore is completely filled with “Galwick” solution, and start the wet-up measuring program. The rough data was proceeded by the software, and the pore information of the membrane sample was calculated according to Young-Laplace equation:

$$p = \frac{4\,\gamma \cos\theta}{D} \qquad (3.1)$$

Where p stands for differential gas pressure required to displace the pore-filled liquid; γ is the surface tension of wetting liquid, here is Galwick; θ is contact angle; D is pore diameter.

3.6.2 Characterization of membrane chemistry

3.6.2.1 ATR-FTIR spectroscopy

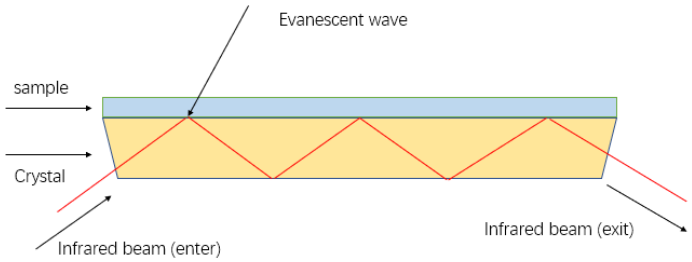

Fig. 3.14 Schematic presentation of the mechanism of ATR-FTIR.

Attenuated total reflection (ATR) uses total internal reflection property resulting in an evanescent wave (cf. Fig. 3.14). An IR beam is passed through the ATR crystal and forming an evanescent wave at the reflection interface, and this evanescent wave can interact with samples of which have good contact with the ATR crystal surface. Thus, the ATR-FTIR can measure the IR spectrum of the opaque sample, such as the membrane. Varian 3100 FT-IR Excalibur spectrometer (Agilent Technologies, USA) equipped with the ATR extension MIRacle (Pike Technologies, USA) unit was used to understand the surface chemistry of pristine and modified membrane. The used ATR unit is a diamond/ZnSe crystal (refractive index 2.4, angle of incidence 45°), and the penetration depth in the range of 0.5-2 µm. Before the ATR-FTIR measurement, the membrane sample is dry in a vacuum oven at 40 °C for 48 h to eliminate the influence of adsorbed water. In the ATR-FTIR measurement, 64 scans were used with a resolution of 1.0 cm^{-1}.

3.6.2.2 Contact angle (CA)

The hydrophilicity of pristine and modified membranes surface was evaluated by contact angle measurement. The CA measurements were carried out by an optical contact angle goniometer (OCA 15 Plus; Dataphysics GmbH, Filderstadt, Germany). In order to correctly represents the hydrophilicity sample surface, “sessile drop” mode and “captive bubble” mode were used, respectively, depends on the surface condition, e.g., the surface with high surface free energy on which liquids spread out, such as hydrogel surface, is particularly better used “captive bubble” mode. In “sessile drop” mode, 5 µL of Milli-Q water were

dropped on the measuring surface by micro-syringe, then a picture was taken by device and later proceed the date via Young-Laplace model to calculate the CA. In “captive bubble” mode, the measuring surface was immersed into Milli-Q water upside-down, and an air bubble with the volume of ~ 5 µL was dispensed to the measuring surface, and a picture will be taken and later proceed the date via Ellipse model to calculate the CA of air bubble. The CA of water was calculated by subtracting the air bubble CA from 180°.

3.6.2.3 Zeta potential

The surface charge of the pristine and modified membranes was measured by SurPASS electro-kinetic analyzer (Anton-Paar GmbH, Austria). Two membranes are needed, and the gap height between two membrane samples is set as 100 (± 10) µm. 550 mL of 1 mM KCl solution was used as an electrolyte and pre-adjust its pH value to around 3. The measurement always starts from pH = 3 to pH = 11. The set rinsing time is 300 s in each step, ensuring the accurate and stable pH value at the membrane surface and the target operation pressure is 300 mbar. Each data point contains four replicates and the comprehensive data were automatically proceeded by the software according to Helmholtz-Smoluchowski equation:

$$\zeta = \frac{dl}{dp} \cdot \frac{\eta}{\varepsilon_r \cdot \varepsilon_0} \cdot \frac{L}{A} \qquad (3.2)$$

Where ζ stands for zeta potential of measuring surface; dl is streaming current; dp is the applied pressure difference; $\eta$is the electrolyte viscosity; ε_r and ε_0 stand for the permittivity of electrolyte solution and free space, respectively;L is the length of the streaming channel;A is the cross-section of the streaming channel.

3.6.3 Characterization of membrane filtration performance

3.6.3.1 Flux measurement

The membrane compaction is done prior to measuring the flux. For the UF membrane, the compaction was performed at the pressure that double the testing pressure, e.g., compact the membrane at 2.0 bar when the test pressure of 1.0 bar for flux measurement. While for MF membrane, the pressure for compaction is triple the test pressure. In both cases, the compaction will be carried out for 30 min. The flux measurements were done by measuring three parallel membrane samples.

3.6.3.2 Membrane resistance

The flux will keep decreasing during the infiltration modification, and the flux decline can be interpreted as increasing of filtration resistance or membrane resistance:

$$J = \frac{\Delta P}{\eta * R} \tag{3.3}$$

Where J is the flux during the PEI modification, where EtOH was used as the solvent; ΔP is the trans-membrane pressure during the PEI modification; η is the dynamic viscosity of the solvent. In the infiltration modification, the total membrane resistance contains a fixed resistance coming from the intrinsic membrane resistance, and a dynamic resistance varies along with the infiltration process:

$$R_{total} = R_m + R_i \tag{3.4}$$

Where R is the membrane resistance and the R with the subscript of total and m correspond to total resistance and the resistance of pristine PES50, respectively; R_i refers to the resistance due to the modification, including hydrogel resistance and concentration polarization. The R_{total} is defined as the resistance at the cessation of the infiltration modification. Furthermore, an index a was introduced to describe the extent of flux decline:

$$a = \frac{R_i}{R_m} = \frac{R_{total} - R_m}{R_m} \quad (3.5)$$

A lower a value indicates a lower flux decline during the infiltration medication. Thus a value would give a clear indication for parameter optimization in the infiltration step, i.e., the modification with a low a value is preferable.

3.6.3.3 Use of fouling models for analysis of the infiltration process

In the section 3.3.1.1 and 3.3.1.2, the polymer PEI and PEI-OH were infiltrated into the support layer of PES50 membrane, and the size of both PEI and PEI-OH is ten times higher than the MWCO of PES50 leading to full rejection. However, the rejected PEI and PEI-OH still possible to penetrate into the pores of the selective layer leading to pore blocking, i.e., dramatic flux decline. This infiltration modification can be seen as a fouling process, and its mechanism can be reflected by the certain flux variation along with the infiltration time. Studying this infiltration process based on different fouling models could give a preliminary vision of the PEI and PEI-OH location during the infiltration modification. Typically, four kinds of fouling models are proposed widely in the membrane field: internal pore blocking, complete pore blocking, cake filtration, and partial pore blocking [109-112]. The flux variation along with infiltration time can be plotted and calculated according to the Hermia equation:

$$\frac{\mathrm{d}J}{\mathrm{d}t} = -k(J)^{3-\mathrm{n}} \quad (3.6)$$

Where t is the filtration time; V is the permeate volume; J is the flux; n refers to an index characterizing fouling mechanism. The n value can represent the dominating fouling mechanism: 1) n = 2 presents complete pore blocking mechanism; 2) n = 1.5 presents internal pore blocking mechanism; 3) n = 1 presents partial pore blocking mechanism; 4) n = 0 presents cake filtration mechanism. However, in the practical situation, different mechanisms will take place simultaneously; hence, in most of cases, the n value would locate in between two adjacent values. Towards the data analysis, plot the log(dJ/dt) against log(J) according to the recorded flux data during the infiltration modification where

the slop is 3-n; furthermore, the value of n can be finally determined.

3.6.3.4. Molecular weight cut-off (MWCO) determination

MWCO describes the sieving property of the membrane. A mixture of dextran solution was used to measure the MWCO of the pristine and modified membrane. For the dextran filtration, a dextran mixture contains five different molecular weight of dextran (15, 35, 40, 70, and 100 kDa) were used, and the total dextran concentration was 1 g/L. During the dextran mixture filtration, the flux should be as low as possible to minimize the effect of concentration polarization; hence, an operation pressure of around 0.02 bar was used. Based on the GPC result of the dextran distribution in permeate, a rejection curve can be obtained by deducting the background, which is the dextran distribution in the feed solution, and the MWCO is defined at the 90% of retention for the selected dextran mixture.

3.6.4 Characterization of membrane adsorption performance

3.6.4.1 Boron determination

Curcumin has a specific binding with boric acid in EtOH and showing adsorption at the wavelength of 540 nm, giving a good R^2 (cf. Fig. 3.15). First, the curcumin stock solution is prepared: dissolve curcumin (0.2 g) and oxalic acid dihydrate (34.9 g) in 200 mL of absolute EtOH, then 37% HCl (21 mL) was added and finally filled EtOH up to 500 mL. This stock curcumin solution should be stored at ~ 5°C.

For boron determination, the 40 µL of boron solution sample (< 5 mg/L) was added into the ceramic evaporating dish, then 2 mL of prepared curcumin solution was added, and then evaporate the mixture at 55 °C for 50 min. The final rose-red crystal of boron-curcumin complex was dissolved by 10 mL of absolute EtOH, showing color development depending on boron concentration. The absorbance of this complex can be measured via Uv-Vis at the wavelength of 540 nm. The actual boron concentration can be figured out by using the pre-done calibration curve.

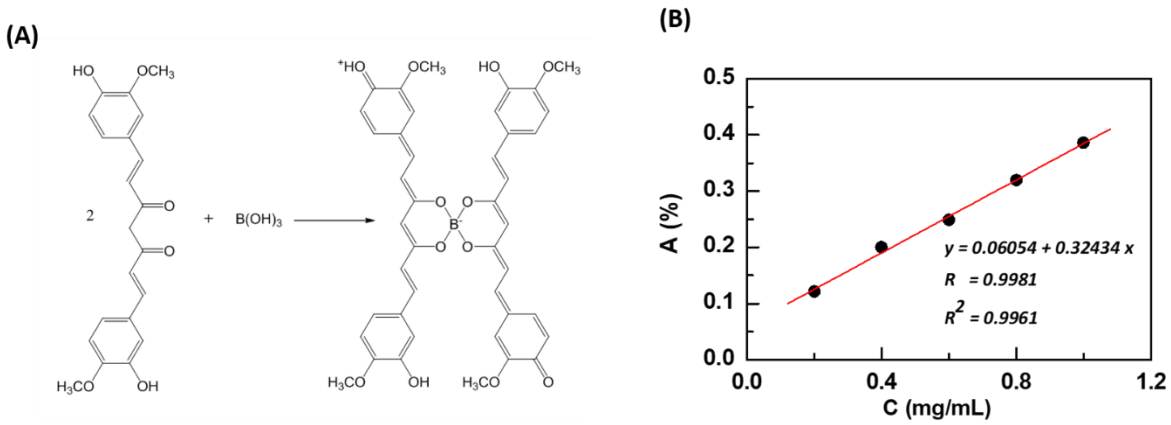

Fig. 3.15 (A) Complexation between boron and curcumin; (B) calibration curve of boron determination via curcumin method.

3.6.4.2 Boron adsorption isotherm

The information regarding the equilibrium in an adsorbate/adsorbent system is necessary that provides the basis for assessing the adsorption process. Two-parameter adsorption models, Langmuir (eq. 3.6) and Freundlich (eq. 3.7) were used to investigate the boron adsorption isotherm of the modified membrane.

$$q = -\frac{q_m * b * c}{1 + b * c} \tag{3.7}$$

In the Langmuir Model, q stands for adsorption capacity; q_m stands for maximum adsorption capacity; c describes equilibrium concentration of adsorbate in solution; b is the Langmuir adsorption constant. The Langmuir model can perfectly describe a homogeneous reversible adsorption process in which each adsorption process in between adsorbate and binding sites has equal sorption energy. Thus, in the Langmuir isotherm curve, saturated adsorption can be achieved when all the binding sites have been occupied at high concentration range.

$$q = K * C^{n} \tag{3.8}$$

In the Freundlich Model, q stands for adsorption capacity; K is the adsorption coefficient describing the strength of adsorption; n is an isotherm parameter related to energetic

heterogeneity of the adsorbent surface; c_e refers to the equilibrium concentration of adsorbate in solution. Freundlich Model can describe heterogeneous adsorption process, i.e., multilayer adsorption.

Towards the boron isotherm of the modified membrane, the pristine and modified membranes with an effective modified area of 3.46 cm^2 were immersed into 4 mL of boron solution with various initial boron concentrations. Place the adsorption containers onto the shaker for 18 h at room temperature (~20 °C). The equilibrium adsorption of the modified membrane, q_e, at the corresponding equilibrium bulk boron concentration, C_e, can be determined by measuring boron concentration via the curcumin method. After receiving the specific q_e date at the corresponding C_e, the model fitting can be done via Origin 8.1. Finally, the fitting result of each isotherm parameter and R^2 can be adapted to evaluate the boron binding capacity and mechanism.

3.6.4.3 Boron adsorption kinetics

The adsorption process can be classified into four steps: 1) transport of adsorbate from bulk to the hydrodynamic boundary layer (bulk connection); 2) transport from the boundary layer to the adsorbent surface via diffusion (film diffusion); 3) transport into interior of adsorbent via diffusion, while it has limited influence on membrane adsorber (intra-particle diffusion); 4) energetic interaction between adsorbent and adsorbate. The adsorption process takes time to reach equilibrium conditions because of these four mass transfer processes. And the adsorption kinetic study is necessary to understand the limiting step in mass transfer and evaluate the characteristic mass transfer parameter. Three kinetic models have been introduced to understand the mass transfer mechanism in both pristine and modified membranes.

Pseudo-first-order model:

$$\frac{dq_t}{dt} = k_1 \cdot (q_e - q_t) \qquad (3.9)$$

Where k_1 is the pseudo-first-order rate coefficient (min^{-1}), which represents how fast to reach the equilibrium condition; q_e and q_t are the values of the amount of adsorbed

mass at equilibrium and the specific time t, respectively. The pseudo-first-order model assumes that the rate-controlling step during the adsorption process is film diffusion.

Pseudo-second-order model:

$$\frac{dq_t}{dt} = k_2 \cdot (q_e - q_t)^2 \qquad (3.10)$$

Where k_1 is the pseudo-first-order rate coefficient ($cm^2 \cdot mg^{-1} \cdot min^{-1}$ or $g \cdot min^{-1}$); q_e and q_t are the values of the amount of adsorbed mass at equilibrium and the specific time t, respectively. The pseudo-second-order model assumes that the rate-controlling step is the interaction between adsorbent and adsorbate.

Intra-particle diffusion model:

$$q_t = k_i \cdot t^{0.5} + C \qquad (3.11)$$

Where k_i is the Intra-particle rate; q_t is the value of the amount of the adsorbed mass at the specific time t; C is a constant. The intra-particle diffusion model assumes that the rate controlling step is the intra-particle diffusion.

To measure the boron kinetics of the modified membrane, the pristine and modified membranes with an effective modified area of 3.46 cm^2 were immersed into 4 mL of boron solution with an initial boron concentration of 5 mg/L. The adsorption containers have been placed onto the shaker at room temperature (~20 °C). At each time interval, 0.1 mL of boron solution was taken for boron determination via the curcumin method. Finally fits the data with three kinetic models via Origin 8.1, thus giving the fitting result of each kinetic parameter and R^2.

3.6.4.4 Flow through adsorption

The adsorption performance of the membrane adsorber in the flow-through process is studied by breakthrough curve, which is the time-resolved effluent concentration at the outlet. The flow-through adsorption experiments were carried out in a dead-end mode. For the single-pass flow-through adsorption experiment, a modified membrane was assembled

in a reusable syringe filter where the effective filtration area is 3.46 cm^2; for the dual-pass flow-through adsorption experiment, two built syringe filters were connected in series. In the flow-through adsorption experiments, either single-pass or dual-pass apparatus, 30 mL of 5 mg/L of boron solution was filtrated under the given flow rate or pressure. The permeate was collected and boron concentration of each permeate sample were measured via the curcumin method. Finally, a breakthrough behaviour can be found when plotting the outlet boron concentration against filtration time or filtration volume.

3.6.4.5 Membrane regeneration

The regenerability of modified membranes is an essential factor in evaluating the adsorbent in terms of the economic point of view. According to the boron adsorption mechanism, a solution with high proton concentration can be used for boron desorption, i.e., for absorbent regeneration. In the static regeneration process, the modified membranes with an effective modified area of 3.46 cm^2 were immersed into 4 mL of 1 N or 0.1 N HCl for 24 hours, and then the membranes were washed sequentially by Milli-Q water, a basic solution (pH=9), and Milli-Q water. In the regeneration procedures, the saturated membranes were regenerated by filtrating 1 N or 0.1 N HCl at the same operation pressure or flow rate upon the flow-through adsorption process. Afterward, wash the membrane sequentially with Milli-Q water, basic solution (pH=9), and Milli-Q water. Finally, the regenerated membranes were ready for the next adsorption cycle.

3.7 The calculation related to mass transfer in the membrane adsorption process

3.7.1 Reynolds number

$$Re = \frac{d \cdot v_s \cdot \rho_f}{\mu} \tag{3.12}$$

The Reynolds number (*Re*) can be used to predict the flow conditions in the different fluid flow situations. Here, the *Re* number was used to predict the flow condition in the membrane pores. Where d refers to the pore diameter (m); v_s refers to linear fluid velocity (m/s); ρ_f refers to fluid density (kg/m^3); μ refers to fluid viscosity (kg/(m·s));

3.7.2 Peclet number

$$Pe = \frac{\text{advective transport rate}}{\text{diffusive transport rate}} = \frac{l * v}{D} = \frac{\tau * d * v}{D} \tag{3.13}$$

The Peclect number (*Pe*) is defined as the ratio of the advective transport process and the diffusive transport process. Where l refers to the length of transport path along with flow direction; v refers to the flow velocity; D refers to the diffusion coefficient of boron. To better represent the ratio of boron mass transfer condition in the membrane pores, the l can be interpreted as $\tau * d$, where τ refers to tortuosity of membrane and d refers to the thickness of the membrane.

3.7.3 Fourier number

$$F_0 = \frac{(\text{length})^2}{(\text{diffusion coefficient}) * (\text{time})} = \frac{l^2}{D * t} = \frac{(\tau * d)^2}{D * t} \qquad (3.14)$$

The Fourier number (F_0) can be used to solve the time-dependent mass diffusion problem. When set the F_0 as 1, this equation can be used to estimated how long or how far the mass transfer has occurred. Where l refers to the length of transport path; D refers to the diffusion coefficient of boron; t refers to the required time that mass transfer occurred. The l can be interpreted as $\tau * d$, where τ refers to the tortuosity of membrane and d refers to the membrane's thickness.

3.7.4 Knudsen number

$$K_{\mathrm{n}} = \frac{l_{free}}{d} \qquad (3.15)$$

Knudsen number (K_{n}) is defined as the ratio of the molecular mean free path (l_{free}) to the length scale, which can be the membrane pore size (d). When K_{n} < 0.01, the molecular transport through the membrane pore via convective flow; when 0.01 < K_{n} < 0.1, the molecular transport through the membrane pore via Knudsen diffusion; when 0.1 < K_{n} < 10, the molecular transport through the membrane via surface diffusion; when K_{n} > 10, the molecular transport through the membrane pore via Knudsen solution-diffusion mechanism.

3.8 Cost estimation for boron removal

To better understand the usability of the modified membrane in the practical scenario, the boron removal cost has been calculated. In the foregoing discussion (cf. Table 2.5), the total boron removal cost comprises implementation cost, material cost, energy consumption, reagents cost, maintenance, etc. For the modified membrane, the cost of modification should be taken into consideration additionally. The cost estimation in this work is interpretated by: 1) the cost of modification per treated 1 m^3 of seawater; 2) the reagent cost for regeneration to treat 1 m^3 of seawater.

3.8.1 The modification cost per treating 1 m^3 seawater

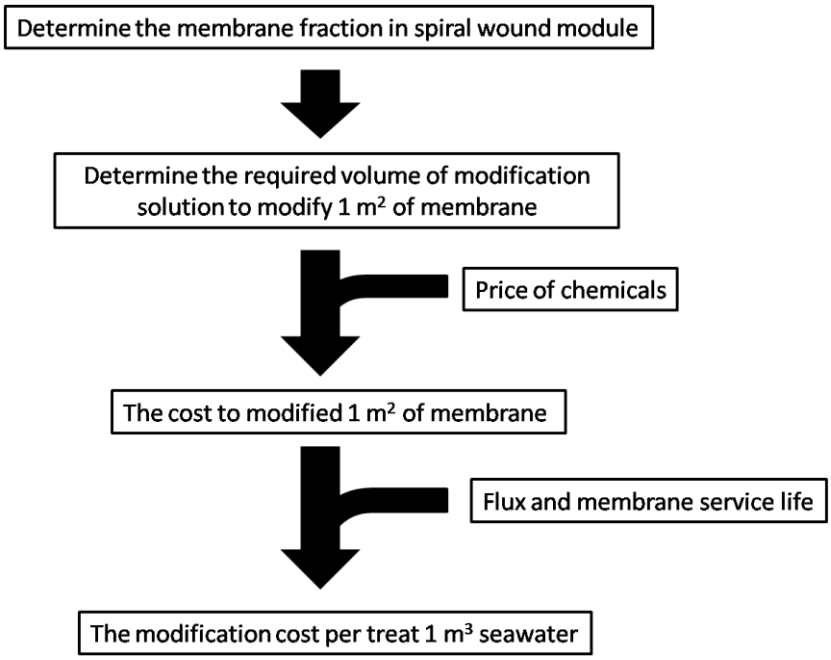

Fig. 3.16 The flow chart of modification cost calculation.

The calculation of modification cost follows with the procedures shown in Fig. 3.16, and the details can be found in Appendix B, Section B1. Specifically, the membrane fraction in the spiral wound module should be first determined where the spacer's thickness should be considered (cf. Section B 1.1). Secondly, the required volume of modification solution to modified 1 m^2 of the membrane can be known (cf. Section B1.2). Afterward, inputting the chemical price and required chemical concentration for modification, the modification cost per m^2 of the membrane can be calculated (cf. Section B1.3). Additionally, the modification cost can be represented by modification cost per volume of treated water. For this, the data of operation flux and membrane service life is introduced and the modification cost per MGD and the modification cost per treat 1 m^3 of seawater can be calculated (cf. Section B1.4).

3.8.2 The regent cost per treating 1 m^3 seawater

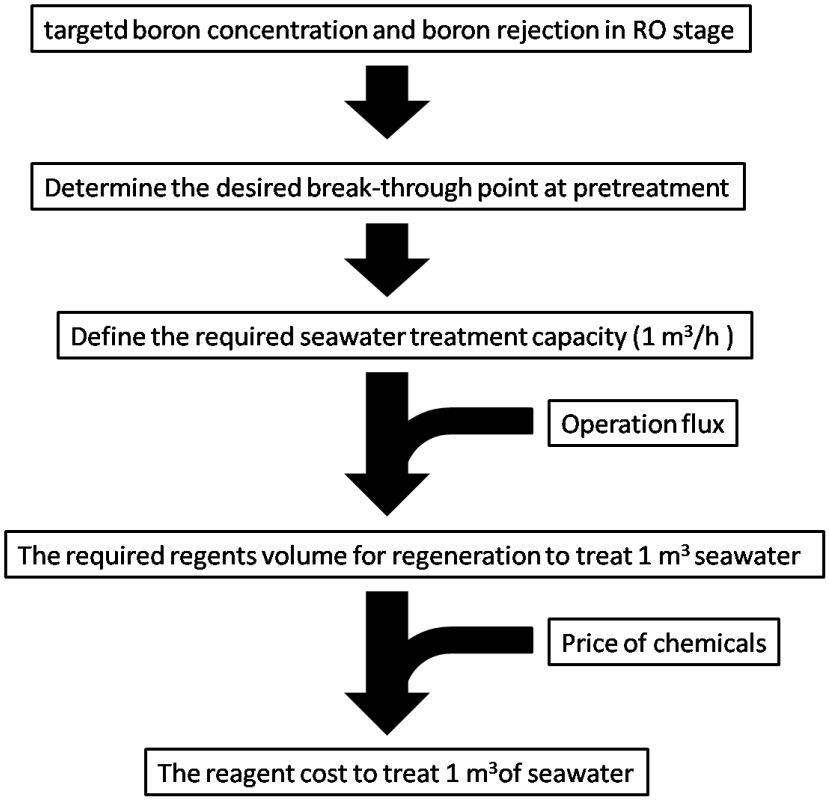

Fig. 3.17 The flow chart of reagent cost calculation.

The calculation of reagent cost is based on the procedures as shown in Fig. 3.17, and the details can be found in Appendix B, Section B2. Specifically, the target boron concentration and the boron rejection in the RO stage should be first defined. Secondly, the desired break-through point can be determined (cf. Section B2.1). Afterward, a capacity of 1 m^3/h for seawater treatment is set, and the required regent volume for regeneration can be calculated under the specific operation flux (cf. Section B2.2). Finally, when inputting the chemical price and reagent concentration for regeneration, the reagent cost to treat 1 m^3 of seawater can be known.

4. Results and discussion

4.1 Modification of the UF membrane via infiltration and cross-linking of PEI/5-Acl or PEI-OH/5-Acl

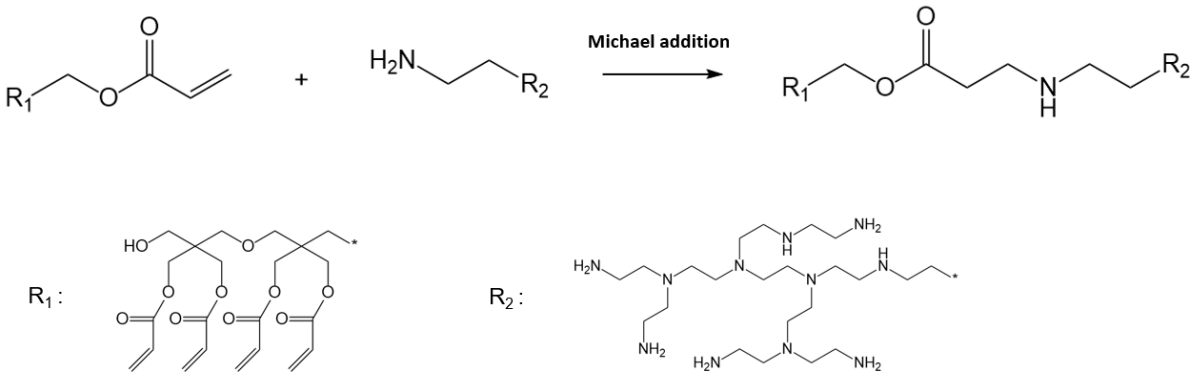

Fig. 4.1 The reaction between primary amine groups in PEI and acrylate groups in the cross-linker 5-Acl.

An infiltration process was applied to modify the support layer of flat sheet UF membrane. The filtration orientation was switched, making sure the support layer faces a feed solution that the chemicals can be infiltration to the support layer. The modification solution contains cross-linker (5-Acl) and PEI, where the 5-Acl can cross-link the primary amine groups in PEI-OH or PEI via Michael addition in EtOH, and the cross-linked PEI-OH or PEI coating can be formed (cf. Fig. 4.1). During the infiltration process, PEI-OH or PEI should be retented by UF membrane; therefore, PES50 is selected as the pristine membrane where the Mw of PEI-OH or PEI is ten times larger than the MWCO of PES50 of 50 kDa ensure a full retention of PEI-OH or PEI in the support layer.

In this section, prior to membrane modification, the solubility of PEI-OH and PEI will be first investigated. Afterward, the gelation point of PEI-OH/5-Acl and PEI/5-Acl will be investigated to define the appropriate substance concentration for infiltration cum cross-linking modification (Section 4.1.1). The membrane modification via the infiltration of PEI/5-Acl and PEI-OH/5-Acl will be discussed regarding coating formation mechanism. After comparing the flux decline and boron adsorption capacity of the respective bulk hydrogel, PEI/5-Acl was selected for membrane modification (Section 4.1.2). The hydroxyl post-modification was performed to functionalize active PEI coating, and several

characterizations have been done (Section 4.1.3). The filtration performance and boron removal performance of modified membrane have been evaluated via various criterions, giving a concrete overview of this modification approach (Section 4.1.4). Finally, the optimal modification parameter in flat sheet membrane modification has been transferred to the Multibore® module (Section 4.1.5).

4.1.1 Hydroxyl functionalization of PEI

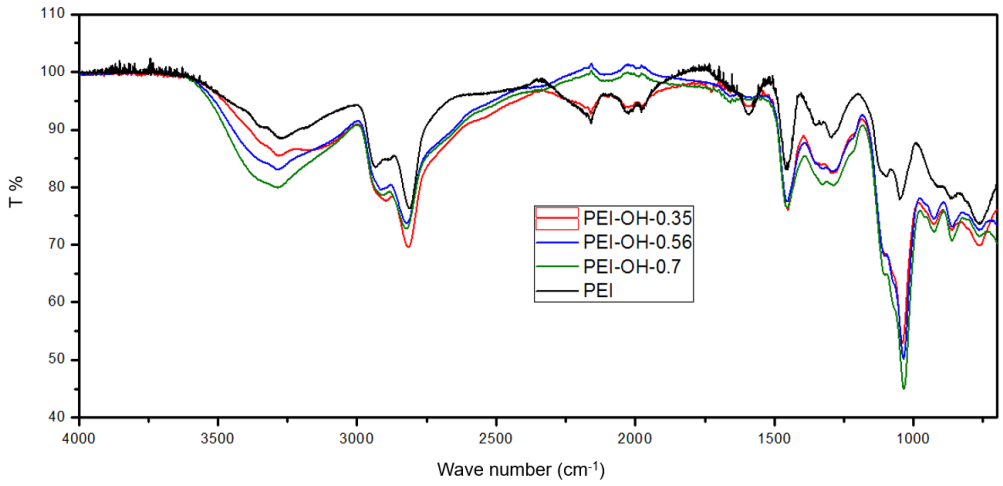

Fig. 4.2 The ATR-FTIR spectrum of the membrane premodified by infiltration and cross-linking of PEI-OH-0.35/5-Acl (red curve), PEI-OH-0.56/5-Acl (blue curve), PEI-OH-0.7/5-Acl (green curve), and pure PEI (black curve).

PEI-OH with three kinds of hydroxyl functionalization degrees, PEI-OH-0.35, PEI-OH-0.56, and PEI-OH-0.7, have been synthesized (cf. Fig. 3.6). The molar ratio of the nitrogen in PEI to glycidol in three synthesized EPI is 1:0.35, 1:0.56, and 1:0.7, respectively. The higher molar ratio of nitrogen to glycidol indicates a higher hydroxyl functionalization degree. The ATR-FTIR spectrum in Fig. 4.2 shows that both three PEI-OH products present absorption at the range from 3100 cm^{-1} to 3500 $cm^{-1,}$ which corresponds to N-H and O-H vibration, respectively [119]. Along with the higher hydroxyl functionalization degree, the intensity of N-H and O-H vibration increase.

The Michael addition between primary amine and acrylate (5-Acl) presents high conversion in EtOH [113,114]. Besides, the pristine membrane, PES-50, is tolerant with EtOH. Hence the EtOH can be used as the media for membrane modification. Towards the solubility of

different PEI-OH products in EtOH, a lower solubility can be found in the PEI-OH with a higher hydroxyl function degree (Table 4.1). Considering the above perspectives, PEI-OH-0.35 is thought to be a suitable substance for infiltration modification among these three kinds of PEI-OH products. Additionally, the PEI-OH-0.35 has a higher fraction of primary amine groups providing more cross-linking sites for the higher cross-linking degree.

Table 4.1 The solubility of PEI, PEI-OH-0.35, PEI-OH-0.56, PEI-OH-0.7 in different solvents.

Solvent	**PEI**	**PEI-OH-0.35**	**PEI-OH-0.56**	**PEI-OH-0.7**
Water	Yes	Yes	Yes	Yes
DMSO	Yes	Yes	Yes	Yes
EtOH	Yes	Yes	No	No
Isopropanol	Yes	No	No	No

The gelation point of the PEI-OH-0.35/5-Acl system is an important parameter that can give useful information that refers to the boundary condition of gelation. Since the cross-linking between primary amines in PEI-OH and 5-Acl occurs simultaneously within the infiltration process, the undesired gelation should be avoided in the bulk modification solution. Thus the PEI-OH and 5-Acl concentration in the bulk modification solution should be kept below the gelation point. During the infiltration of PEI-OH-0.35/5-Acl solution, the PEI-OH-0.35 accumulates in the support layer due to the rejection of PEI-OH-0.35 by the PES-50 membrane. The PEI-OH-0.35 concentration would surpass the overlapping concentration, forming a cross-linked network inside the support layer. Table 4.2 shows the gelation points of the PEI-OH-0.35/5-Acl system when altering the PEI-OH-0.35 and 5-Acl concentrations. The PEI-OH-0.35/5-Acl can form a cross-linked network within a board concentration range. Besides, a faster gelation time can be achieved by either increasing PEI-OH-0.35 concentration or 5-Acl concentration.

Table 4.2 Gelation test of PEI-OH-0.35/5-Acl solutions.

Probe	$C_{PEI\text{-}OH\text{-}0.35}$ (g/L)	$C_{5\text{-}Acl}$ * (wt%)	Gelation points (s)
1	200	12.5	Before measurement (< 1 min)
2	200	5	Before measurement (< 1 min)
3	200	2	20 - 30
4	200	1	140 - 150
5	150	12.5	Before measurement (< 1 min)
6	150	5	Before measurement (< 1 min)
7	150	2	160 -170
8	150	1	No gelation
9	100	25	Before measurement (< 1 min)
10	100	12.5	90 - 100
11	100	5	280 - 290
12	100	2	No gelation

*: it's a relative concentration (wt %) to the mass of PEI-OH-0.35

Table 4.3 gives the information about the gelation points of PEI/5-Acl at different concentration windows. Because of the higher fraction of primary amine in the PEI, which provides more available cross-linking sites, PEI shows higher gelation ability than PEI-OH-0.35. In the selected PEI and 5-Acl concentration window, the PEI either forms cross-linked gel immediately or no gelation at all. This phenomenon probably arises from the higher reactivity between PEI and 5-Acl. The idea polymer (PEI and PEI-OH-0.35) and cross-linker (5-Acl) concentration for such infiltration modification should prevent bulk gelation during the modification. Therefore, a low polymer (PEI and PEI-OH-0.35) concentration of 0.3 g/L and cross-linker (5-Acl) concentration of 2, 5, 10, and 25 wt% are chosen in the infiltration modification to prevent bulk gelation. And the infiltration time runs from 50 min to 250 min depends on the specific filtration conditions.

Table 4.3 Gelation test of PEI/5-Acl solutions.

Probe	C_{PEI} (g/L)	$C_{5\text{-Acl}}$ * (wt%)	Gelation points (s)
1	200	25	Before measurement (< 1 min)
2	200	12.5	Before measurement (< 1 min)
3	200	5	Before measurement (< 1 min)
4	200	2	Before measurement (< 1 min)
5	200	1	Before measurement (< 1 min)
6	150	25	Before measurement (< 1 min)
7	150	12.5	Before measurement (< 1 min)
8	150	5	Before measurement (< 1 min)
9	150	2	Before measurement (< 1 min)
10	150	1	No gelation
11	100	25	Before measurement (< 1 min)
12	100	12.5	Before measurement (< 1 min)
13	100	5	Before measurement (< 1 min)
14	100	2	No gelation
15	100	1	No gelation

*: it's a relative concentration (wt %) to the mass of PEI

4.1.2 Modification of PES-50 by infiltration and cross-linking of PEI-OH/5-Acl or PEI /5-Acl

In this section, a further optimization has been done, and the modified membrane is evaluated by two criterions: 1) the flux decline after the modification, which can be reflected by a value (cf. section 3.6.3.2); 2) and the boron adsorption capacity of bulk hydrogel prepared from PEI/5-Acl and PEI-OH-0.35/5-Acl.

Table 4.4 The calculated a value for the respective infiltration condition.

P / $C_{Cross-linker}$	0.5 bar		1.0 bar		1.5 bar	
	PEI	PEI-OH	PEI	PEI-OH	PEI	PEI-OH
25 wt%	32.8	76.6	38.7	56.3	38.9	75.0
10 wt%	30.5	37.4	34.5	55.0	37.3	96.4
5 wt%	19.3	\	35.8	\	29.8	\
2 wt%	28.0	38.6	17.1	20.9	33.4	54.4

According to the gelation point result, the modification solution condition has been preliminary determined: 1) PEI or PEI-OH-0.35 concentration of 0.3 g/L; 2) cross-linker concentration of 2, 5, 10, and 25 wt%. And infiltration modifications were carried out under three operation pressure, 0.5, 1.0, and 1.5 bar. The a value of each modification is shown in Table 4.4, where the a value describes the ratio between the resistance coming from the modification and the pristine membrane resistance (see 3.6.3.2). Obviously, the membrane modified by PEI-OH/5-Acl has a higher a value indicating that the membrane modified by PEI-OH-0.35/5-Acl will create more resistance (R_i) leads to dramatic flux decline. This resistance (R_i) comes from two parts: 1) an additional layer of PEI-OH gel; 2) and the resistance due to the concentration polarization of PEI-OH and 5-Acl during the infiltration process. With respect to flux decline, the modification via infiltration of PEI/5-Acl is superior to infiltration of PEI-OH-0.35/5-Acl.

Table 4.5 The boron uptake of different PEI/5-Acl and PEI-OH/5-Acl bulk hydrogels ($C_{0\text{-}boron}$ = 5 mg/L, t = 48 hours).

Polymer	$C_{5\text{-}Acl}$ (wt%)	Remaining C_{Boron} (mg/L)	Boron removal rate (%)
PEI *	**25**	0.076 ± 0.002	98.5
PEI *	**10**	0.334 ± 0.007	93.3
PEI *	**2**	-	-
PEI-OH	**25**	1.532 ± 0.013	69.4
PEI-OH	**10**	0.806 ± 0.033	83.9
PEI-OH	**2**	1.211 ± 0.028	75.8

*: the bulk PEI/5-Acl gel needs to be post-functionalized by glycidol.

The boron binding capacity of the modified affinity coating is another crucial criterion to evaluate the modified membrane. Hereof, the boron binding performance of bulk hydrogel out of different hydrogel compositions has been studied to figure out the potential modification parameter (cf. Section 3.4.4). As shown in Table 4.5, after 48 hours of adsorption, the hydrogel prepared byPEI/5-Acl remains less boron in the bulk solution, i.e., more boron has been bond. A simple explanation can be made: the PEI/5-Acl hydrogel carries more binding sites after completely hydroxyl functionalization, while only 35% molar fraction of primary amide groups converts to boron binding sites in PEI-OH-0.35/5-Acl gel.

Based on the membrane resistance study and boron adsorption test on various bulk hydrogels, modifying the membrane via infiltration of PEI/5-Acl is thought to be prominently superior compared to PEI-OH/5-Acl infiltration.

4.1.3 Characterization of the membranes modified via two steps: first infiltration and cross-linking of PEI /5-Acl and subsequently post-hydroxyl functionalization

Since PEI/5-Acl infiltration has been used to prepare cross-linked coating in the support layer of commercial UF membrane, PES50, this coating location needs to be further studied. PEI with a Mw of 750 kDa can be rejected by the chosen UF membrane (PES50, 50 kDa)

during the infiltration process. The rejected PEI will be cross-linked by 5-Acl in the membrane support layer forming a cross-linked coating, and this retentive PEI coating can be treated as a type of 'fouling'. Thus it's possible to explain the PEI coating location and coating forming mechanism by means of applying fouling models. Four kinds of coating formation are proposed: 1) the PEI gel would penetrate to the pores of the selective layer, result in internal pore blocking; 2) PEI gel will completely block the pores; 3) PEI gel would cover the pores forming a cake layer; 4) PEI gel will partially cover the pores leading to partial pore blocking. The above four different scenarios can be reflected by certain flux variations along with infiltration time.

Table 4.6 The R^2 of linear fitting for the fouling model (cf. eq. 3.6) and the corresponding n value for the membranes modified by PEI/5-Acl.

P / **$C_{Cross\text{-}linker}$**	**0.5 bar**		**1.0 bar**		**1.5 bar**	
	R^2	n	R^2	n	R2	n
25 wt%	0.987	0.33	0.982	0.50	0.999	0.50
10 wt%	0.980	0.20	0.934	0.33	0.983	0.08
5 wt%	0.993	0	0.994	0.37	0.996	0.25
2 wt%	0.987	0.02	0.986	0.29	0.998	0.18

During the infiltration process, the flux variation has been monitored and recorded. When log(dJ/dt) was ploted against log(J) (see Appendix A7-A9), a slope of 3-n can be obtained by performing linear fitting. Finally, the PEI gel location and forming mechanism can be interpreted by n value (see section 3.6.3.3). As shown in Table 4.6, all of the infiltration experiments performed under three different operation pressures showing *n*-value within the range between 0 and 1.0, which indicates that PEI and 5-Acl infiltration will lead to partial pore blocking and forming a layer cover the pores simultaneously. And the layer coverage plays the predominant effect during the infiltration because the *n*-value is close to zero. And the SEM image of the modified membrane also supports this statement.

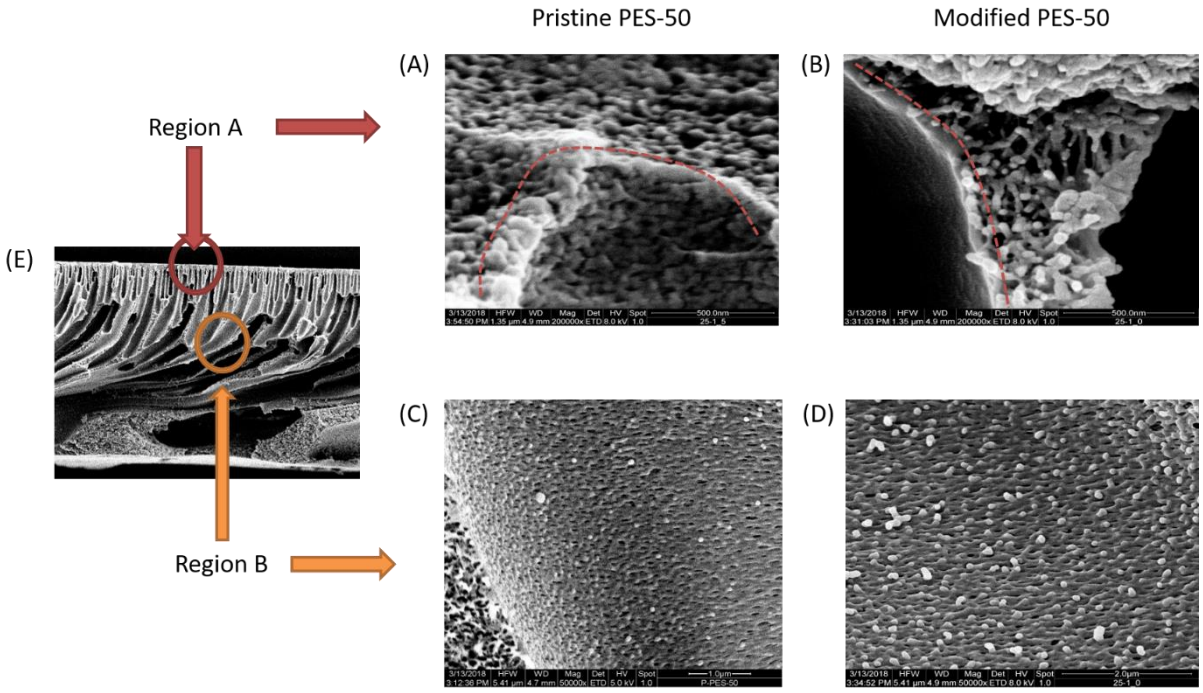

Fig. 4.3 SEM images of pristine PES-50 (A, C, and E) and PEI/5-Acl modified membrane (B and D).

Fig. 4.3 shows the SEM images of the membrane modified via infiltration of PEI/5-Acl with a degree of grafting of 25 wt%. In the cross-section SEM images, a thin coating layer can be found at the upper part of modified membranes (Region A), indicating the success of infiltration modification. This coating layer covers the pores and forming a cake layer during infiltration of PEI/5-Acl, which is in good agreement with the n value in Table 4.6. While in the middle of the support layer (Fig. 4.3, Region B), no noticeable coating can be observed. This indicates that the PEI coating only forms at the upper part of the support layer.

The same conclusion can be made when checking the ATR-FTIR spectrum of the final modified membrane (cf. Fig. 4.4). It should be noticed that the sample named PEI-25 wt%-1.5P has been treated with glycidol, i.e., the PEI coating has been post-functionalized by hydroxyl groups. When measure the IR absorption by placing the membrane upside down (PEI-25 wt%-1.5P-nor), i.e., contact the selective layer with ATR unit (diamond/ZnSe crystal), two clear board absorption can be found at around 3400 $cm^{-1}$and 2800 cm^{-1}, which is corresponding to -O-H and the -C-H vibration (polymer backbone), respectively. And the IR spectrum of bulk hydrogel shows the same characteristic peak of -O-H and the -C-H vibration as PEI-25 wt%-1.5P-nor. Interestingly, when flipping over the measuring

orientation (PEI-25 wt%-1.5P-op), i.e., support layer contact with ATR unit, no observation at the 3400 $cm^{-1}$and 2800 cm^{-1}. Both SEM images and IR spectrum come to the same conclusion of inhomogeneous modification in which the modified coating accumulates at the upper part of the membrane. Nevertheless, the modification has been done successfully, and the coating sticks tightly in the support layer.

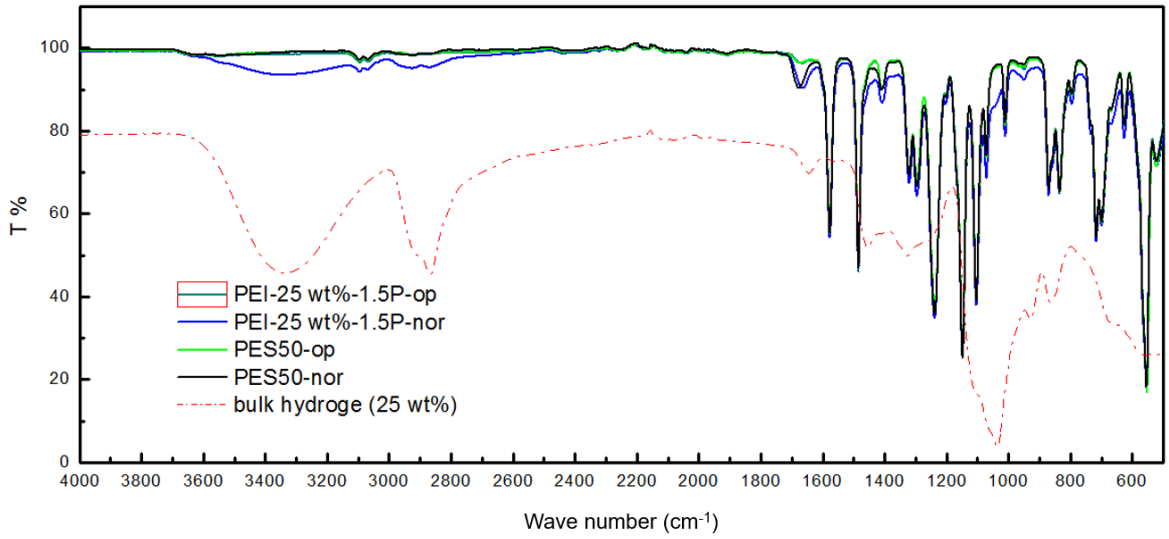

Fig. 4.4 ATR-FTIR spectra of selective layer (PES50-nor) and bottom (PES50-nor) of the pristine membrane, the selective layer (PEI-25 wt%-1.5P-nor) and bottom (PEI-25 wt%-1.5P-op) of the membrane premodified via the condition of PEI-25 wt%-1.5P, and PEI bulk hydrogel.

4.1.4 Membrane performance

The membrane can be successfully modified via infiltration and cross-linking of PEI/5-Acl and later post-functionalizing by glycidol. Based on the previous discussion, three kinds of modified membranes were selected to characterize filtration and adsorption performance (cf. Table 4.7).

Table 4.7 The optimal modification conditions.

Name	$C_{5\text{-Acl}}$ (wt%)	Operation pressure (bar)
PEI-10	10	1.5 bar
PEI-5	5	1.5 bar
PEI-2	2	1.5 bar

4.1.4.1 Filtration and sieving performance

The pure water permeability and MWCO of the pristine membrane (PES50) and three modified membranes can be found in Table 4.8. After the modification, it has a 76 - 82 % flux decline depending on the modification parameters. Based on the discussion in Section 4.1.3, such flux declined is due to the coverage of PEI gel during the infiltration modification of PEI/5-Acl, and this PEI gel coverage causes additional filtration resistance. On the other hand, the part of PEI gel or PEI chains can plug in the selective layer's pores during the infiltration process, resulting in partial pore blocking. The partial pore blocking can also be reflected by characterizing the sieving performance of the modified membrane. The MWCO of pristine and modified membrane can be found in Table 4.8, where the MWCO of PES-50 is 70 kDa. Interestingly, the three selected modified membranes all present similar MWCO of around 17 kDa, 16.2 kDa, and 16.3 kDa, indicating that the pore size decreases after modification. And the pore size diminution is independent of cross-linking degree. The similar MWCO of these three modified membranes can be interpreted by the partial pore blocking of PEI gel or PEI chain plug-in effect. This statement is in good agreement with the fouling model study (cf. Section 4.1.3, Table 4.6), in which all the PEI/5-Aclgel formation during the infiltration process presents a combined mechanism of partial pore blocking and pores coverage.

Table 4.8 The MWCO and permeability of the pristine membrane and three selected modified membrane.

Name	Permeability (LMH bar)	MWCO (kDa)
PES50	210 ± 28	70
PEI-10	38	17
PEI-5	44	16.2
PEI-2	50	16.3

4.1.4.2 Boron adsorption isotherm

Based on the previous discussions, three modifications have been selected for further characterization on boron removal performance. Adsorption isotherm can provide useful information regarding binding capacity as well as the binding mechanism. Fig 4.5 gives information about the adsorption isotherm curve of three modified membranes.

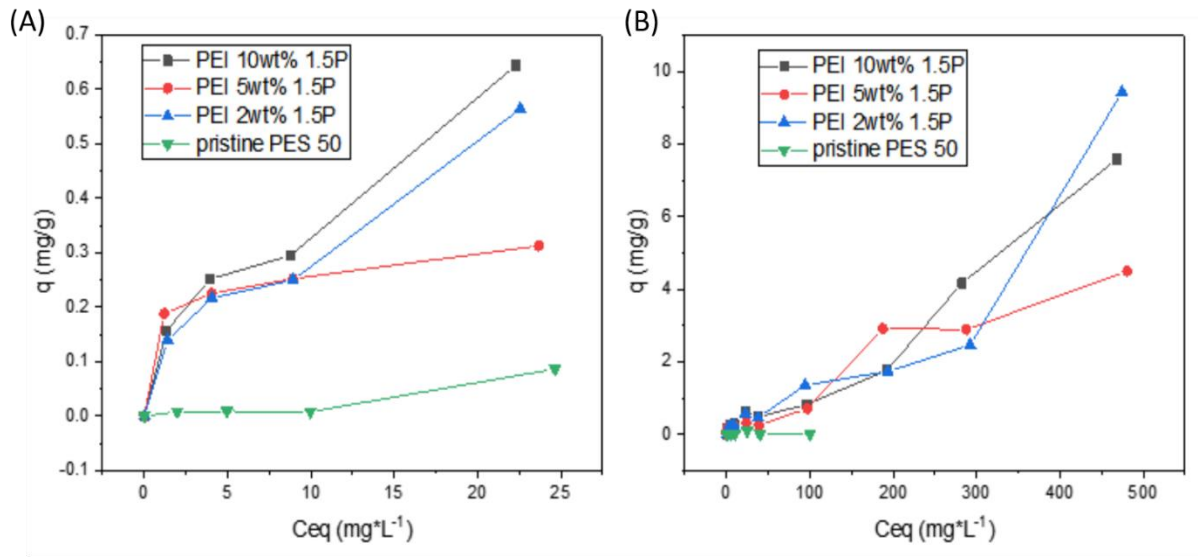

Fig. 4.5 The adsorption isotherms of the three selected membranes at two boron concentration windows of (A) from 2 – 25 mg/L and (B) from 2 – 500 mg/L.

As shown in Fig. 4.5, the modified membrane presents a specific boron binding capacity, while the pristine membrane has almost no boron uptake. Within the applied initial boron concentration range of 2 - 500 mg/L, all three modified membrane presents higher boron uptake as the boron concentration increases, but none of them reach the adsorption plateau. Moreover, both three modified membranes are subject to S-type isotherm indicates a possibility of cooperative adsorption [120,121]. The cooperative adsorption

occurs when there is strong adsorbate-adsorbate interaction, especially at the high adsorbate concentration. In the case of boron in the aqueous phase, boron presents as boric acid and various poly-nuclear species when boron concentration excess 25 mM or 270 mg/L[H, H1]. And different boron species would lead to a complicated adsorption mechanism. Thus in high boron concentration, competitive adsorption occurs: 1) one boron ligand binds with one boric acid; and 2) one boron ligand binds with one poly-nuclear species. This complicated adsorption process could be the main reason for the S-type adsorption isotherm.

However, the boron adsorption at low boron range is of great interest because the original boron concentration in seawater is around 5 mg/L. Hereof, it is more reasonable to study the boron adsorption mechanism at the low boron concentration window. Langmuir and Freundlich isotherms models have been used to analyze the boron adsorption with the initial boron concentration from 2 - 25 mg/L, and the fitting result can be found in Table 4.9. It was found that the Freundlich isotherms model gives better fitting for both of the three modified membranes. The Freundlich isotherms model describes a heterogeneous adsorption process of which having different adsorption energy when boron binds to the ligands. The *n* value is a heterogeneity index between 0-1, and the n value is close to 0, indicating the more heterogeneous adsorption process. The sample PEI-5 has good fitting (R^2 = 0.998) with Freundlich isotherms, and presents most binding capacity (*k* = 0.178 mg/g) and significant heterogeneous adsorption process (*n* = 0.173).

Table 4.9 The fitting result of adsorption isotherm by Freundlich and Langmuir isotherm models.

Sample	Langmuir isotherm fitting			Freundlich isotherm fitting		
	q_m (mg/g)	b (L mg^{-1})	R^2	K (mg/g)	n	R^2
PEI-10	1.099	0.059	0.940	0.102	0.583	0.970
PEI-5	0.297	1.180	0.971	0.178	0.173	0.998
PEI-2	0.018	0.051	0.931	0.084	0.599	0.965

4.1.4.3 Boron adsorption kinetics

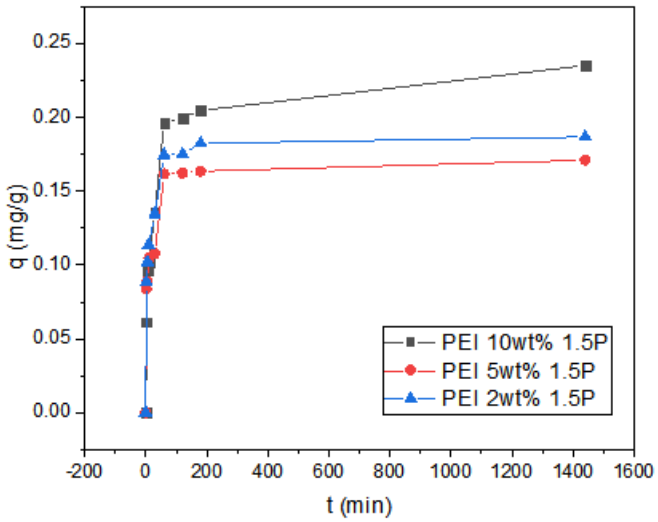

Fig. 4.6 The boron adsorption kinetics of three selected membranes.

Adsorption kinetics characterization gives useful information regarding the mass transport process during the adsorption process, and it is one of the essential assessments toward the quality of adsorbents. The time-dependent adsorption kinetics has been studied by conducting batch adsorption for the selected three modified membranes, and the target initial boron concentration is 5 mg/L. As Fig. 4.6 shows, all three modified membranes present similar adsorption profile, i.e., rapidly adsorption at the first 60 min, then come to an adsorption plateau. Moreover, the membrane PEI-10 shows the highest boron binding capacity, where the membrane PEI-5 has the lowest boron binding capacity.

Table 4.10 The fitting result of adsorption kinetics by Pseudo-first-order, Pseudo-second-order, and intra-particle models.

Sample	Pseudo-first-order			Pseudo-second-order			intra-particle		
	q_e (mg/g)	k_1 (min^{-1})	R^2	q_e (mg/g)	k_2 (g mg^{-1} min^{-1})	R^2	C	k_i (g mg^{-1} $min^{-0.5}$)	R^2
PEI-10	0.176	3.931	0.914	0.215	0.519	0.995	0.045	0.014	0.835
PEI-5	0.138	1.553	0.599	0.170	0.927	0.993	0.053	0.010	0.716
PEI-2	0.158	1.782	0.76	0.186	0.934	0.997	0.059	0.011	0.722

The rate-controlling steps during the adsorption process should be identified to further understand the mass transport process during the boron binding. As the previous discussion in Section 3.6.3.7, three models have been introduced, i.e., pseudo-first-order model, pseudo-second-order model, and intraparticle diffusion model. The fitting results can be found in Table 4.10. The pseudo-second-order model fits better with the experimental adsorption kinetics results for three modified membranes ($R^2 > 0.99$). This good fitting with the pseudo-second-order model indicates that the rate-controlling step during the boron adsorption is the interaction between the binding site and boron. Moreover, the k_2 value describes adsorption rate constants, so a higher k_2 value refers to faster adsorption, i.e., lower adsorption resistance in terms of the mass transport process. A clear tendency can be seen, in which a denser hydrogel (PEI-10) shows the slowest adsorption rate of 0.519 g mg^{-1} min^{-1}; vice versa, the low cross-linked hydrogel (PEI-2) gives the fastest adsorption rate of 0.934 g mg^{-1} min^{-1}. This tendency can be interpreted by the slower mass transport of boron in the dense hydrogel network. Table 4.11 presents the q_e (in mg/g or mg/m^2) obtained from the batch experiment of three replicates. The experimental q_e value gives a similar value with the fitted q_e value in Table 4.10 due to the good fitting ($R^2 > 0.99$).

Table 4.11 The boron uptake of three selected membranes by bath adsorption experiment.

Name	Experimental q_e (mg/g)	Experimental q_e* (mg/m^2)	Fitting q_e (mg/g)	$C_{0\text{-Boron}}$ (mg/L)
PEI-10	0.25 ± 0.02	10.7 ± 0.9	0.22	5
PEI-5	0.23 ± 0.03	9.7 ± 1.3	0.17	5
PEI-2	0.22 ± 0.02	9.5 ± 0.9	0.19	5

*: the data here represent the experiment q_e in mg/m^2.

4.1.4.4 Regeneration

A static membrane regeneration has been done to investigate the reusability of modified membranes. In the regeneration protocol, the saturated membrane has been first treated by 1 N HCl as a boron desorption step. Afterward, the membrane was recovered by subsequent neutralization and washing step, and the detailed procedures can be found in Section 3.6.3.9. As shown in Fig. 4.7, five adsorption cycles, i.e., four regenerations, were performed. The equilibrium adsorption results have been nominalized by setting the q_e of the first adsorption as 1. In both three modified membranes, the boron binding capacity only remains about 50 % after first generation. The binding capacity declined may due to: 1) there is part of non-adherent hydrogel been trapped inside the support layer of membrane, and it would be washed out during the regeneration process; 2) there are irreversible boron binding sites in the affinity coating that cannot be regenerated; 3) the PEI was cross-linked by 5-Acl, an acrylates cross-linker, which is unstable in strong acidic condition. However, after the first regeneration, the binding capacity of both of the three membranes keeps constant in the following adsorption/desorption cycles confirming the stable grafting of the boron affinity coating inside the support layer of the membrane.

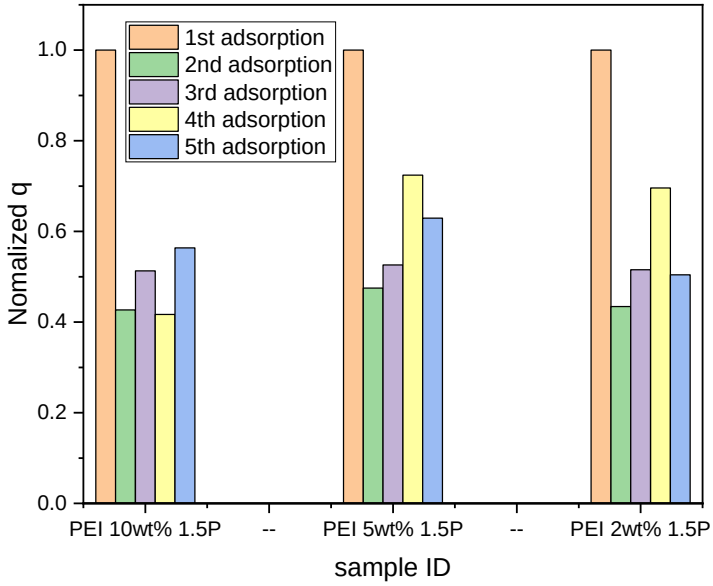

Fig. 4.7 The regeneration performance of three selected membrane.

4.1.4.5 Flow-through adsorption

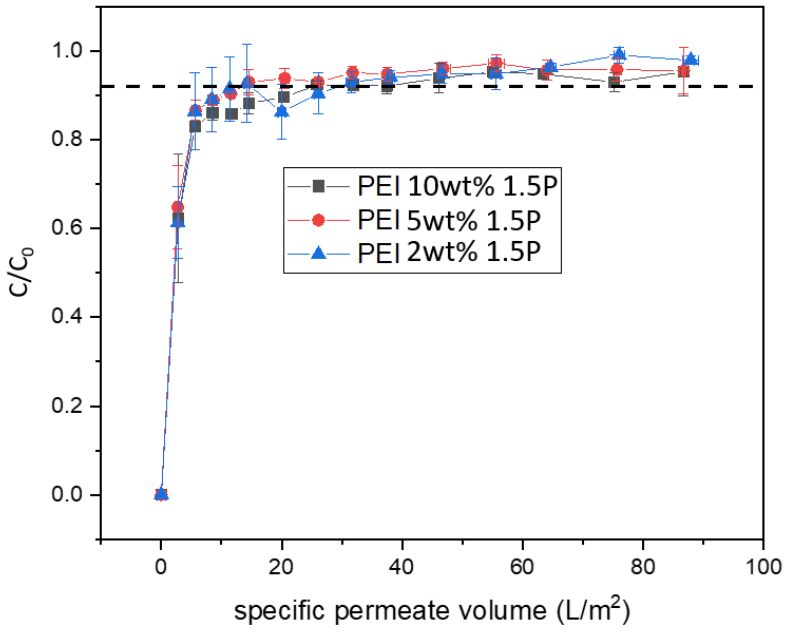

Fig. 4.8 The breakthrough curve of the three selected membranes.

The flow-through adsorption experiment has been done to estimate the boron removal performance of the modified membrane. Three replicates were done to assure the

reproducibility of the adsorption experiment. In the flow-through experiment, a boron solution of 5 mg/L was used as feed solution, and the applied transmembrane pressure was 1.0 bar.

As shown in Fig. 4.8, a boron breakthrough curve can be obtained from the flow-through adsorption experiment. It has a steep breakthrough curve and reaches 90 % of adsorption capacity at the early specific permeate volume, and then the membrane can still keep binding boron slowly until saturated. Such breakthrough behaviour can be interpreted by different mass transport scenarios: 1) first, the bulk convection flow can easily access the binding sites at the hydrogel surface and saturated quickly; 2) the binding site in the hydrogel only can be reached by diffusive transport. Obviously, the diffusive transport has high mass transport resistance leading to a slow absorption rate.

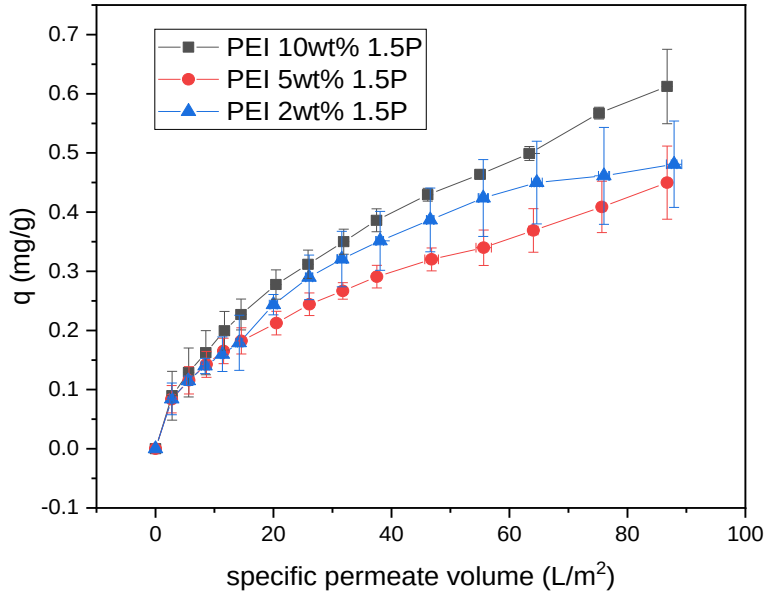

Fig. 4.9 The boron accumulation in the three selected membranes during flow through adsorption

In terms of boron uptake of the modified membrane in the flow-through process, the total boron uptake has been calculated based on the flow-through adsorption, and the result is shown in Fig 4.9. No adsorption plateau can be observed in two of three modified membranes indicating the unsaturated state at the specific permeate volume of 90 L/m^2.

However, the corresponding boron uptake ($q_{\text{flow-through}}$) of 0.61 mg/g, 0.45 mg/g, 0.48 mg/g can be obtained in PEI-10, PEI-5, and PEI-2 membrane, respectively. Interestingly, the modified membrane has more than double boron uptake in the flow-through process compared to bath adsorption ($q_{\text{flow-through}}$, cf. Table 4.12). Such a huge gap (q_{bath}- $q_{\text{flow-through}}$) may be due to insufficient mass transport of boron solution from bulk to the membrane pores in the batch adsorption experiment, which is an inevitable error. And the inefficient mass transport process will be further discussed together with the modified MF membrane in Section 4.3.4.

Another possibility is due to the different driving forces of the boron binding process. Compared with static adsorption, the convection flow in the flow-through protocol would eliminate boron depletion at the coating surface due to the boron adsorption, thus improving boron transport driving force across the hydrogel layer. When assuming that there is no insufficient mass transport in the batch adsorption experiment, then the $q_{\text{flow-through}}$-q_{bath} value would indicate the improvement of applying convection flow.

Table 4.12 The boron uptake difference between bath adsorption and flow through adsorption.

Name	q_{bath} (mg/g)	$q_{flow-through}$ (mg/g)	$q_{flow-through} - q_{bath}$ (mg/g)	$\frac{q_{flow-through} - q_{bath}}{q_{flow-through}}$ (%)
EI-10	0.25 ± 0.02	0.61	0.36	59 %
PEI-5	0.23 ± 0.03	0.45	0.22	49 %
PEI-2	0.22 ± 0.02	0.48	0.26	54 %

4.1.5 Transfer of modification condition to the capillary membranes

The filtration and boron removal performance of three modified PES flat-sheet membranes has been globally disused in the previous section. The modification condition of PEI-5 and PEI-2 have been proportionally transferred to a commercial capillary PES membrane branded Multibore® module. Table 4.13 gives a pure water permeability of pristine Multibore® module, modified Multibore® module, and modified PES50 (flat sheet membrane). In both two transferred modification conditions, the modified Multibore® module presents similar water permeability as Modified PES-50. With respect to the membrane resistance point of view, the leading membrane resistance would dominate the

final flux, and obviously, the predominant resistance comes from the grafted coating, which is approx. 2-3 order higher than intrinsic membrane resistance. Thus a similar permeability was obtained when applied same modification on different membranes.

Table 4.13 The permeability of the pristine membrane, the modified flat sheet membrane (PES-50), and the modified Multibore® module.

Modification condition	Pristine Multibore (LMH bar)	Modified Multibore (LMH bar)	Modified PES50 (LMH bar)
PEI-5	1140 ± 25	53	38
PEI-2	940 ± 20	53	59

Regarding the boron removal performance, boron uptake of modified Multibore® module via flow-through process has been done under identical operation conditions. Fig. 4.10 presents the breakthrough curve and total boron uptake of modified Multibore® module and modified PES-50, respectively. In both modification parameters, the breakthrough curve of modified Multibore® module nearly overlaps with the breakthrough curve of modified PES50. Moreover, the modified Multibore® module has comparable total boron uptake (boron accumulation) as modified PES50. The similar boron removal performance and water permeability indicate a reproducible modification and a successful parameter transfer from the modified flat sheet membrane to the commercial capillary membrane, Multibore® module.

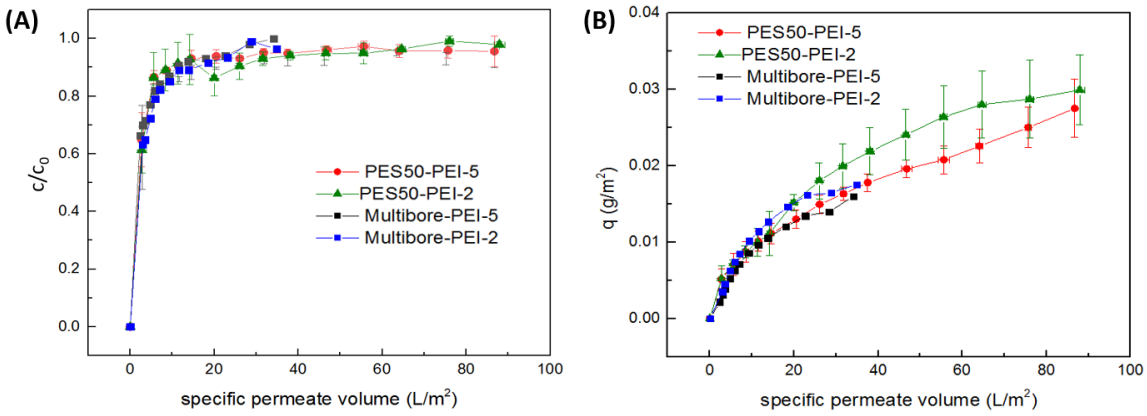

Fig. 4.10 Comparison of (A) breakthrough curve of modified flat sheet membrane and Multibore® module; (B) boron accumulation in flat sheet membrane and Multibore® module.

4.1.6 Interim summary for Section 4.1.

Gelation point determination, solubility test, and bulk hydrogel test have been used to pre-screen the modification conditions. Moreover, different models have been introduced to reveal the possible location and coating formation mechanism during the premodification step. Premodifying the support layer of UF membrane by PEI/5-Acl active coating and later adapting post-hydroxyl functionalized is thought to be a better route to impart boron selective binding to membrane filtration.

The modified membranes only retain 18-24 % of the original flux after modification, and the flux is positively associated with the cross-linking degree of coating. The MWCO decreases from 70 kDa to around 17 kDa after the modification and has no clear association with the cross-linking degree. This phenomenon can be interpreted by the partial pore plugging effect during the modification.

The adsorption isotherm and kinetics have been studied to reveal the boron binding mechanism. It shows a heterogeneous boron binding, and the rate-controlling step is the interaction between boron and binding sites. Also, the flow-through adsorption has been conducted and interestingly gives different adsorption capacity compared to batch adsorption. This inconsistency may due to the different mass transport conditions. However, the boron binding capacity is still relatively low in comparison with commercial ion

exchange resin (cf. Fig. 2.3). The relatively low boron binding can be mainly attributed to the inhomogeneous modification where the coating locals close to the selective layer instead of the overall accessible area in the support layer.

4.2 MF membrane modification via surface-initiated polymerization using redox pair of macro-initiator and persulfate

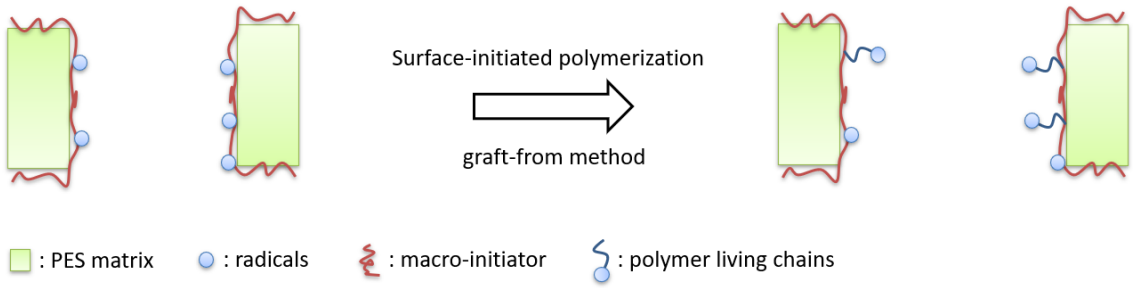

Fig. 4.11 Schematic representation of macro-initiator meditated surface-initiated polymerization (graft-from method).

In the preceding study (cf. section 4.1), it was found that improving the modification homogeneity is essential to accomplish ideal boron binding capacity. One of the attractive modification strategies is to pre-modify the overall accessible membrane surface area with unique compounds through adsorption, where the adsorbed compounds contain specific functional groups to initiate polymerization. Thus, a coating can be grafted onto the surface via surface-initiated polymerization (cf. Fig. 4.11). By virtue of the homogeneous adsorption of initiation groups, the later polymerized layer can evenly cover the overall pre-modified surface. As introduced in Section 2.4.3, the redox initiation system, i.e. APS/TEMED, gains lots of interest because of its prominent initiation efficiency and moderate initiation condition. A similar idea has been introduced into the membrane surface modification by Quilitzsch et al. [78,96]. In these works, a macro-initiator containing anchor groups and tertiary amine moieties (PBD-300) was first adsorbed by PES membrane via hydrophobic-hydrophobic interaction. The adsorbed tertiary amine moieties can decompose persulfate (APS), thus generate free radicals for polymerization. In this section, the feasibility of applying such modification on MF membrane will be first discussed in terms of monomer activity and initiation efficiency of the redox system (Section 4.2.1). And the adsorption condition of PBD300 will be later discussed to optimize the PBD adsorption (Section 4.2.2). Afterward, a coating was modified via surface-initiated polymerization, and several characterizations have been done to ensure the coating grafting (Section 4.2.3). Parameter

optimization has been done to approach higher boron binding with less flux decline (Section 4.2.4). Finally, few comments were made towards potential alternatives (Section 4.2.5).

4.2.1 Feasibility test of this modification method

4.2.1.1 Gelation and boron adsorption test of GAEMA-based affinity hydrogels

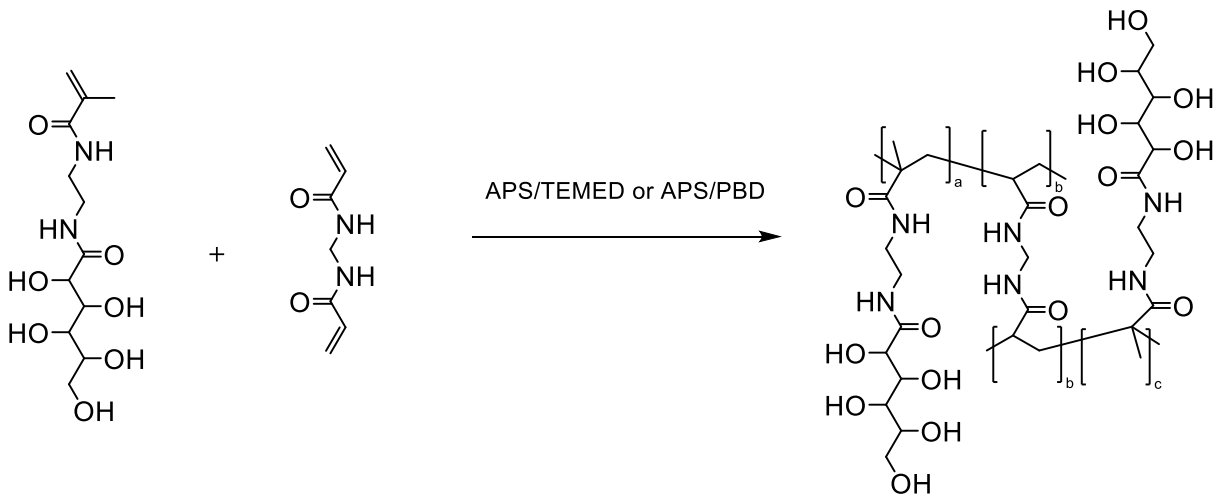

Fig. 4.12 Schematic representation of cross-linking between GAEMA and MBA under APS/TEMED or APS/PBD initiation system.

Prior to performing the modification, self-prepared GAEMA has been firstly tested in terms of gelation activity with MBA as cross-linker monomer (cf. Fig. 4.12). Table 4.14 shows the rheological data of the monomer solution containing three different amounts of cross-linker concentrations, where the relative cross-linker concentration to monomer mass is 15, 10, and 5 wt%, respectively. All three monomer solution contains 0.2 mg/L of APS. Right before the measuring, TEMED was added to these three monomer solutions and then well mixed. All three samples present gelation points indicating cross-linked network formation, and the gelation points decrease with the increase of cross-linker concentration (cf. Table 4.14). Usually, the higher cross-linking degree will lead to a higher elastic modulus (G'). The same tendency can be observed that the sample with the highest cross-linking degree (15 wt%) has a significantly larger G' of 761 Pa.

Table 4.14 The gelation points and rheological data of GAEMA hydrogel with the different cross-linking degrees.

$C_{Cross\text{-}linker}$ / Parameters	15 wt% *	10 wt% *	5 wt% *
gelation point	before measurement	21 min	7.33 min
G'' (Pa)	16.6	1.15	0.102
G' (Pa)	761	84.8	0.399
tan δ	0.022	0.0135	0.257

*: it's a relative concentration (wt %) to the mass of monomer GAEMA.

After verifying the feasibility of gelation of GAEMA, the boron affinity of prepared hydrogel should be further confirmed. A monomer solution containing 100 mg/mL of the monomer, 2 mg/mL of APS, and 10 mg/mL of MBA (10 wt% to the mass of GAEMA) was used to prepare bulk hydrogel for the boron uptake test. The adsorption was carried out by using an initial boron concentration of 5 mg/L, an adsorbent dosage of 2 g/L, a pH value of ~8.0, and an adsorption time of 48 hours. Two replicates have been done, and the result was shown in Table 4.15. Under the given adsorption condition, the prepared GAEMA gel shows slightly less boron uptake than the adsorbent prepare from PEI/5-Acl gel (cf. Table 4.5). Towards the PEI/5-Acl gel, it contains higher amount of proton acceptor, such as secondary and tertiary amine, and the existence of proton acceptor moieties would facilitate boron complexation [25,49,122,123]. In comparison, the GAEMA gel lacks proton acceptor moieties thus presumably yielding less boron binding affinity than PEI/5-Acl gel. However, the boron binding capacity still comparable with commercial ion exchange resin [24,33,34,50,124].

Table 4.15 The boron uptake of 10-10-2 bulk hydrogel in bath adsorption experiment (C_0 = 5 mg/L).

Probe	C_0 (mg/L)	Remaining Boron (C_e) (mg/L)	removal rate (%)	q (mg/g)
1	5	0.89	82.1	2.054
2	5	1.09	78.2	1.956

4.2.1.2 Feasibility test of surface initiation by macro-initiator

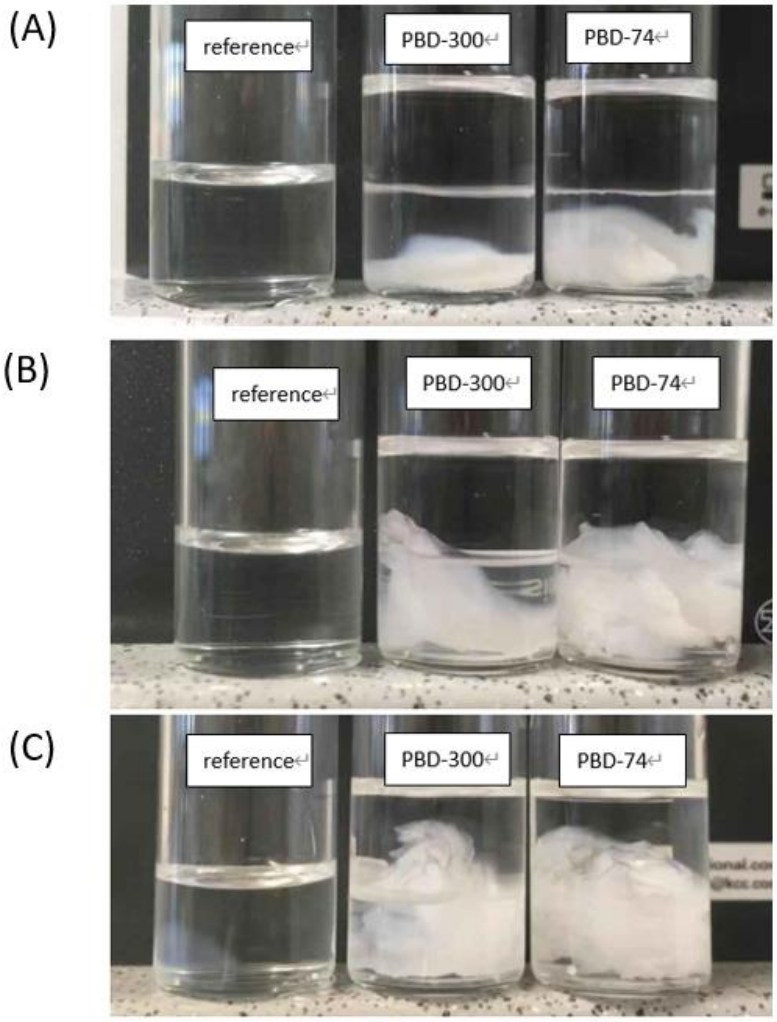

Fig. 4.13 Optical images of hydrogel formation initiated by a two-phase system after 5 h (A), 24 h (B), and 48 h (B) where the upper (organic) phase is octanol, and the bottom (aqueous) phase is water. The organic phase contains PBD300 (middle bottle) or PBD74 (right bottle).

Apart from GAEMA reactivity, the initiation efficiency of the macro-initiator/APS system is another imperative test before transferring the modification to the membrane. For the sake

of monomer synthesis difficulty, a commercial monomer, acrylamide (AAm), was used to test the initiation efficiency of macro-initiator/APS. To mimic the initial surface process, a classical two-phase system of octanol/water was used, where octanol was used as the organic phase. The octanol phase contains 1 g/L of PBD300 (the middle bottle in Fig. 4.13) or PBD74 (the right bottle in Fig. 4.13). The aqueous phase contains 150 mg/mL of AAm, 7.5 mg/mL of MBA (5 wt% to the mass of AAm), and 2 mg/L of APS. The macro-initiator PBD300 and PBD-74 will be retained in the organic phase, and the majority of AAm (log KOW = -0.78) and MBA (log KOW = -1.52), as well as all of APS (insoluble in octanol), is retained in the aqueous phase. A control group with the same monomer solution (the left bottle in Fig. 4.13), which is macro-initiator absent, was used to assess the influence of self-decomposition of APS. As shown in Fig 4.13, a visible white cross-linked AAm gel appears after 5 hours, while the control group remains transparent, and no AAm gel can be visually observed. It keeps gaining more AAm gel in the two-phase system in the following 48 hours, and a small piece of cross-linked AAm gel finally can be found at the bottom after 48 hours which is due to the self-decomposition of APS. This two-phase initiation system gives an obvious and confident result to affirm the feasibility of the macro-initiation system.

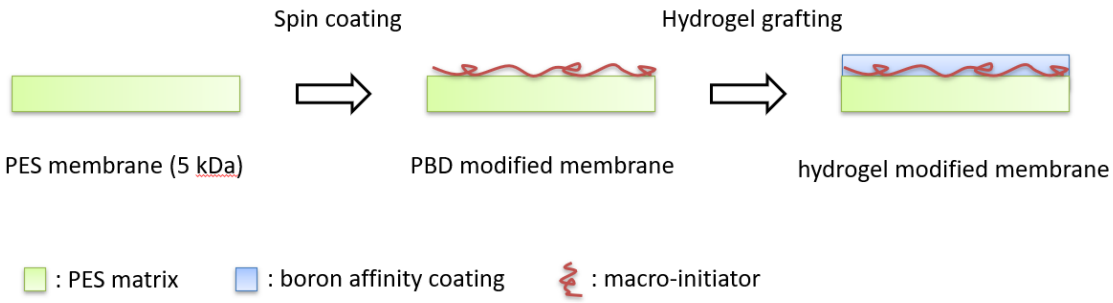

Fig. 4.14 Schematic presentation of surface coating test via macroinitiator assist surface initiation polymerization approach.

Moreover, the modification has been preliminarily performed onto the membrane surface via spin coating (cf. Fig. 4.14). A PES membrane with the MWCO of 5 kDa was used as the pristine membrane, ensuring that the coated PBD would not penetrate to the pores. 100 µL of a solution of PBD in isopropanol (5 g/L) was dropped to the 25 mm of PES membrane, and the spin coating is carried out at 150 rpm for 10 s. After the complete evaporation of

isopropanol, the PES membrane can be covered with 67 μg/cm^2 of PBD (cf. Table 4.16). The premodified PES membrane was later immersed into a degassed GAEMA monomer solution consisting of 100 mg/mL of GAEMA, 10 mg/mL of MBA, and 2 mg/mL of APS. And no APS was added in the control group. After hydrogel grafting, the total mass increase to 104 μg/cm^{2,} and the total GAEMA coating mass is 37 μg/cm^2, while the control group has no apparent change in terms of mass gain.

Table 4.16 Mass gain and contact angle of the PBD-300 modified PES-5 and the final modified membrane coated by GAEMA layer with or without using APS in the monomer solution.

	Total Mass gain (μg/cm^2)	Hydrogel mass (μg/cm^2)	Contact angle (°)
Pristine membrane	/	/	30
Premodified membrane	67	/	40
Monomer solution with APS	104	37	25
Monomer solution without APS	67	0	38

The contact angle (CA) of each membrane has been measured via captive bubble mode to reflect the change of surface wettability (cf. Table. 4.16). The pristine membrane has a CA of 30 ° because of the utilization of hydrophilic additives during the manufacture. After membrane coat with PBD, the CA increases to 40 °, which is in good agreement with the reported value in Quilitzsch's work [78]. When the membrane coat with GAEMA coating, the CA decreases from 40 ° to 25 ° because of the hydrophilic nature of GAEMA coating. The control group sample has a little CA change from 40 ° to 38 °, indicating limited surface grafting of GAEMA coating because of APS absence in the control group.

4.2.2 Modification step 1: Macroinitiator adsorption

4.2.2.1 Adsorption of PBD300 in MicroPES-2F

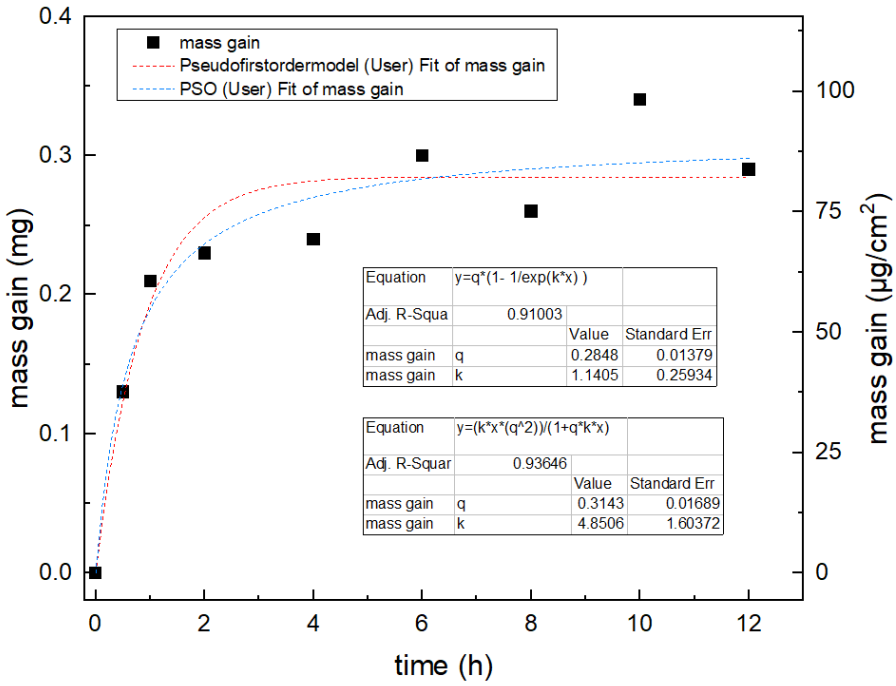

Fig. 4.15 The adsorption kinetics of PBD-300 adsorption via recirculation mode.

So far, the monomer (GAEMA) reactivity and initiation feasibility have been verified in the previous discussion. Since the core in the premodification step is adsorption, the adsorption kinetic of the macro-initiator could provide some valuable information for designing better modification conditions. As described in Section 3.3.2.1, the adsorption of the PBD solution was carried out via a recirculation mode. Thus recirculation time should be carefully defined to assure saturated adsorption of PBD. The Adsorption kinetic of PBD on commercial MF membrane with a labeled pore diameter of 0.2 μm (MicroPES-2F) has been carried out with a 3 mL/min flow rate. According to the kinetic curve in Fig. 4.15, a clear adsorption plateau can be observed after one hours' recirculation. For the sake of assurance, 6 h was chosen as the recirculation time in the subsequent experiments.

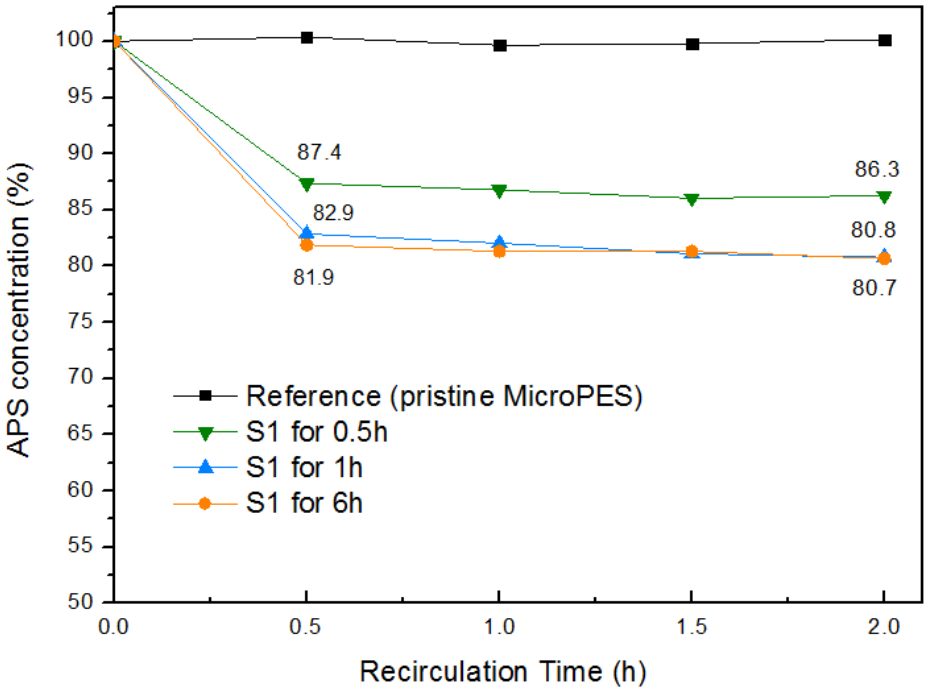

Fig. 4.16 The remaining APS concentration when recirculating APS solution through the pristine membrane and the membrane premodified by PBD-300 for 0.5, 1, and 6h.

In Section 4.2.1.2, the initiation feasibility of this macro-initiation system has been qualitatively established via CA and mass gain method. However, it would be interesting to study the initiation efficiency quantitatively, i.e., decomposition efficiency of APS, of this initiation system. The persulfate concentration can be measured via UV/Vis method. Briefly, the persulfate will stoichiometrically oxidize Fe^{2+} to Fe^{3+}, and the Fe^{3+} will complex with $[SCN]^-$ forming $[Fe(SCN)(H_2O)_5]^{2+}$, leading to a specific absorbance at a wavelength of 450 nm. A degassed APS solution in water (2 mg/L) was pumped through three kinds of premodified membranes and recirculated for two hours. The recirculation APS solution was sampled every 30 min during the recirculation, and measured the remaining persulfate concentration. The APS concentration variation along with recirculation time can be found in Fig 4.16. The persulfate concentration keeps constant when recirculated APS for 6 hours in the pristine membrane, which means no APS decomposition. For the membrane experienced by 0.5 hour of premodification, the persulfate concentration drops to 87.4 % in the first 30 min and slowly decreases to 86.3 % in the rest of recirculation time. While

for membrane experienced 1 and 6 hours' premodification, it remains a similar level of persulfate to 82.9 % and 81.9 %, respectively, and the persulfate concentration keeps decreasing to around 81 % in the rest of recirculation time. According to the pseudo-second-order model, the PBD loading at 1 hour and 6 hours is close to saturation adsorption. It means that the APS decomposition is proportional to the amount of adsorbed PBD. Hereof, a clear conclusion can be made: the initiation efficiency depends on PBD-300 loading, where more PBD-300 adsorbed leads to more free radicals generated at the membrane surface.

Table 4.17 The APS consumption and the mass of adsorbed DMAEMA moieties in macroinitiator PBD.

Consumed APS (μmol)	Grafted DMAEMA (μmol)	The ratio of APS/DMAEMA
21.74	3.63 ± 0.5	6

To have a rough estimation of initiation efficiency, the consumed APS and grafted tertiary amine moiety (DMAEMA segments) in the system are calculated and present in Table 4.17. It should be noticed that the grafted DMAEMA is calculated from the membrane experienced 6 hours' premodification. The consumed persulfate is around 6 times higher than grafted tertiary amine moiety in terms of molar ratio. In the APS/tertiary amine redox initiation system, two radicals will be first generated, persulfate radicals and tertiary amine radicals, and the tertiary amine radicals can extract hydrogen from water or trace isopropanol (the solvent used in premodification), forming new tertiary amine. And such recovered tertiary amine would keep accelerating the decomposition of APS, leading to non-stoichiometric APS consumption.

4.2.3 Modification step 2: Surface grafting of GAEMA-based hydrogel

4.2.3.1 Determination of modification time for hydrogel grafting

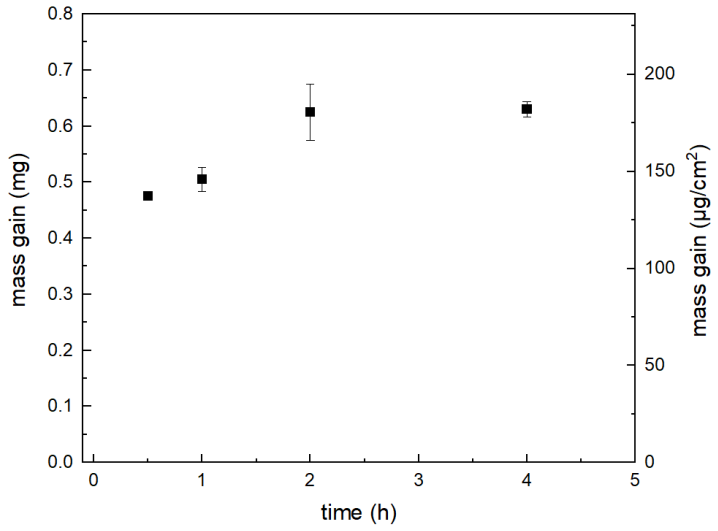

Fig. 4.17 The hydrogel mass gain change over applying recirculation time.

The selection of modification time in the premodification step has been resolved based on the concrete results in previous sections. The evolution of hydrogel grafting loading along with the recirculation time should be studied, thus able to determine the suitable modification time via recirculation apparatus. Fig. 4.17 presents the GAEMA hydrogel mass gain after recirculating monomer solution for specific recirculation time. As can be seen that the hydrogel loading has no obvious change when recirculating monomer solution after two hours. Additionally, the initiation test by monitoring the persulfate concentration shown in Fig. 4.16 giving the information that most of the persulfate will be consumed in 30 min. The presented result comes out with the conclusion of sufficient GAEMA grafting can be achieved when recirculating monomer solution through the premodified membrane for two hours or more.

4.2.3.2 The surface chemistry changes after modification

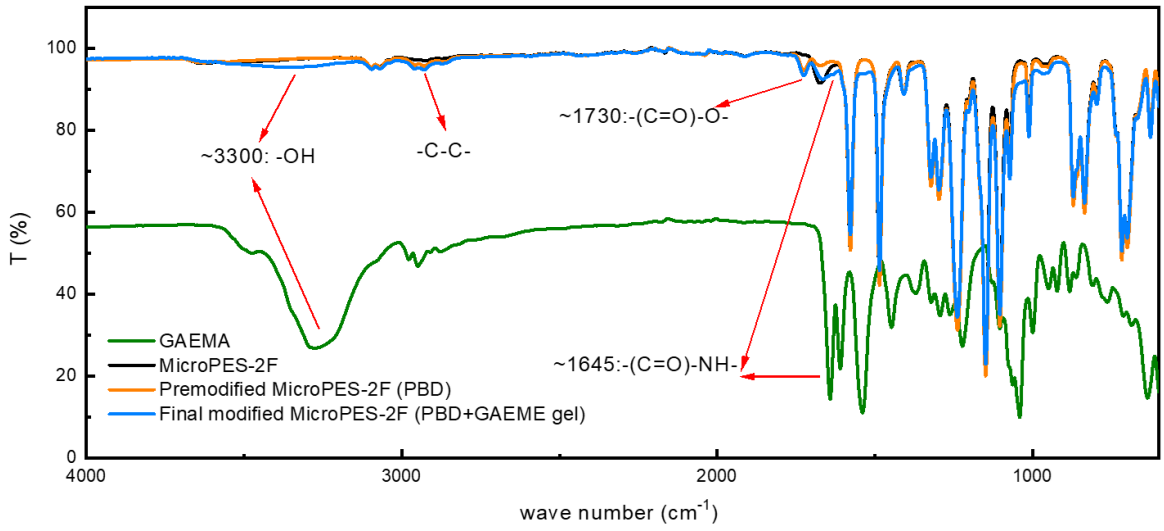

Fig. 4.18 The ATR-FTIR spectrum of the pristine membrane (black curve), premodified membrane (orange curve), GAEMA hydrogel coated membrane (blue curve), and bulk GAEMA bulk hydrogel (green curve).

ATR-FTIR was used to reveal the surface chemistry change in each modification step, and the spectra are shown in Fig. 4.18. When the MicroPES-2F is premodified by macro-initiator, new absorbance at the wavenumber of 2930-2955 cm^{-1} and 1730 cm^{-1} appears, which is corresponding to the backbone C-C- vibration and -(C=O)-O- vibration, respectively. And these two absorptions attribute to characteristic peaks for macroinitiator, PBD. Apart from the absorbance of PBD, new peak at ~ 3300 cm^{-1} appears, which belongs to the -O-H vibration from the GAEMA layer. The ATR-FTIR of premodified and final modified membrane gives solid evidence of successful modification performed on MicroPES-2F membrane.

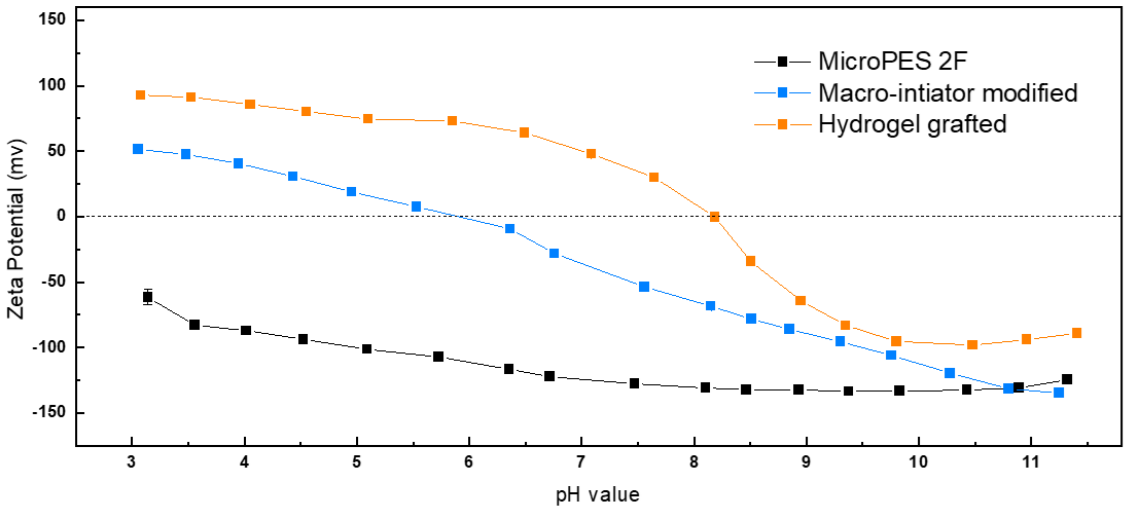

Fig. 4.19 The zeta potential of the pristine membrane (black curve), premodified membrane (blue curve), and GAEMA hydrogel coated membrane (orange curve).

The surface charge alteration with modification step has been investigated as well (cf. Fig. 4.19). The pristine membrane MicroPES-2F shows a strongly negatively charged surface over the measuring pH range, although the pristine membrane has been intensively washed by Milli-Q water and isopropanol. The durable negatively charged surface arises from a partially sulfonated polyethersulfone that is blended into the membrane matrix during the manufacturing process for the sake of wettability improvement. The negatively charged membrane surface reverses to positively charge (charge overcompensation effect) and showing an observable isoelectric point (IEP) of about 5.9 after the premodification step. The overcompensation is due to an extension of a few chain segments into the z-direction, i.e., the protonated DMAEMA moiety presents in loops and tails segment in the adsorbed PBD [125–128]. It should be noticed that the adsorption of PBD was carried out at a pH of 3 where the tertiary amine moieties in DEAEMA are protonated to carry a positive charge. The adsorption of polymer follows with the loops and tails mechanism, where only part of the polymer segment anchor to the solid surface via specific interaction [125,126]. The projected mechanism for macro-initiator attachment was via hydrophobic interaction between BMA segments and the PES membrane matrix. However, there could be an extra contribution of adsorption energy of Coulombic interaction between protonated DMAEMA moiety and negatively charged membrane surface. So far, it is clear that the PBD adsorption

is a synergistic effect of Coulombic interaction and hydrophobic interaction. After the membrane is modified by GAEMA hydrogel coating, the surface shift to move positively charged because the surface is covered by GAEMA coating, and the IEP of the final modified surface is 8.2, which is in good consistent with a report IEP value from glycopolymer [129,130].

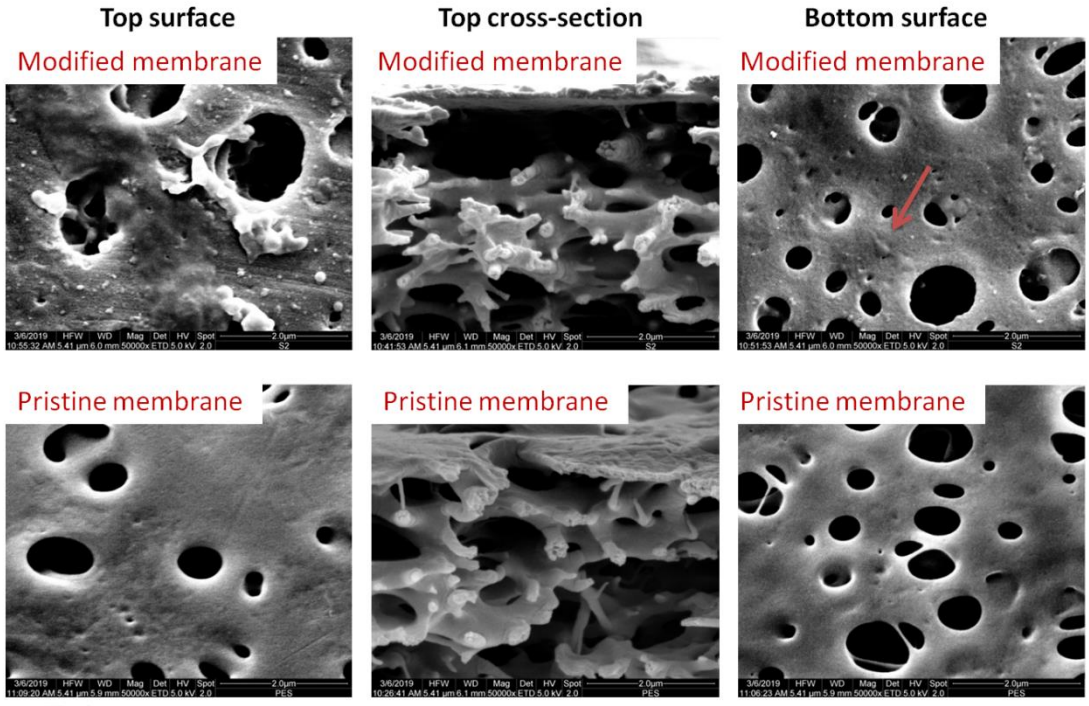

Fig. 4.20 SEM images of pristine membrane and the membrane modified at a monomer condition 15-5-2.

The SEM images of the pristine and modified membrane are shown in Fig. 4.20. It should be classified here that the definition of the so-called 'top surface' is the surface contacted with non-solvent during the membrane manufacturing via phase separation method, and 'bottom surface' is the membrane surface contact with the substrate. A considerable amount of GAEMA hydrogel has been coated onto the membrane top surface results in a distinguishable morphology different from the top surface morphology of the pristine membrane. And the cross-section image of the modified membrane gives positive feedback that no pore blocking can be observed after the modification. Moreover, it has observable surface roughness difference between modified and pristine membranes, where the rougher surface comes from the modified membrane indicating the existence of GAEMA coating. However, it has a significantly different modification degree between the

top and bottom surface, leading to a hint of uneven modification in this approach.

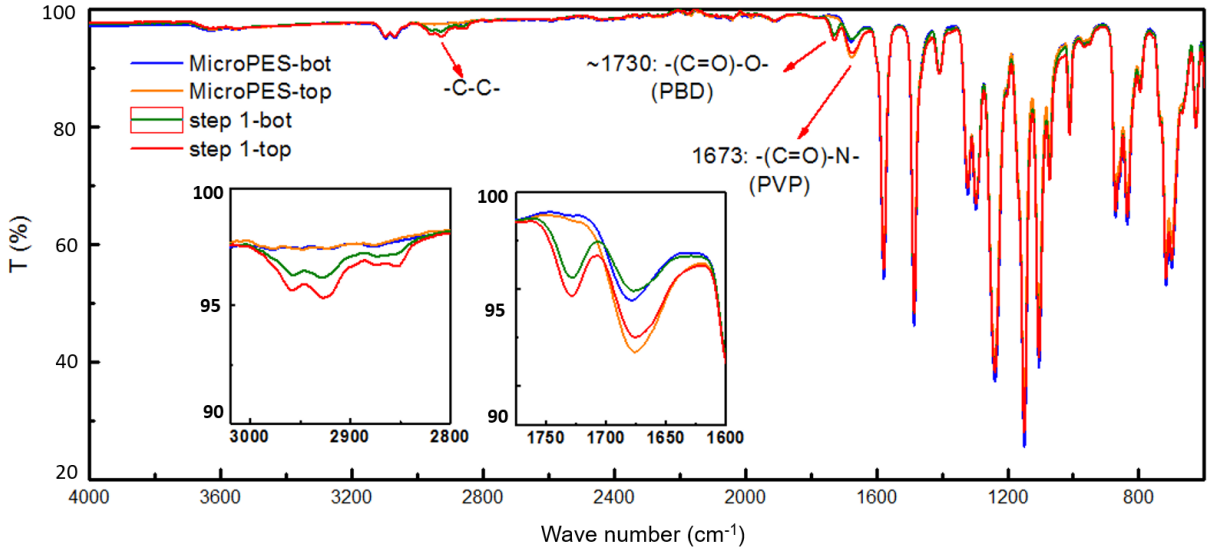

Fig. 4.21 The ATR-FTIR spectra of the top surface of the pristine membrane (orange curve), the bottom surface of the pristine membrane (blue curve), the top surface of the premodified membrane (red curve), and the bottom surface of the premodified membrane (green curve)

The ATR-FTIR spectrum of both the top surface and bottom surface of the pristine and premodified membrane has been measured (Fig 4.21). Interestingly, the -(C-O)-N- vibration (1673 cm^{-1}) from PVP additives shows higher absorbance in the top surface of both pristine and premodified membrane. On the other hand, the top surface adsorbs more PBD than the bottom surface when checking the peak area at 2800 - 3000 cm^{-1}, which belongs to the backbone -C-C- vibration. As previously mentioned, the membrane producer will blend sulfonated polyethersulfone and PVP endow membrane better wettability, and the added sulfonated polyethersulfone and PVP would accumulate at the membrane top surface during the phase separation process [133, 134]. The ATR-FTIR here gives the same conclusion of PVP accumulation at the membrane top surface. Also, the sulfonated polyethersulfone would accumulate at the top surface due to its hydrophilic nature. However, it's challenging to find out the IR peaks for sulfonated polyethersulfone from Fig. 4.21. Overall, higher sulfonated polyethersulfone content affording a stronger Coulombic interaction with protonated DMAEMA moiety leading to a higher adsorption amount of PBD at the membrane top surface. Under the context of initiation efficiency study in Section 4.2.2.1, a higher amount of PBD will decompose more persulfate result in

more GAEMA grafting. So far as the discussion here, the uneven modification degree is mainly due to the inhomogeneous additives distribution across the membrane. Such heterogeneity nature of commercial membrane directly affects the modification homogeneity.

4.2.4 Parameter optimization

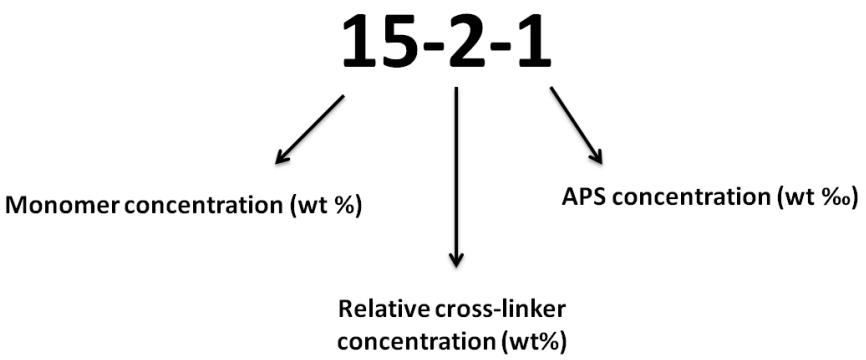

Fig. 4.22 the explanation for the name of monomer condition.

The premodification and the surface-initiated polymerization process have been intensively studied and discussed. The parameter optimization will be addressed in this section aiming to achieve a higher grafting degree with less permeability loss. In order to classify the different factors and the corresponding levels, each monomer condition can be named by three numbers (cf. Fig. 4.22). The first number refers to the GAEMA concentration in wt%, e.g., 15 means 15 wt% equal to 150 mg/mL; the second number refers to a relative MBA concentration to the mass of monomer in wt%, e.g., 2 means 2 wt% to monomer; the third number refers to APS concentration in wt‰, e.g., 1 means 1 wt‰ equal to 1 mg/mL.

4.2.4.1 Influence of monomer solution conditions

The monomer, cross-linker, and the APS concentrations would directly affect the polymerization rate in free radical polymerization, leading to different grafting degrees in this membrane modification. The 10-5-3, 10-5-2, and 10-5-.5 in Table 4.18 give information about the influence of APS concentration on hydrogel loading and permeability. No

significant difference can be found regarding hydrogel loading and permeability when increasing the APS concentration from 0.5 wt‰ to 3 wt‰ while fixing the GAEMA and MBA concentration. A similar tendency can be found as well when comparing sample 15-5-2 and 15-8-0.5. It seems that the APS concentration variation has limited contribution to altering hydrogel grafting. In the surface-initiated polymerization, the graft PBD will accelerate the decomposition of APS. It has around 20% of APS consumed in the case of APS concentration of 2 wt‰, and the consumed APS is six times higher than grafted PBD (cf. Section 4.2.2), which means the APS amount is already superfluous and the free radical generation is mainly subject to adsorbed PBD.

Table 4.18 The permeability and grafting degree (volumetric loading) of the membrane modified by different monomer conditions.

Monomer condition	**P. (LMH bar)**	**Total loading * (mg/cm^3)**	**Hydrogel loading (mg/cm^3)**
10-5-3	6400 ± 300	11.8 ± 2.5	5.4 ± 2.5
10-5-2	7600 ± 800	11.0 ± 1.2	4.6 ± 1.2
10-5-0.5	5400 ± 1400	12	5.6
15-5-2	1000 ± 200	14.4 ± 0.5	8 ± 0.5
10-10-2	6000 ± 1000	11.2 ± 3.2	4.8 ± 3.2
15-5-0.5	5900 ± 1000	13.8 ± 2.5	7.4 ± 2.5

* the total loading includes PBD loading and GAEMA loading.

When increasing the monomer concentration from 10 wt% to 15 wt%, about 130-170 % more hydrogel can be grafted to the membrane where a higher hydrogel loading can be found in sample 15-5-2 (8 ± 0.5 mg/cm^3) and 15-5-0.5 (7.4 ± 2.5 mg/cm^3) in comparison with the sample 10-5-2 (4.6 ± 1.2 mg/cm^3) and 10-5-0.5 (5.6 mg/cm^3), respectively. The degree of polymerization is mainly determined by the ratio of monomer to radicals and the chain termination rate. As widely known that enhancing monomer concentration will increase the ratio of monomer to radicals, e.g., living chain, thus higher degree of polymerization is achieved. In addition, under the scenario of surface-initiated polymerization, the free radical locals in the front of hydrogel growing surface, thus the

termination rate is dependent on grafting density and surface morphology (will be discuses later in Section 4.2.4) [131–134]. It has restricted living chains motion in the denser hydrogel surface, leading to a lower chain termination rate, since higher monomer concentration tends to form denser hydrogel coating. Speaking of the living chains' motion in the hydrogel surface, a higher cross-linker concentration gives positive input to create higher cross-linked hydrogel networks that suppress the living chain's motion. However, when comparing the result of 10-5-2 (4.6 ± 1.2 mg/cm^3) and 10-10-2 (4.8 ± 3.2 mg/cm^3), no obvious difference regarding hydrogel loading can be found. In summary, monomer concentration variation plays a dominant effect on the hydrogel loading, while the cross-linker degree and APS concentration have no significant influence.

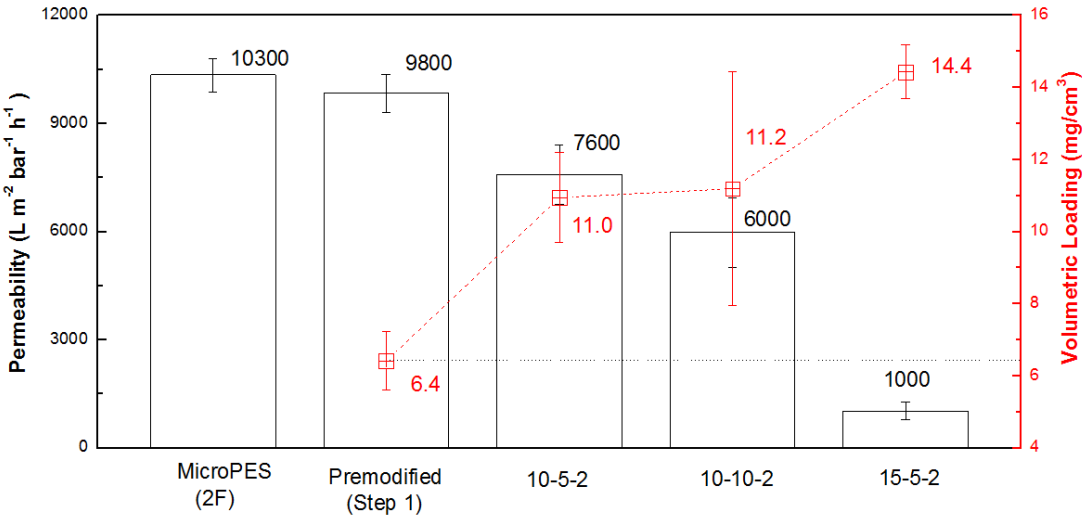

Fig. 4.23 The permeability and grafting degree (total volumetric loading) of the pristine membrane (MicroPES-2F), premodified membrane, and the GAEMA coated membrane (10-5-2, 10-10-2, and 15-5-2).

Permeability is another criterion to evaluate the usability of the modified membrane in terms of filtration performance. Fig. 4.23 shows the pure water permeability variation along with the modification procedures. The pristine membrane has a pure water permeability of 10300 LMH bar, and it shows a slight permeability decline to 9800 LMH bar after premodifying the pristine membrane by PBD-300. An obvious tendency of permeability decreasing with higher hydrogel loading can be found. Higher hydrogel grafting will lead to a less effective water transport path by narrowing the pore diameter (cf. Fig. 4.23). Moreover, the membrane modified by using monomer condition of 15-5-2 will leads to border pore size distribution, as shown in Fig 4.24. The border pore size distribution mainly due to partial pore blocking that can be verified by SEM images (cf. Fig 4.20).

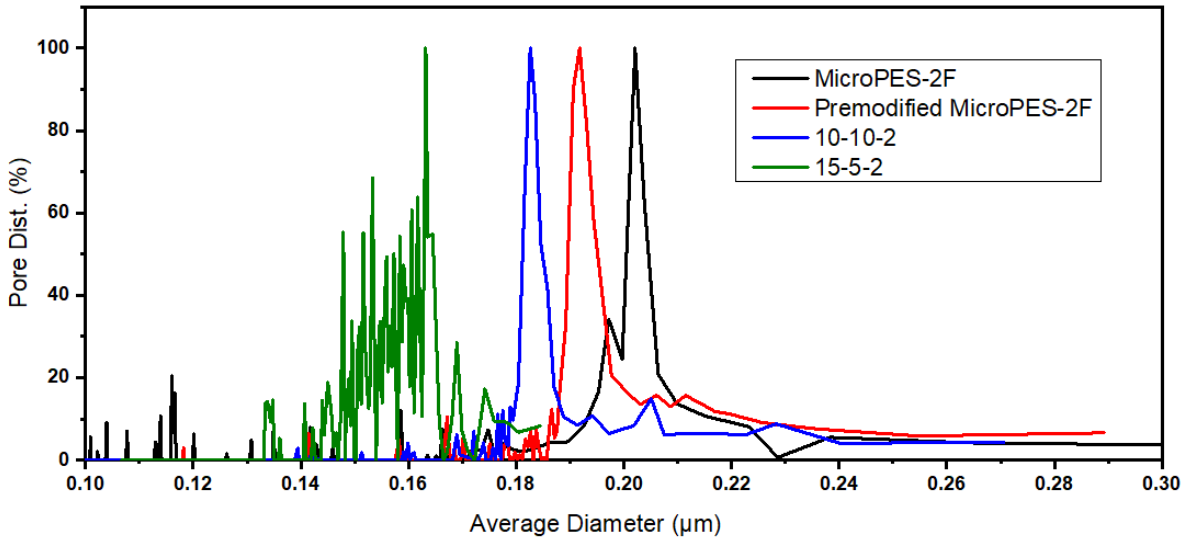

Fig. 4.24 Pore size distribution of pristine membrane, premodified membrane, and the GAEMA coated membrane (10-10-2 and 15-5-2)

4.2.4.2 Influence of circulation flow rate during monomer recirculation

Operation conditions should be considered, especially the applying circulation flow rate, which could impact the mass transport condition and flow condition in the membrane modification process. A good mixing can maintain a constant monomer, cross-linker, and APS concentration inside the membrane pore and to compensate the consumed chemicals duly, i.e., an efficient chemicals replacement. Conversely, there is a negative effect from the over stirring or over mixing that would facilitate the live chain motion at the hydrogel growing surface, which will enhance the termination rate, resulting in a lower degree of grafting [115]. Table 4.19 presents the result of hydrogel loading by applying different flow rates during the recirculation of monomer solution.

Table 4.19 The permeability, grafting degree (hydrogel loading) and calculated residence time in different modification conditions.

Monomer condition	Flow rate (mL/min)	Residence time (s)	P. (LMH bar)	Total loading (mg/cm^3)	Hydrogel loading (mg/cm^3)
15-5-2	1.5	1.6	1000 ± 200	14.4 ± 0.5	8 ± 0.5
15-5-2	4.5	0.5	1300 ± 400	14.8 ± 0.8	8.4 ± 0.8
10-5-2	0.5	4.8	7300 ± 900	10.5 ± 1.3	4.1 ± 1.3
10-5-2	1.5	1.6	7600 ± 800	11.0 ± 1.2	4.6 ± 1.2
10-5-2	4.5	0.5	-	11.5 ± 0.25	5.1 ± 0.25

Apparently, for the monomer condition of 15-5-2 and 2, increasing the flow from 1.5 to 4.5 mL/min doesn't have a significant difference regarding hydrogel loading and permeability after modification. The same conclusion can also be found when comparing the hydrogel loading and permeability of the membranes modified by 10-5-2 of monomer condition under 0.5, 1.5, and 4.5 mL/min flow rate. The circulation flow rate would directly affect the flow condition inside the membrane pores, leading to various mixing conditions. For such, the flow condition should be defined, i.e., the Re number at the specific recirculation flow rate.

To qualitatively estimate the flow condition, here assume that the tube diameter is equivalent to pore diameter, and the *Re* number can be calculated via Eq. 4.12. The calculated *Re* is in the scale of ~4.8 x 10^{-6} – 4.3 x 10^{-5}, corresponding to the flow rate from 0.5 - 4.5 mL/min. Such a small *Re* number is indicating a laminar flow condition during the modification. Hereof, varying the flow rate from 0.5 - 4.5 mL/min would not change the flow condition. Since the monomer solution presents as laminar flow during the recirculation, the flow velocity at the solid surface (within the boundary layer), i.e., hydrogel growing surface, would not have a significant difference under three selected flow rates of 0.5, 1.5, and 4.5 mL/min. Thus the living chain motion at the hydrogel growing surface is similar under the selected flow rates window, which leads to similar termination rates. On the other hand, the residence time of monomer solution can be easily calculated as 4.8, 1.6, and 0.5 s when the applied flow rate is 0.5, 1.5, and 4.5 mL/min, respectively. The orders of magnitude with respect to the applied residence time is higher than the

typical radical lifetimes that are in the lower microsecond (ms) range. Therefore, the adapted flow rate would not impact the polymerization step. Beside, such small residence time variation from 0.5 - 4.8 s would not significantly differentiate monomer replacement efficiency inside the membrane pores.

4.2.4.3 Influence of membrane pore size

Table 4.20 The information of MicroPES-2F and MicroPES-6F

Membrane	Thickness (μm)	Pore size (μm)	Porosity (%)	Surface charge
MicroPES-2F	116	0.2	80.0	Negative
MicroPES-6F	109	0.6	74.0	Negative

Table 4.21 The membrane performance and absolute hydrogel loading of the modified MicroPES-2F and MicroPES-6F.

Note	Pristine membrane	P. (LMH bar)	Total loading (mg/cm^3)	Hydrogel loading (mg/cm^3)
Premodified	MicroPES-2F	9800 ± 500	6.4± 0.8	-
10-5-2	MicroPES-2F	7600 ± 800	11.0 ± 1.2	4.6
10-10-2	MicroPES-2F	6000 ± 1000	11.2 ± 3.2	4.8
15-5-2	MicroPES-2F	1000 ± 200	14.4 ± 0.5	8.0
Premodified	MicroPES-6F	31200 ± 1200	2.4 ± 1.0	-
10-5-2	MicroPES-6F	27000 ± 600	6.5 ± 0.7	4.1
10-10-2	MicroPES-6F	25800	11.6 ± 2.3	9.2

Two membranes, MicroPES-2F and MicroPES-6F, were used to investigate the influence of pore size on hydrogel loading, and the information of each membrane can be found in Table 4.20. As shown in Table 4.21, MicroPES-2F can adsorb more PBD-300 (6.4 ± 0.8 mg/cm^3) than MicroPES-6F (2.4 ± 1.0 mg/cm^3). The higher adsorbed mass of PBD300 in MciroPES-2F is due to the higher specific area because of the smaller pore size and higher porosity. Although the MicroPES-6F adsorbed less PBD-300, the final modified MicroPES-6F showed comparable hydrogel loading as PBD-300 modified MicroPES-2F. A

similar hydrogel loading can be found when using monomer condition of 10-5-2 to treat premodified MicroPES-2F (4.6 mg/cm^3) and MicroPES-6F (4.1 mg/cm^3). When applying monomer condition of 10-10-2, more hydrogel can be grafted onto the MicroPES-6F (9.2 mg/cm^3) than MicroPES-2F (4.8 mg/cm^3). Seemingly the modification applied onto the MicroPES-6F gives a more promising result in terms of hydrogel loading and turnability of modification. It could be a hint that the membrane with a larger pore size is preferable for higher functionalization. The change of membrane pore size would lead to different flow conditions and different pore curvature. For the flow condition in MicroPES-6F, the calculated *Re* number is 1.4 x 10^{-5} – 1.3 x 10^{-4}, which is still showing laminar flow condition in the pores of MicrPES-6F. Thus, the better hydrogel loading can't be interpreted by flow condition variation. The surface-initiated polymerization of hydrogel in this work was carried out in the confined environment, i.e., in the membrane pores. And it has been widely reported that surface parameters restrict the polymerization kinetics and the molecular weight is affected by the concave surface parameters such as pore size [135–138]. In cased of the concave surface, the higher curvature will lead to a decrease in molecular weight. In this work, the typical grafted layer is in the range of 10 - 100 nm (cf. Fig. 4.24), which is the same scale of membrane pores (200 - 600 nm), thus the polymerization kinetics would be significantly affect by the curvature of membrane. And this conclusion perfectly fits the scenario where the pores in membrane MicroPES-6F are less concave than MicroPES-2F due to the larger pore size in MicroPES-6F. Therefore, a thicker GAEMA coating is prone to be formed in the less concave surface, i.e., the membrane with a larger pore size.

4.2.4.4 The Influence of PBD molecular weight

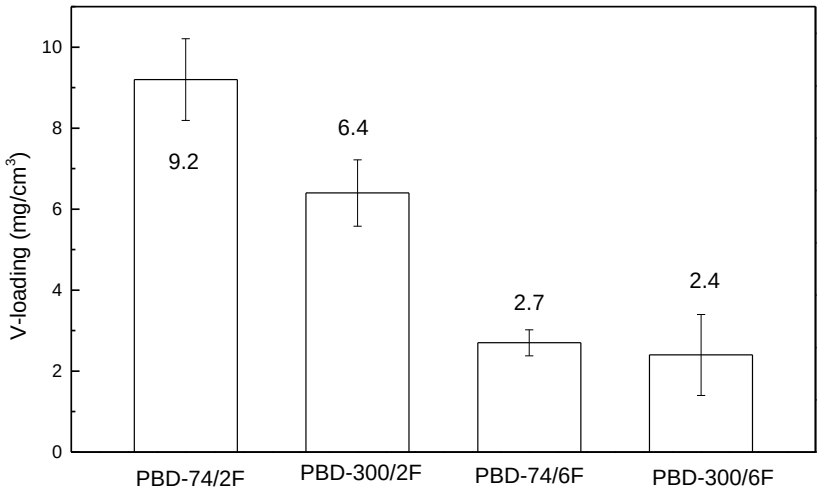

Fig. 4.25 The volumetric loading of the macroinitiators PBD-300 and PBD-74 on the membranes MicroPES-2F and MicroPES-6F, respectively.

Since macro-initiator plays an important role in accelerating APS decomposition for free radicals generation, the influence of PBD size will be discussed here. The polymer adsorption is on the basis of loops and tails mechanism, where the only a part of chain will anchor to the solid surface and the rest of segments is forming loops or tails on the z-direction relative to the solid surface. Thus the size of the adsorbed polymer impacts the adsorption behaviour. Generally, the polymer with higher molecular weight is more prone to adsorb than low Mw polymer because of the less stability of large polymer in the solution [125]. On the other hand, due to the larger size of higher Mw polymer, loosen packing on the membrane surface will lead to a relatively lower amount of adsorption, especially in the case of charged polymers because of repulsion between polymers chains. When speaking of stability, the larger adsorbed macromolecules would have higher stability due to more anchor sites on the substrate. Fig. 4.25 presents the PBD-300 and PBD74 adsorption onto MicroPES-2F and MicrpPES-6F, respectively. Firstly, MicroPES-2F can adsorb more PDB-74 and PBD-300 than MicroPES-6F because of the higher specific adsorption area in MicroPES-2F. Interestingly, when macroinitiator adsorption on

MicroPES-2F, the membrane can uptake more PBD-74 than PBD-300. The molecular weight of prepare PBD-300 and PBD-74 are characterized by size exclusion chromatography. Therefore, the Mw obtains from GPC measurement can give a strong indication of the coil size of PBD-300 and PBD-74. The higher adsorption of PBD-74 on MicorPES-2F is due to the denser packing of PBD-74 because of its smaller coil size. It also gives a same conclusion when MicroPES-6F adsorber PBD-300 (2.4 mg/cm^2) and PBD-74 (2.7 mg/cm^2).

4.2.5 Adsorption performance of the selected membrane adsorbers

The boron removal performance has been preliminarily assessed by recirculating 4 mL of 5 mg/L of boron solution through the membrane with an effective membrane area of 3.46 cm^2, and the adsorption process was carried out for 18 h. The boron uptake and boron removal rate are shown in Table 4.22. Additionally, the boron removal performance of modified UF membranes is enclosed for comparison. The modified MF membrane shows poor boron uptake (1.6, 1.2, and 2.4 mg/m^2 for samples 10-5-2, 10-10-2, and 15-5-2, respectively) in comparison to the modified UF membrane. Such poor boron removal performance can be mainly blamed due to the insufficient hydrogel grafting amount and inhomogeneous grafting.

Table 4.22 The boron uptake of modified UF membrane (Section 4.1) and modified MicroPES-2F MF membrane (this section).

Probe	Monomer condition	Pristine membrane	Macroinitiator	Boron uptake (mg/m^2)	removal rate (%)
1	PEI-10	PES-50	-	10.7	12.4
2	PEI-5	PES-50	-	9.7	11.3
3	PEI-2	PES-50	-	9.5	11
4	10-5-2	MicroPES-2F	PBD-300	1.6	1.9
5	10-10-2	MicroPES-2F	PBD-300	1.2	1.4
6	15-5-2	MicroPES-2F	PBD-300	2.1	2.4

4.2.6 Interim summary for Section 4.2

So far, the feasibility of macro-initiator meditated surface-initiated polymerization has been qualitatively and quantitatively verified by several experiments. The adsorbed macro-initiator showed a good co-initiation effect to decompose APS and generating free radicals for later polymerization. Most importantly, the hydrogel can be successfully grafted onto the membrane surface via this macro-initiator meditated surface-initiated polymerization.

The influence of monomer solution condition, flow rate, membrane pore size on hydrogel loading amount has been discussed. Regarding the monomer solution condition, only monomer concentration plays a dominant effect on final hydrogel loading mass, where the influence of APS and cross-linker concentration have a limited impact.

Apart from the monomer solution conditions, the influence of the applied recirculation flow rate is discussed. In the selected flow rate ranging from 0.5 – 4.5 mL/min, it has no apparent impact on hydrogel loading. It shows laminar flow in the membrane pore at the selective flow rate window.

Moreover, two kinds of macro-initiators are used in the premodification step, and the smaller polymer can be adsorbed by both two membranes, MicroPES-2F and MicroPES-6F. Also, the membrane with a smaller pore size can adsorb more macro-initiator because of its larger specific surface area.

However, the modified MF membrane showed suboptimal boron adsorption capacity, which is mainly due to the inhomogeneous modification and the relatively low hydrogel loading.

4.3 MF membrane modification via an integrated initiation system (surface and bulk initiation)

The discussion in Section 4.2 provides lots of value in guiding several possibilities to improve hydrogel functionalization degree. In the premodification step (macroinitiator adsorption), the membrane with a larger pore size and the macro-initiator with a smaller size is preferable; for the monomer solution conditions, higher GAEMA concentration can lead to higher hydrogel loading. Besides, homogenous modification on the overall accessible modification area is thought to be the core of achieving higher hydrogel loading. For another, applying an additional initiation process to assist hydrogel grafting can also be put into the contest. Based on the above comments, a new modification strategy has been figured out to improve hydrogel grafting, and the details will be discussed here.

In this section, an integrated initiation system was applied for membrane surface modification by a GAEMA hydrogel coating. The concept will be first introduced (Section 4.3.1). Before applying the modification to the pristine membrane, the feasibility of this integrated initiation system will be evaluated (Section 4.3.2). After that, the modification parameters have been pre-screened for the subsequent parameter optimization (Section 4.3.3). A two-stage parameter optimization has been done: the modification parameters were first optimized via the Design of Experiment (DOE); the additional parameter fine screening has been done on the ground of the given parameters window from DOE (Section 4.3.4). Finally, the boron and filtration performance of the optimal membrane have been comprehensively studied (Section 4.3.5)

4.3.1 Concept

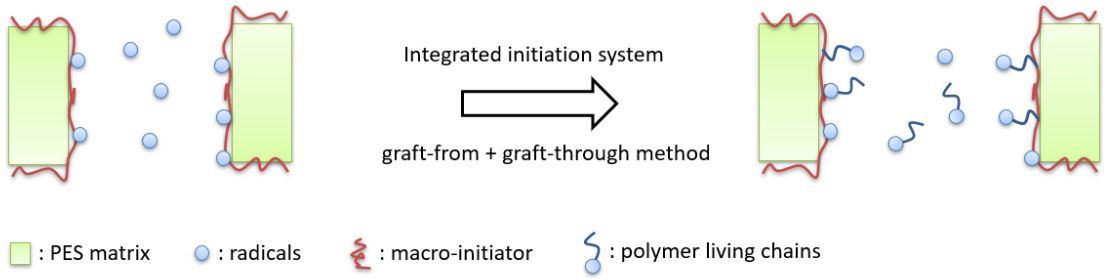

Fig. 4.26 Schematic presentation of the principle of integrated initiation system with simultaneous surface-initiated and bulk polymerization.

In this section, an integrated initiation system has been introduced to achieve a higher degree of GAEMA hydrogel grafting. Fig. 4.26 shows the principle of the surface initiation system and the integrated initiation system. The membrane in both systems has been premodified by a macroinitiator, thus accelerating the decomposition of APS and generating free radicals at the membrane surface. For the integrated initiation system, free radicals are also created at the bulk solution to form the living polymer chains in the bulk phase by adding TEMED as an accelerator. Thus the integrated initiation system can be considered as the membrane surface modification via simultaneous graft-through and graft-from strategy. More hydrogel is thought to be grafted onto the membrane surface because of the extra initiation in the bulk solution. However, because of the free radicals in the bulk phase, the gelation of monomer solution should be avoided, otherwise, the gel would completely block the membrane pores and the tubing system in the recirculation apparatus. For this reason, the monomer and cross-linker concentration should be carefully designed to prevent undesired gelation in the bulk solution. Based on the gelation result of different monomer solution compositions in Appendix A (cf. Table A1), the security window of monomer solution, in which no bulk gelation occurs, can be found in Table 4.23. Briefly, when monomer concentration is 10 and 15 wt%, the relative cross-linker concentration to monomer shouldn't be excess 2 wt%; while to the monomer concentration of 5 wt%, the relative cross-linker concentration to monomer shouldn't be below 5 wt%.

Table 4.23 The security window for monomer condition to prevent bulk gelation.

C_{GAEMA} (wt %)	C_{APS} (wt‰)	APS/TEMED	$C_{cross-linker}$ (wt %)
15	2	2.25	≤ 2
10	2	2.25	≤ 2
5	2	2.25	≤ 5

4.3.2 Feasibility test of the integrated initiation system

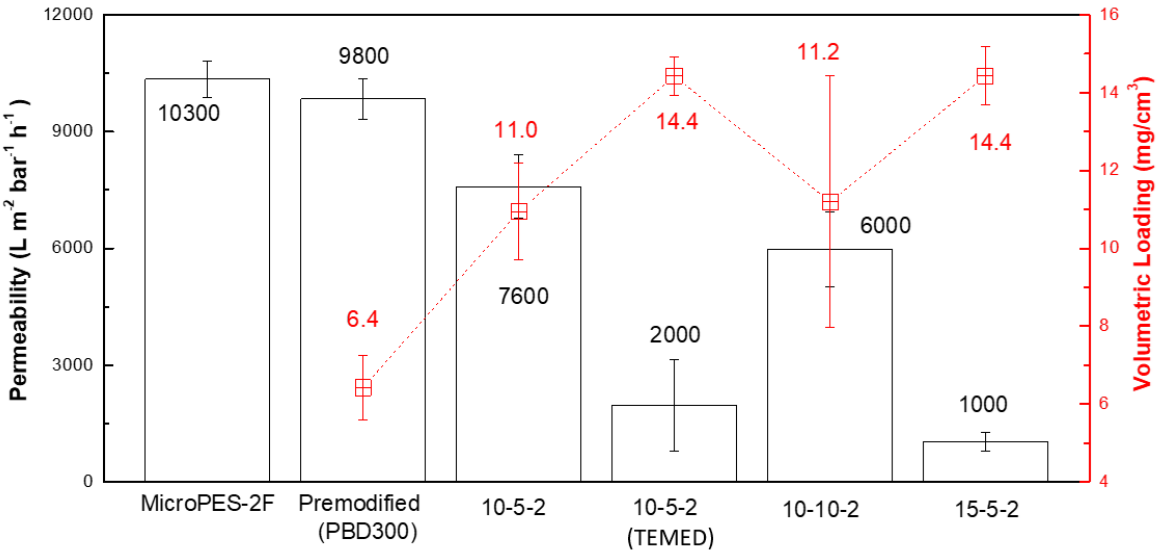

Fig. 4.27 The permeability and grafting degree (volumetric loading) of the pristine membrane, PBD-300 premodified membrane, and the GAEMA coated membrane prepared via integrated initiation system (10-5-2 TEMED) or surface initiation system (10-5-2, 10-10-2, 15-5-2).

The assessment of this integrated initiation system has been done by comparing the hydrogel loading of a controlling experiment in which no TEMED was used. Fig. 4.27 presents the membrane performance evaluation along with modification procedures on MicroPES-2F. It has total loading of 11.0 mg/cm^3, i.e., hydrogel loading of 4.6 mg/cm^3, when is TEMED absent in the monomer solution of 10-5-2. In comparison, the total loading can be improved to 14.4 mg/cm^3, i.e., hydrogel loading of 8 mg/cm^3, after introducing free radicals in the bulk phase under the same monomer solution condition. Moreover, the membrane modified by monomer condition of 15-5-2 without TEMED presents the same total loading as the membrane modified by monomer solution of 10-5-2 containing TEMED.

With respect to the membrane permeability, obviously, the higher hydrogel loading leads to lower permeability. Still, for the modified membrane with the same total loading of 14.4 mg/cm^3, the membrane modified by the integrated system has higher permeability (10-5-2 with TEMED, 2000 LMH bar) than the membrane modified without TEMED addition (15-5-2, 1000 LMH bar). Such a positive result indicates more efficient hydrogel grafting in such an integrated initiation system (10-5-2 with TEMED) compared to the membrane modified by monomer conditions with adding TEMED (10-5-2 and 15-5-2).

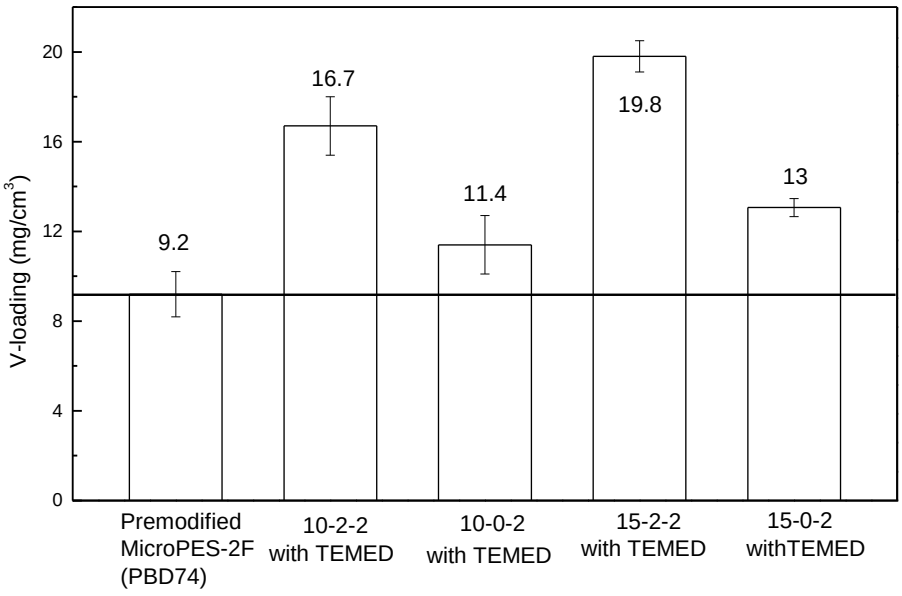

Fig. 4.28 Grafting degree (volumetric loading) of the pristine membrane, PBD-74 premodified membrane, and the GAEMA coated membrane via surface initiation system (without TEMED) or integrate initiation system (with TEMED).

The necessity of using cross-linker in the integrated initiation system has also been studied, and the result can be found in Fig. 4.28. In comparison with the monomer solution with cross-linker (10-2-2 and 15-2-2), the membrane modified by a monomer solution without cross-linker shows significantly lower total grafting of 11.4 mg/cm^3 (10-0-2) and 13 mg/cm^3 (15-0-2), respectively. Three reasons can interpret this result: 1) the use of cross-linker attributes to the cross-linked network formation at the membrane surface that will suppress the chain termination rate; 2) the cross-linker increase the double bond

concentration in the system leading to a higher polymerization rate, but it only plays minimum effect; 3) the formed cross-linked network would have physical entanglement with porous membrane structure leading to more stable grafting, and this should be the main reason.

So far, it has been demonstrated the significant advantage of an integrated initiation system regarding hydrogel loading improvement. However, the extra mass gain of hydrogel loading in the integrated initiation system may come from the additional graft-through process by bulk living polymer, i.e., covalently binding, and/or the entanglement between the cross-linked polymer and porous membrane structure, i.e., physically grafting. To figure out the extent of the contribution of the entanglement effect, a control experiment of which no surface initiation polymerization is applied should be done in which no surface initiation polymerization is applied. Table 4.24 presents the boron uptake and filtration performance of the two modified membranes with or without applying pretreatment. When pumping the TEMED included monomer solution through the pristine membrane, i.e., no surface initiation occurs, the contribution of hydrogel grafting comes from the entanglement between bulk polymer and porous membrane structure. Compared with the premodified membrane, directly performing hydrogel grafting on pristine membrane shows a lower boron binding capacity of 1.5 mg/m^2 and higher permeability of 2200-3100 LMH bar. It could indicate the importance of the premodification step, in which the macro-initiator can improve the formation and adhesion of hydrogel coating. The significant improvement in the functionalization degree in the integrated initiation system is contributed by the bulk polymer graft-through process and physical entanglement between cross-linked polymer and porous membrane structure.

Table 4.24 The membrane performance after adapting the factors which giving positive input, i.e., PBD-74, MicroPES-6F and TEMED.

Modification condition	Macro-initiator	Pristine membrane	P. (LMH bar)	TEMED/APS	Hydrogel loading (mg/cm^3)	Boron uptake (mg/m^2)	Boron binding/gel* (mg/g)
10-5-2	PBD-300	2F	7600 ± 800	0	4.6	1.6	3.0
10-10-2	PBD-300	2F	6000 ± 1000	0	4.8	1.2	2.2
15-5-2	PBD-300	2F	1000	0	8.0	2.1	2.3
15-2-2	Without PBD	2F	2200-3100	1	-	1.5	-
15-2-2	PBD-74	2F	870 - 1200	1	10.6	8.6	7.0
15-2-2	PBD-74	6F	550 ± 586	1	34.3	27.4	7.3

* the boron binding per grafted hydrogel was calculated when input the membrane thickness (cf. Table 4.16)

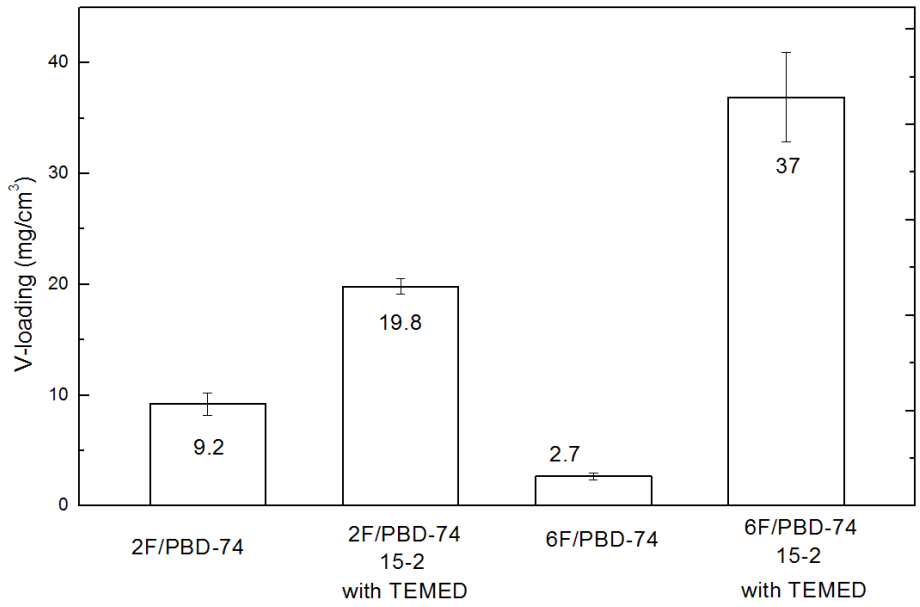

Fig. 4.29 The grafting degree of the modified MicroPES-2F and modified MicroPES-6F via integrated initiation system. The macroinitiator and monomer condition is PBD-74 and 15-2-2, respectively.

The discussion in section 4.2.4 already gives an overview of the influence of monomer condition, membrane pore size, flow rate, and macroinitiator. Larger membrane pore size, higher GAEMA concentration, and smaller macroinitiator may afford positive input regarding the amount of hydrogel grafting. The way to achieve maximum hydrogel loading

is to combine all the parameters enable to provide positive input on the enhancement of hydrogel loading. However, the highest monomer concentration is limited to 15 wt % because of the solubility of GAEMA. Fig. 4.29 presents the total loading result of the two modified membranes, MicroPES-2F and MicroPES-6F, upon the optimal modification condition where: 1) using 15-2-2 as monomer solution condition; 2) PBD-74 macroinitiator in premodification process; 3) integrated initiation system as modification approach. When select MicroPES-2F as the based membrane, it achieves total loading of 19.8 mg/cm^3 (or hydrogel loading of 10.6 mg/cm^3), while it has a total loading of 37 mg/cm^3 (or hydrogel loading of 34.3 mg/cm^3) when adapting analogous modification on MicroPES-6F.

In order to give straight forward assessment between two initiation systems, the boron uptake, the permeability, and the hydrogel loading of each selected modified membrane have been collectively summarized in Table 4.24, additionally. A superior boron uptake performance can be observed when adapting optimal parameters to membrane modification, of which using higher monomer concentration, adapting larger pore size, applying the integrated initiation system. And the superior boron uptake performance mainly due to a higher degree of grafting. Conversely, the membrane with higher hydrogel loading show relatively low permeability of 870 -1200 LMH bar and 550 ± 586 LMH bar, respectively.

The boron binding per grafted hydrogel has been calculated and presented in Table 4.24 as well. It shows 2.2-3.0 mg/g of boron binding capacity for the affinity coating prepared via surface-initiated polymerization, which is in good agreement with the binding capacity for bulk hydrogel (cf. Table 4.15). Interestingly, the boron binding per grafted hydrogel for the affinity coating prepared via an integrated initiation system gives surprisingly higher specific boron binding capacity of 7.0 and 7.3 mg/g, respectively. Theoretically, the specific boron binding capacity is only related to the mass of grafted hydrogel, but it looks like the modification strategy also impacts grafted hydrogel's binding performance. This unusual phenomenon can be interpreted by the outcome of modification homogeneity, of which a homogenous hydrogel coating could provide more accessible binding sites and better mass transport efficiency for boron binding.

4.3.3 Two-stage modification parameter optimization

4.3.3.1 Definition of evaluation criteria for parameter optimization

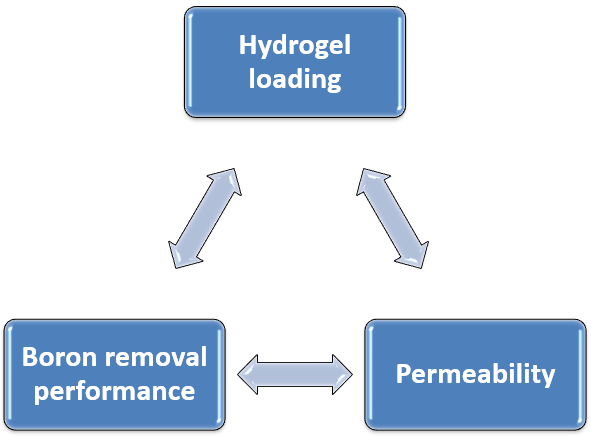

Fig. 4.30 The correlation among hydrogel loading, boron removal performance, and permeability.

It has been found out that several modification parameters will jointly determine the final boron uptake and filtration performance, and each parameter would have various contributions to the final filtration and adsorption performance. An even more complicated situation would appear when the impact of an input parameter depends on the setting of a second input parameter. Thus, it's of extreme importance to define the evaluation criterion prior to move ahead to parameter optimization work. Fig. 4.30 present the three criteria, hydrogel loading, boron removal performance, and permeability, to evaluate respective modification conditions. The hydrogel loading will directly affect the boron removal performance and permeability in two opposite directions: higher hydrogel loading will give positive input on boron removal but negative input on permeability. Thus, for the sake of simplicity, it would be reasonable to focus on only two criteria: boron removal performance and permeability. Also, these two criteria are more attractive because of the practical reason.

Based on the previous discussion, MicroPES-6F membrane, PBD-74, the flow rate of 3 mL/min, and 2 wt‰ of APS were selected as substrate, macroinitiator, operating flow rate, and initiator concentration in the modification, respectively. Hereof, the remaining alterable parameters are monomer concentration, cross-linker concentration, and

TEMED/APS ratio. In order to optimize modification parameters, enough data volume and replicates are necessary. Table. 4.25 summarizes the overall input modification parameters and the corresponding output performance of boron uptake and permeability.

Table 4.25 The membrane performance of the membrane modified by different monomer conditions.

Exp.	Monomer solution	TEMED/APS	Boron uptake (mg/m^2)	Permeability (LMH bar)
1	-	-	-	40200
2	15-2-2	1	27.4	550 ± 586
3	15-2-2	0.5	16.8	429 ± 348
4	15-1-2	1	9.2	6600 ± 1150
5	15-1-2	0.5	6.7	8900 ± 2000
6	10-2-2	0.5	5.7	25700 ±2100
7	10-2-2	1	4.6	16500 ± 2000
8	10-1-2	1	4.0	36600 ± 700
9	10-1-2	0.5	4.9	27800 ± 1300

4.3.2.2 Stage I: Parameter optimization via Design of experiment (DOE)

The membrane modification is carried out under 9 conditions. The change of one or few independent input variables, e.g., cross-linker concentration, monomer concentration, or APS/TMEMD ratio, would change one or few dependent output variables, e.g., boron binding capacity or flux. Thus, applying a scientific analysis tool is of extreme importance for the sake of time efficiency and data reliability. DOE is a statistical methodology aiming to describe and explain the hypothesized correlation between input variables and output variables. The orthogonal array is commonly used in DOE to reduce the number of experiments, and it's suitable for main effect analysis. Besides, when parameter interaction happens, the full factorial array is preferable, and the full factorial array can give reliable information and main effect analysis.

Table 4.26 The selected factors and level for DOE analysis

Factor / Level	$C_{monomer}$ (wt %)	$C_{cross\text{-}linker}$ (wt %)	TEMED/APS
Level 1	10	1	0.5
Level 2	15	2	1

The full factor array (L8 (23)) experiment is conducted in this work to have convincing results. Besides, variability analysis (ANOVA) can be done when a full factorial array experiment is done. Table 4.26 presents the three input factors of monomer, cross-linker, and TEMED concentration, and each factor has two levels. As described in Section 4.3.2.1, the boron uptake and the permeability of the modified membrane are chosen as the output performance.

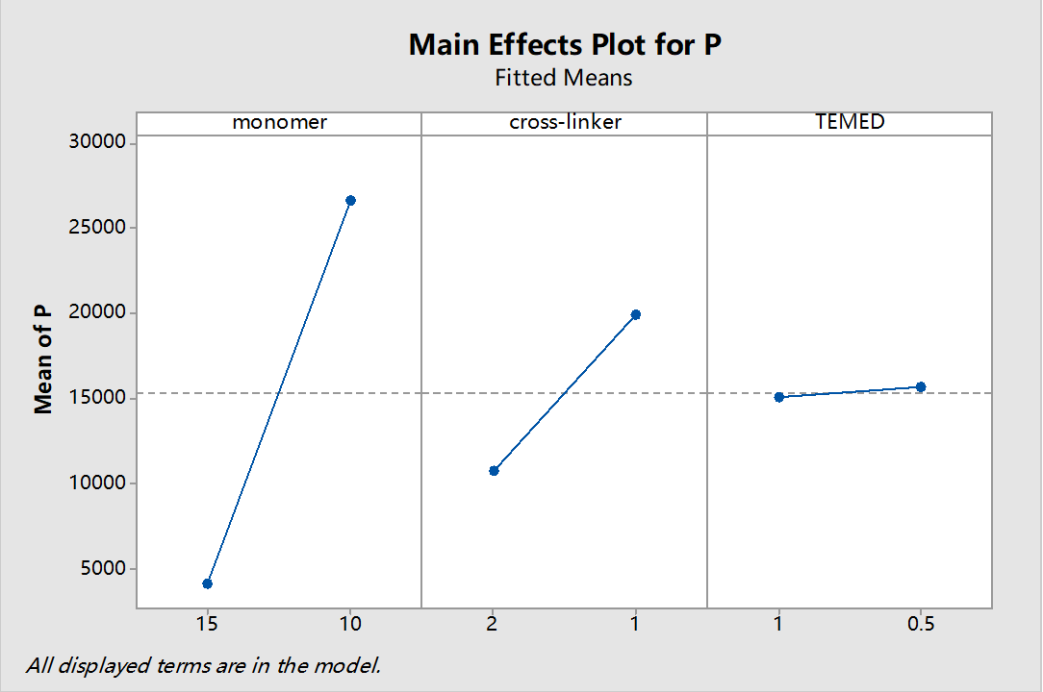

Fig. 4.31 Main effect analysis on permeability in L8 (2^3).

The main effect analysis for membrane permeability has been done, and the main effect plot for permeability can be found in Fig 4.31. Firstly, both $C_{monomer}$ and $C_{cross\text{-}linker}$ obviously influence permeability, while the $C_{monomer}$ plays a predominant effect. Applying lower $C_{monomer}$ or $C_{cross\text{-}linker}$ for membrane modification would lead to a higher permeability. Membrane permeability is strongly dependent on the means pore size and pore distribution. The previous result shows that hydrogel grafting is proportional to the monomer concentration because a higher monomer concentration will promote polymerization rate. A high cross-linked hydrogel coating at the pore wall would lead to higher flux when functionalizing surface via graft-from approach. However, the real scenario in the integrated initiation systems is more complicated where graft-through and graft-from approaches occur simultaneously. Thus, it is difficult to discuss the detail regarding the influence of cross-linker concentration. It is well known that a higher amount of TEMED would lead to a faster decomposition rate of APS, thus increasing free radical concentration in the bulk solution. And the higher free radicals concentration will promote polymerization rate. The faster the polymerization rate, the larger polymer will be form and covalently graft to the membrane surface. Interestingly, the permeability slightly decreases

when increasing TEMED concentration from 0.5 to1.0 wt‰, which means the variation of TEMED/ASP ratio from 1 to 2 has no significant impact on permeability.

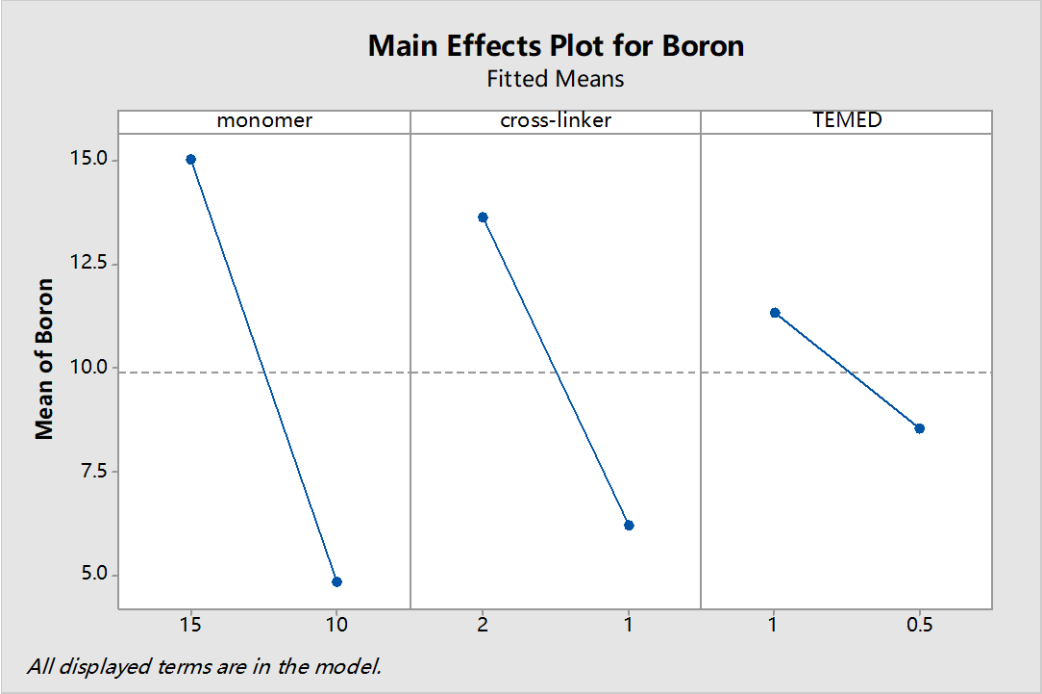

Fig. 4.32 Main effect analysis on boron binding in L8 (2^3).

Fig 4.32 presents the main effect plot for boron binding. Apparently, both $C_{monomer}$, $C_{cross\text{-}linker}$, and TEMED concentration significantly influence boron adsorption capacity, and a higher amount of monomer, cross-linker, and TEMED contribute to more boron binding. The boron uptake capacity is dependent on the number of available binding sites in the coated membrane, and the higher the hydrogel amount would lead to more boron uptake. The amount of hydrogel loading is positively associated with monomer, cross-linker, and TEMED concentration. It shows a contradictory outcome when comparing the influence of TEMED on permeability and boron uptake, where higher TEME leads to more boron biding (cf. Fig. 4.32) but an unapparent influence on permeability (cf. Fig. 4.31). This contradicts conclusion indicates a possible existence of a pair of parameter interaction where the impact of TEMED is dependent on the setting of another input parameter, or vice versa. Thus, performing parameter interaction analysis is imperative.

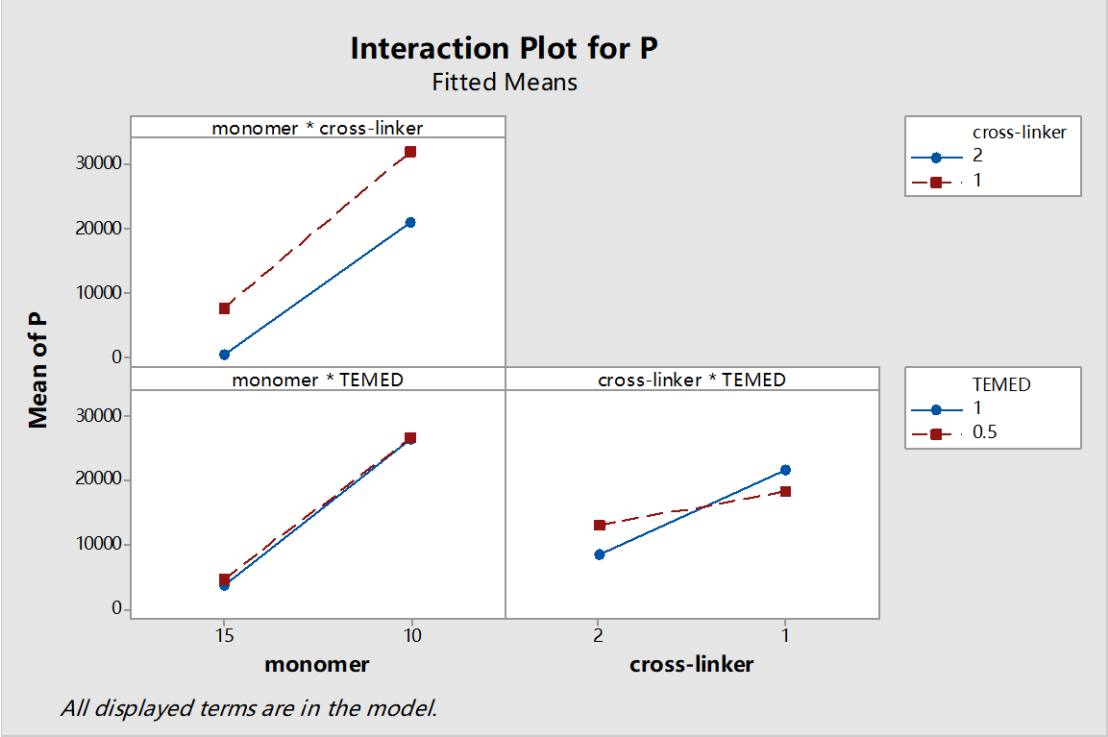

Fig. 4.33 Parameter interaction analysis on permeability in L8 (2^3).

Fig. 4.33 presents the parameter interaction plot for permeability, in which three pairs of parameter interactions are monomer/cross-linker, monomer/TEMED, cross-linker/TEMED, respectively. The top left plot (cf. Fig. 4.33) presents the analysis result of the monomer/cross-linker pair. There is no interaction between monomer and cross-linker because two curves have no observable intersection in the selected concentration window. The monomer/TEMED interaction is shown in the bottom left plot (cf. Fig. 4.33). The interaction effect is negligible because two curves have similar slop and intercept, leading to difficulty distinguishing the intersection. However, due to the similar slop and intercept of two curves in the bottom left plot, the monomer/TEMED interaction can be deemed as a weak interaction if the interaction exists. Finally, when coming to the cross-linker/TEMED interaction, an obvious intersection of two curves can be observed in the bottom right plot (Fig.4.33), indicating a strong interaction. Such strong interaction means that the influence of TEMED can be disturbed when varying the cross-linker concentration simultaneously, and both factors would conjointly impact the output performance of permeability. The parameter interaction analysis reveals the possible reason for the contradictory outcome of TEMED impaction on permeability and boron uptake, as just mentioned previously.

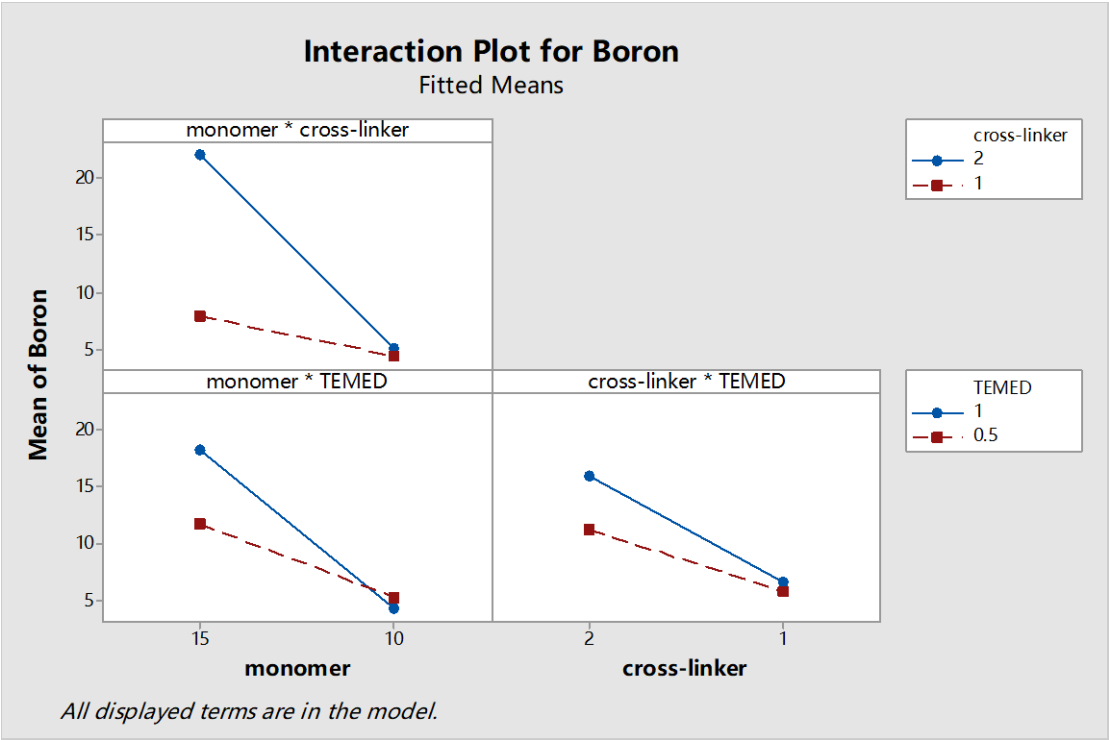

Fig. 4.34 Parameter interaction analysis on boron binding in L8 (2^3).

The interaction plot for boron uptake has been studied additionally, and the result can be found in Fig. 4.34. It only shows interaction regarding monomer/TEMED pair within the selected monomer concentration window of 10-15 wt%. According to the previous discussion that both monomer concentration and TEMED concentration would impact the polymerization rate, the higher polymerization rate may contribute more hydrogel loading, namely more boron binding sites. No apparent interaction can be found within the selected concentration windows for the monomer/cross-linker and TEMED/cross-linker pairs.

Based on the DOE study of main effect analysis and parameter interaction analysis, the tendency of respective parameter influence and parameter association has been revealed. However, the final membrane should have applicable permeability in consideration of practical reasons. For the microfiltration, a permeability around 10000 LMH bar should be usable. Base on the permeability setting of ~10000 LMH, the concentration windows of each parameter can be figured out: 1) the TEMED/APS ratio can be fixed at 1 (i.e., 2 wt ‰) since it wouldn't affect permeability under given monomer and cross-linker concentration but gives a positive input on hydrogel loading; 2) the relative cross-linker concentration can

be fixed at around 2 wt%, or can be slightly increased when applying lower monomer concentration because the impact of cross-linker concentration variation on permeability is less prominent compared to the impact of monomer concentration; 3) at last, it should decrease the monomer concentration from 15 wt% for the sake of higher permeability. Table 4.27 presents the optimal concentration window for membrane modification, and a single-factor experiment can now be employed to efficiently search for the most suitable membrane modification parameters. Notably, the analysis of variance (ANOVA) should be done before moving ahead to the single-factor experiment, where it can reveal the significance level of the impaction of each factor (monomer, cross-linker, and TEMED concentration) on respective responses (boron uptake or permeability). The relevant result and discussion are presented in the next section.

Table 4.27 The monomer condition window for the further monomer solution conditioning.

$C_{monomer}$ (wt %)	$C_{cross\text{-}linker}$ (wt %)	C_{APS} (wt ‰)	TEMED/APS
< 15	> 2	2	1

4.3.2.3 Analysis of variance (ANOVA)

AVONA is part of the DOE methodology, and in the typical AVONA analysis, a null hypothesis is applied. The null hypothesis is a general statement or default setting that there is no significant correlation between input factors and output response. The null hypothesis in this work is specified: the monomer variation, cross-linker variation, or TEMED variation has no statistically significant impact on permeability or boron uptake, and the observed response variation in terms of permeability or boron uptake are just because of the random error in the process, for example, the measuring error in boron uptake or permeability, the inevitable error during monomer solution preparing, boron uptake variation because of the temperature fluctuation, and so on. A probability value (p-value) of 95 % (0.95) was commonly used in the null hypothesis. Thus in the AVONA analysis, the p-value obtained from the data processing result is essential to define whether the pre-specified null hypothesis is true or false. Specifically, when the p-value < 0.05, the pre-specified null hypothesis can be rejected, thus leading to a conclusion that the variation of input factors

(monomer, cross-linker, or TEMED) have a statistically significant impact on the output response (permeability or boron uptake).

Table 4.28 The result of ANOVA analysis.

Input	Response	F-value	P-value	Null hypothesis
Monomer	Permeability	23.46	0.003	true
Cross-linker	Permeability	0.91	0.376	false
TEMED/APS	Permeability	0.00	0.952	false
Monomer	Boron uptake	4.79	0.071	false
Cross-linker	Boron uptake	1.84	0.223	false
TEMED/APS	Boron uptake	0.20	0.668	false

One-way AVONA was used to analyze the p-value of each factor (monomer, cross-linker, and TEMED) to the corresponding responses (permeability and boron uptake). It should be noticed that during the One-way AVONA analysis, the non-objected factors were treated as intragroup factors. To be specific, in order to analyze the correlation between monomer and permeability, the influence of cross-linker and TEMEDM on permeability was treated as an intragroup factor, while the intergroup factors are the monomer concentrations of 15 wt% and 10 wt%. The analogous analysis on each input factor and responses have been applied in the data processing via Minitab 17, and the respective p-value can be found in Table 4.28. The monomer variation has a statistically significant impact on permeability, which is in line with the foregoing discussion. Secondly, the cross-linker doesn't have a statistically significant impact on boron uptake.

4.3.2.4 Stage II: Further optimization based on the DOE results

Based on the DOE and ANOVA analysis, an optimal concentration window for membrane modification can be located (cf. Table 4.27). Under the precondition of permeability of ~ 10000 LMH bar, the single factor experiment was applied to approach the final optimal modification parameter step by step. The overall monomer solution condition variation, the corresponding boron uptake, and permeability performance can be found in Table 4.29.

Table 4.29 The membrane performance of the modified membrane in stage II optimization.

Probe	Monomer solution	TEMED/APS	Boron uptake (mg/m^2)	Permeability LMH bar
1	12.5-1.5-2	1	6.1 ± 2.0	14100 ± 5500
2	12.5-2-2	1	5.7 ± 0.5	24100 ± 4900
3	12.5-2.5-2	1	6.4 ± 2.5	23800 ± 2500
4	12.5-4-2	1	-	blocking
5	13.5-2-2	1	4.9 ± 0	32200 ± 10500
6	13.5-2.5-2	1	6.8	2900 ± 2100
7	14-2-2	1	13.3 ± 0.8	16680 ± 2600

There is a trade-off relation between filtration throughput and appendant functionality, and such trade-off in this work is reflected by permeability and boron uptake, respectively. Fig. 4.35 presents the overview of the trade-off between boron uptake and permeability. The ideal modification should have high boron uptake together with high permeability. The membrane modified by the monomer condition of 14-2-2 with TEMED/PAS of 1 presents as the best trade-off at the giving a boron uptake of 13.3± 0.8 mg/m^2 and final permeability of 16680 ± 2600 LMH bar (highlighted in Fig. 4.35 with red circle). This positive result indicates a successful parameter optimization by applying a two-stage approach.

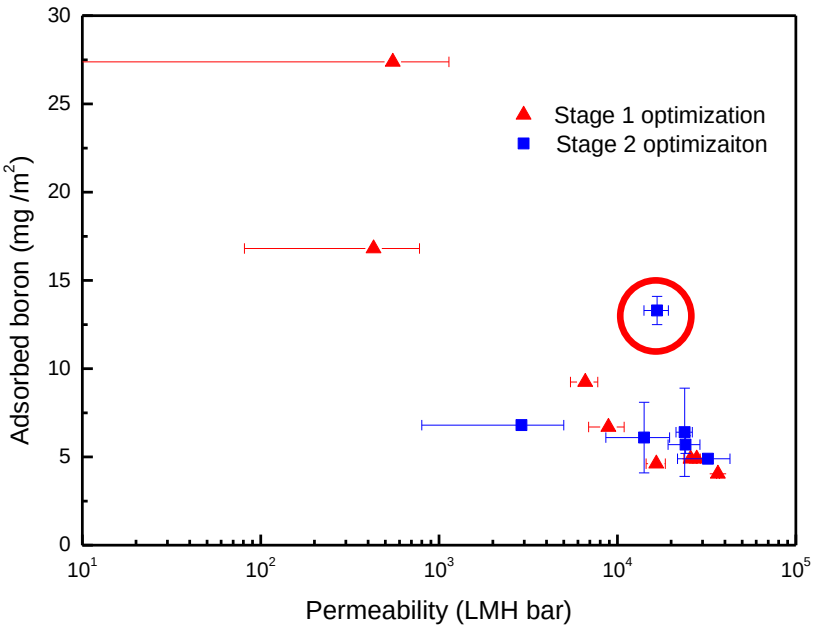

Fig. 4.35 The permeability and boron uptake of each modified membrane.

4.3.4 Boron adsorption performance

After DOE analysis and the subsequent parameter optimization, the optimal modification condition is 14-2-2, with a TEMED/APS ratio of 1 (cf. Table 4.30). This modification condition has been adapted to study the boron adsorption performance. Additionally, to mimic the seawater situation, the artificial seawater (ASW) was used as the media to prepare boron solution (cf. Table 3.3).

Table 4.30 The final optimal monomer condition.

$C_{monomer}$ (wt %)	$C_{cross-linker}$ (wt %)	C_{APS} (wt‰)	TEMED/APS
14	2	2	1

An interesting result can be found in Table 4.31 that the 14-2-2 membrane presents 32% more boron uptake in ASW, although both of ASW and pure boron solution (PBS) have the same initial boron concentration of 5 mg/L. This phenomenon can be interpreted by the buffering effect in ASW. According to the boron binding mechanism, one proton is released

when one boric acid binds to the polyols hydrogel. Regarding the pure boron solution (PBS), the releasing proton will result in a slight increase of proton concentration, i.e., decrease pH value, in the pure boron solution. Besides, the absorption of CO_2 from the atmosphere could also descend the pH value. And the lower pH value will lead to less boron binding. While the ASW has buffering capacity because of the pre-add $NaHCO_3$ making a buffering pair of HCO_3^- and CO_3^{2-} (cf. Fig. 4.36).

$$CO_2 + H_2O \leftrightarrow H_2CO_3 \leftrightarrow H^+ + HCO_3^- \leftrightarrow 2H^+ + CO_3^{2-}$$

Fig. 4.36 Equilibrium between HCO_3^- and CO_3^{2-} in seawater.

The buffering capacity of ASW endows certain tolerance upon extra disturbances, such as atmospheric CO_2 and released proton during the boron binding process. And the self-prepared ASW keeps a stable pH value of ~7.9, which is consistent with the seawater's pH value of 8.0 [139].

Table 4.31 The boron uptake of 14-2-2 membrane in pure boron solution (PBS) and artificial seawater (ASW).

P. (LMH bar)	Adsorption capacity in PBS (mg/m^2)	Adsorption capacity in ASW (mg/m^2)
16700 ± 2600	13.3 ± 0.8	17.6 ± 0.6

Another hypothesis is based on the alleviation of hydrogen bonding inside the GAEMA hydrogel. The used monomer GAEMA has strong intramolecular hydrogen bonding because of the hydroxyl groups. One could imagine that the GAEMA hydrogel also presents strong interior hydrogen bonding in its hydrogel matrix; thus, more energy is required for boron binding. To weakening the intramolecular hydrogen bonding of monomer GAEMA, urea (10 wt%) is added to increase its solubility up to 17.5 wt%. The Na^+, Mg^{2+}, Ca^{2+} in the ASW system akin to urea act as a chaotropic compound weakening the hydrogen binding in GAEMA hydrogel, leading to a lower energy barrier for boron binding, namely, more binding sites are accessible for boric acid.

4.3.4.1 Boron adsorption isotherm

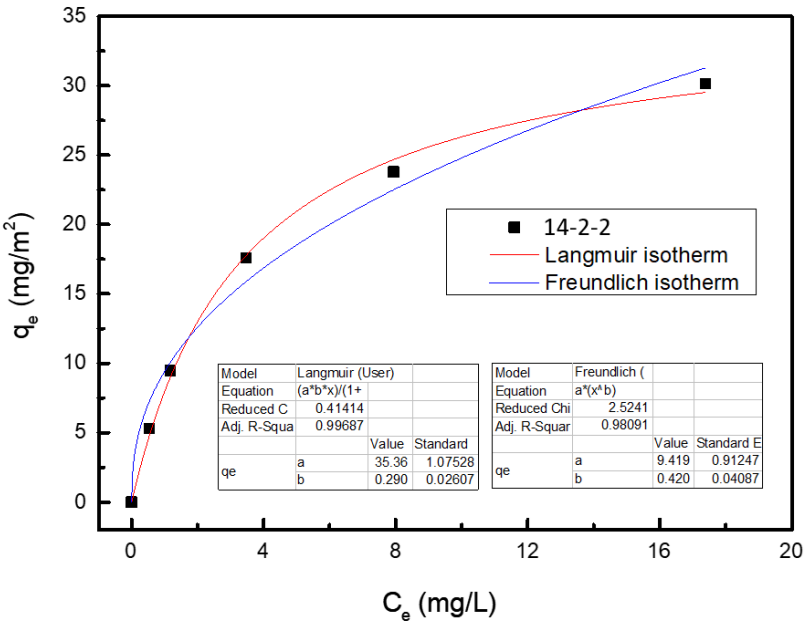

Fig. 4.37 The boron adsorption isotherm of 14-2-2 membrane in ASW.

The adsorption isotherm of 14-2-2 membrane (TEMED/ASP = 1) has been measured, and the result can be found in Fig 4.37, where membrane presents higher boron uptake as the boron concentration increase. The Langmuir isotherm and Freundlich isotherm were tested to fitting the adsorption data of 14-2-2, and the corresponding result is presented in Table 4.32. The adsorption isotherm of the 14-2-2 membrane fits better with the Langmuir model. Langmuir describes the homogenous adsorption, which means the adsorption of each boron has equal sorption energy. At the selected boron concentration window, there is no evidence of multilayer adsorption. Since the result has good fitting R^2 on Langmuir models, the theoretical q_e value of 14-2-2 membrane can be calculated via Langmuir models affording an equilibrium adsorption capacity of 21 mg/m^2 at C_e = 5 mg/L.

Table 4.32 The fitting result of boron adsorption isotherm of 14-2-2 membrane by Langmuir and Freundlich models.

	Langmuir isotherm fitting			Freundlich isotherm fitting		
	q_m (mg/m^2)	b (L mg^{-1})	R^2	K (mg/m^2)	n	R^2
Value	35.36	0.29	0.997	9.42	0.42	0.981
Std.	1.08	0.03		0.91	0.04	

Additionally, according to the isotherm fitting result, the 14-2-2 membrane has a different adsorption mechanism than the modified UF membrane, PEI-10, PEI-5 and PEI-2 (cf. Table 4.9), which fit better with Freundlich isotherm, i.e., a heterogeneous adsorption process occurred in modified UF membrane. The different adsorption mechanism for the modified UF and MF may be due to different boron ligands used and the different adsorption media. The GAEMA hydrogel only provides polyols without additional proton acceptor moieties, while the coating in the modified UF membrane contains tertiary amine as a proton acceptor to promote boron binding with polyols. On the other hand, the adsorption experiment of modified UF membrane was carried out in PBS solution, while the ASW was used as media in the adsorption experiment of the 14-2-2 membrane, and the different media could interfere with the boron binding process.

4.3.4.2 Boron adsorption kinetics via the static method and flow through method

In the previous adsorption results presented in UF modification (cf. Section 4.1), a significant difference in boron adsorption capacity is observed between static adsorption (batch adsorption) and the flow-through adsorption process. Few hypotheses are made regarding the accessibility of boron binding sites and different mass transfer conditions. In order to have a more precise overview of the boron binding mechanism in the dynamic scenario, the boron adsorption kinetic has been done via a static method and recirculation method (3 mL/min, equivalent to 390 LMH), respectively. The respective adsorption kinetic curve of the 14-2-2 membrane can be found in Fig.4.38. And both adsorption kinetic data

have been fitted by pseudo-first-order model, pseudo-second-order model, and intraparticle model to investigate the rate controlling step.

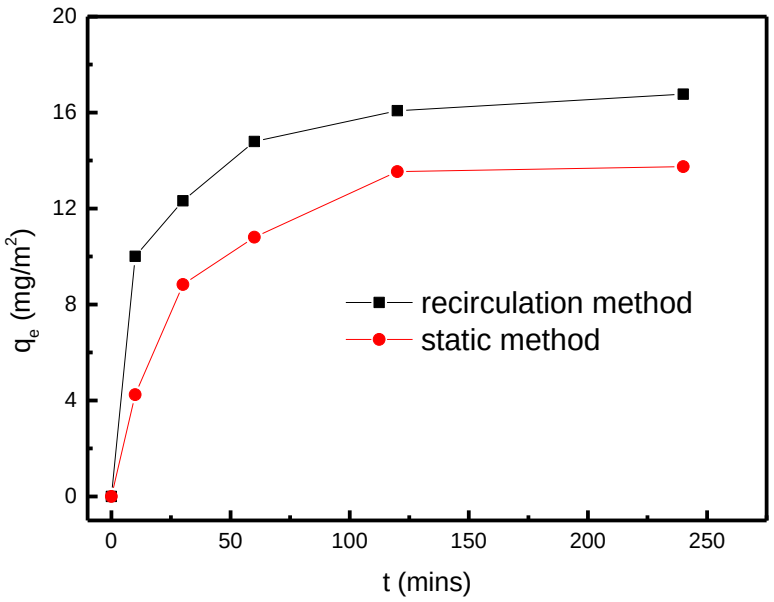

Fig. 4.38 The boron adsorption kinetics of 14-2-2 membrane measured by recirculation (3 mL/min) and static method. The ratio of boron solution to filtration area is 4 mL per 3.46 m^2.

The adsorption experiment performed via static and recirculation methods comes to the same conclusion: both kinetic results fit well with the pseudo-second-order model (cf. Table 4.33), indicating that the rate-controlling step for boron binding is the interaction between polyols ligands and boron. It's clear that the recirculation methods can improve bulk convection but not disturb complexation between boron ligands and boric acid. However, adsorption carried out by recirculation methods has higher boron uptake (q_e = 17.45 mg/m^2) and faster adsorption (k = 0.006 g mg^{-1} min^{-1}) in comparison with the adsorption performed via static method (q_e= 15.24 mg/m^2, k = 0.003 g mg^{-1} min^{-1}). It gives a convincing statement of faster boron adsorption and higher uptake can be achieved by means of improving bulk convection. Besides, the q_e of 17.45 mg/m^2 obtained from pseudo-second-order model fitting is in good agreement with the experiment result of 17.6 ± 0.6 mg/m^2 (cf. Table 4.31), which is due to the good model fitting (R^2 = 0.999).

Table 4.33 The fitting result of boron adsorption kinetics of 14-2-2 membrane by pseudo-first-order, pseudo-second-order and intra-particle models.

	Pseudo-first-order			Pseudo-second-order			Intra-particle		
	q_e (mg/m^2)	k_1 (min^{-1})	R^2	q_e (mg/m^2)	k_2 (m^2 mg^{-1} min^{-1})	R^2	C	k_i (m^2 mg^{-1} min$^{-0.5}$)	R^2
Static	13.98	21.95	0.921	15.24	0.003	0.997	3.93	0.76	0.759
Flow through	16.68	7.05	0.934	17.45	0.006	0.999	9.37	0.54	0.820

To investigate the gap of adsorption kinetic between the static method and recirculation method, the boron uptake difference has been calculated and summarized in Fig 4.39. Comparing to the static method, the boron adsorption process done by the recirculation method gives around 17% improvement on boron binding capacity (see the black curve in Fig. 4.39). Regarding the difference of the boron uptake ($q_{e\text{-flowthrough}}$ - $q_{e\text{-static}}$ in Fig. 4.39), the boron adsorption carried out by recirculation method shows more boron uptake of 5.8 mg/m^2 in the early stage, while this gap decreases and then remains constant to around 2.5 - 3 mg/m^2 in the rest of experimental period.

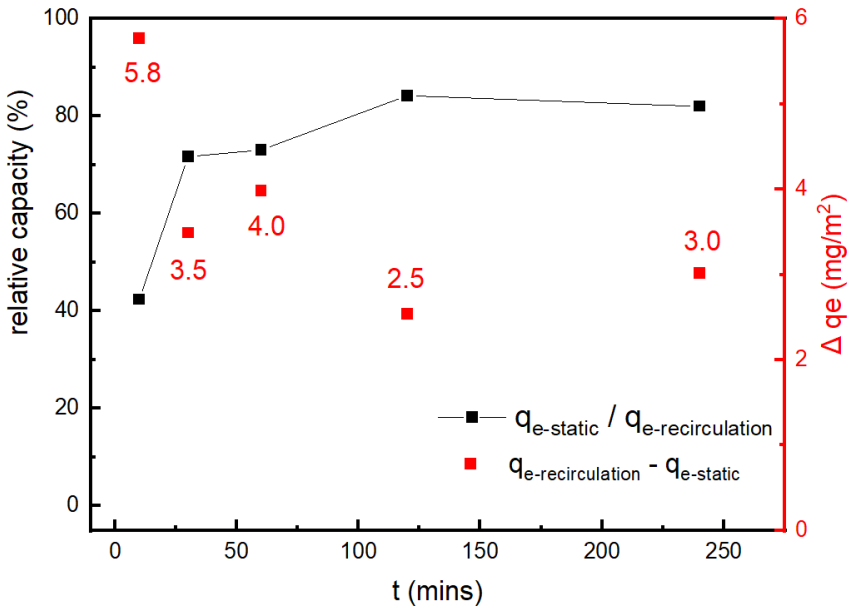

Fig. 4.39 The difference of boron uptake measured by recirculation (3 mL/min) and static method

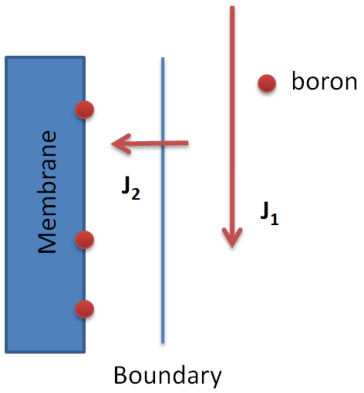

Fig. 4.40 Schematic presentation of boron mass transfer in membrane pore.

The discussion in Section 4.1.4.5 already gives a possible explanation for this discrepancy of adsorption data obtained in the static and recirculation method, which is due to the different mass transport conditions. In this part, the influence of the insufficient mass transfer process on boron binding in the static method will be studied further. As shown in Fig. 4.40, the boron mass transfer process in membrane adsorber contains two steps: 1) the axial boron flux from the outside feed solution to the membrane pores (J_1); 2) the radial boron flux through the boundary layer towards membrane surface (J_2). The boron adsorption carried out by static and recirculation method would have similar J_2 driven by concentration gradient between the interface of bulk and boundary layer and the membrane surface. This J_2 can be mathematically represented by Fick's first law (eq. 4.1).

$$j_i = \frac{D}{l} \cdot \Delta C \tag{4.1}$$

$$j_i = \sqrt{\frac{D}{\pi t}}^{\frac{-z^2}{4Dt}} \cdot \Delta C \tag{4.2}$$

Where D refers to the diffusion coefficient of solute, and the D of boric acid in seawater is $1.11 \pm 0.03 \times 10^{-5}$ cm^2 s^{-1} [140]; l refers to the length of transport path; t refers to particular time during the mass transfer; ΔC refers to the driving force of transport; z is the position in the diffusion profile. The J_1 in the static method is driven by the boron diffusion from the outside feed solution to the membrane pores. In contrast, the J_1 in the

recirculation method is driven by the applied flow velocity. The J_1 in the static method can be mathematically presented by Fick's second law (Eq. 4.2), where the flux changes along with t. The value of J_1 is of great interest that defines the time of completely wetting the membrane pores with feed boron. Apparently, the J_1 difference between the static and recirculation method could be the main factor responsible for the boron uptake difference.

In order to further investigate the time scale of filling feed boron in membrane pores, either can use Fick's second law to calculate J_1 or Fourier module (Eq. 3.12). This is analogous to Fick's second law that can be handily applied to resolve a time-dependent mass transport problem, for example, estimate how far or how long does mass transfer occur [141]. In order to apply the Fourier module correctly, few assumptions should be made: 1) the diffusion coefficient of boron is independent of the boron concentration; 2) the feed boron concentration is constant; 3) the boron transport mechanism in the membrane pore refers to bulk diffusion. Assumption 3 is the basis of applying the Fourier module. And the boron diffusion condition can be determined by checking the K_n number according to the Eq. 3.13. The estimated K_n number is 10^{-4} - 10^{-5} for the boric acid transport in MicroPES-6F (pore size = 600 nm) at ASW as median, therefore the boron transport in membrane pores complies with bulk diffusion. The voids diameter in the UF membrane (PES-50) support layer is in the range of µm so that the boron transport in modified PES-50 also complies with bulk diffusion.

After defining the boron transport mechanism is bulk diffusion in the MicroPES-6F and PES-50 membrane, Fourier module now can be used by setting Fourier number, F_0, as 1. It should be noticed that when calculating transport path (l) in the MicroPES-6F, the effective thickness for boron transports should be half of the membrane thickness because the boron mass transport takes place from both membrane sides. While for PES-50 membrane, the l can be calculated by using overall membrane thickness due to the selective layer that the boron transport from the dense selective later can be negligible. Finally, the respective time of mass transfer occurs, t, can be found in Table 4.34.

Table 4.34 The calculated time requirement for boron mass transport from the bulk solution to membrane pores.

Membrane type	t (s)
MicroPES-6F	11 - 98
PES-50	44 - 392

The calculated time for mass transfer in MicroPES-6F and PES-50 is in the time scale of ~10^1 - 10^2 s or ~10^{-1} - 10^1 min. However, the adsorption experiment is carried out within a time scale of 10^2 - 10^3 min (cf. Fig. 4.38 and Fig. 4.6). Thus the mass transfer difference between static and recirculation methods only occurs at the early stage of adsorption. And this statement is in line with the result presented in Fig. 4.39, where adsorption difference of 5.8 mg/m^2 at the early stage of adsorption and the gap of adsorption difference decrease to 2.5-3.0 mg/m^2 in the rest of the adsorption time.

4.3.4.3 Flow-through adsorption

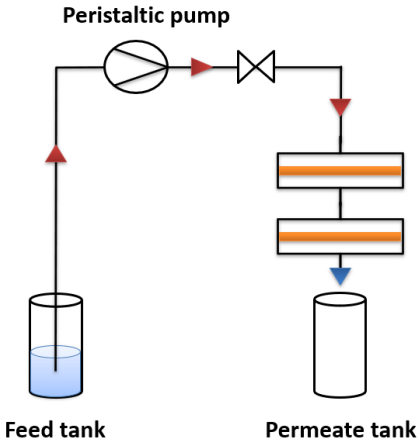

Fig. 4.41 The configuration of dual-pass flow-through adsorption.

Two kinds of filtration apparatus were used in the flow-through adsorption, single-pass and dual-pass configurations (cf. Fig. 4.41). Experiments with these two apparatuses were carried out at the same flow rate of 3 mL/min with an equivalent flux of 390 ± 15 LMH (cf. Fig. 4.42). Such stable flux makes sure a comparable mass transfer process in two apparatuses since flow rate variation would disturb adsorption efficiency and mass transfer

steps during the flow-through process, as previously discussed.

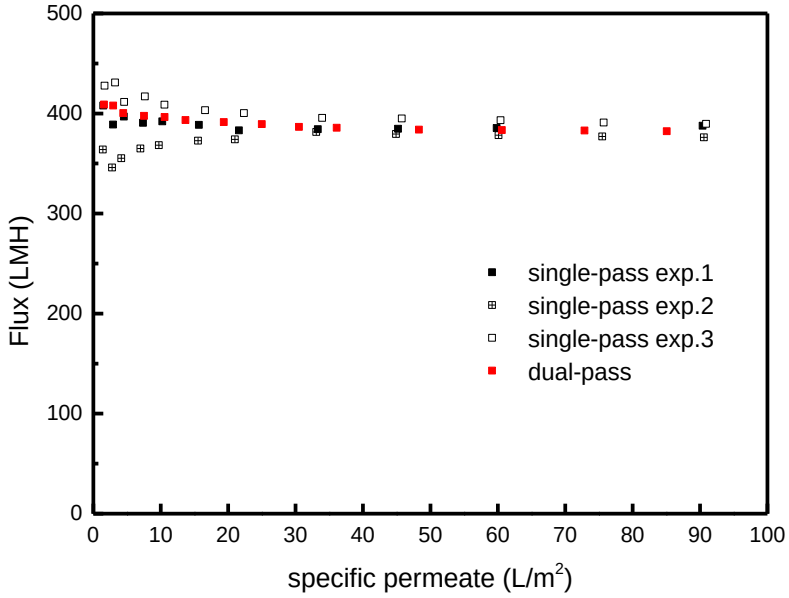

Fig. 4.42 The actual flux in flow-through adsorption at the pumping flow rate of 3 mL/min.

The breakthrough curve of single-pass and dual-pass configurations can be found in Fig. 4.43. The flow-through adsorption carried out by single-pass configuration shows a steeper breakthrough curve and reaches saturated adsorption faster than dual-pass configurations. The dual-pass configurations have a gradual breakthrough curve at the early adsorption stage (specific permeate < 20 L/m^2), then the permeate boron concentration slowly creeping up to the feed concentration. However, both of the configurations show no 0% breakthrough points. The shape of the breakthrough curve is affected by axial diffusion, adsorbate dispersion, the adsorption kinetics and isotherm of adsorbent [141]. The adsorbate dispersion takes the major responsibility for the breakthrough behavior above all of the four mentioned phenomena; thus, the possible reason for the missing 0% breakthrough points will be first discussed in the aspect of the influence of adsorbate dispersion in the flow-through experiment.

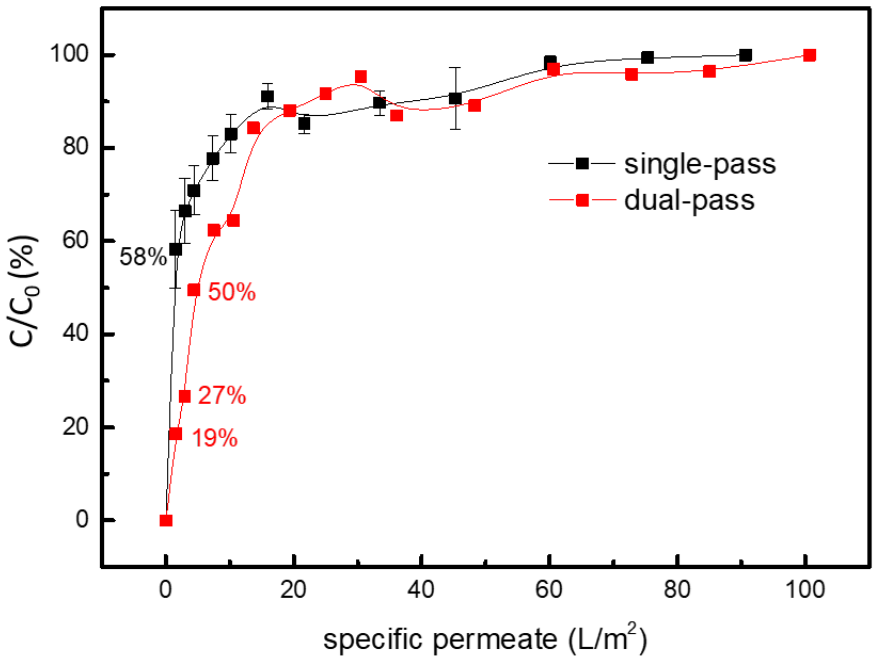

Fig. 4.43 The boron break-through curve in single-pass and dual-pass methods.

The uneven boron dispersion occurs for three reasons. Firstly, the uneven boron dispersion is an outcome arising from the distribution of pore size in the membrane adsorber, and the uneven pore size will lead to the diverse axial flow rate across the membrane porous structure. The Taylor dispersion in the laminar flow could be another reason that the shear flow smears out the concentration distribution in the flow rate direction leading to uneven boron acid diffusion and low rate direction [103,104]. And the third reason is the uneven flow distribution and effluent collection in the syringe membrane module, which is basically due to the poor module design (cf. Fig. 4.44). Such radial flow distribution resulted in various residence times distributed at the radial direction in the membrane, therefore the boron breakthrough from the central area of the membrane prior to the outer radial positions.

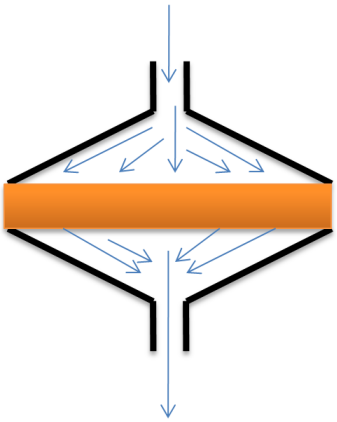

Fig. 4.44 Schematic presentation of flow distribution in a poorly designed syringe membrane holder.

However, the foregoing discussion of the flow dispersion effect is based on the precondition that the membrane can be perfectly saturated at the given flow rate. In this paragraph, the correlation of applied flow rate and residence time will be discussed. The boron flux can be divided into two directions (cf. Fig. 4.40): 1) boron transport along with the flow direction, J_1, which is directly controlled by flow rate; 2) diffusion through the boundary layer to the membrane surface, J_2, which is perpendicular to the flow direction. Thus, the applied flow rate, i.e., the residence time of feed boron solution, is an important factor since it has the same J_2 in the single-pass and dual-pass configuration. The residence time of feed boron solution during the single-pass and dual-pass process can be calculated according to:

$$\mathrm{t_{residence}} = \frac{d \cdot \tau}{\mathrm{F}} \tag{4.3}$$

Where d is the thickness of the membrane, which is 110 µm in single-pass configuration and 220 µm in dual-pass configuration; τ is the tortuosity of the membrane; F is the flux of 390 ± 15 LMH used in the experiment. The calculated residence time is 1.02τ in single-pass setup configuration and $2.04\,\tau$ in dual-pass configuration. When assuming the tortuosity of the MF membrane as 2, thus the actual residence time of feed boron solution should be 2.0 s and 4.1 s for single-pass and dual-pass setup configuration, respectively. While in column adsorption (filled by resins), the residence time is commonly around 15-20 min, which is equivalent to ~10^3 s according to the literature [142]. Hereof, the residence time in the single-pass and dual-pass configuration is two orders of magnitudes lower than

column adsorption. Besides, the prepared 14-2-2 membrane would need more than 100 min (> 6 x 10^3 s) to reach saturated adsorption according to the boron adsorption kinetics results (cf. Fig. 4.38). In summary, such short residence time would possibly lead to unsaturated adsorption during the flow-through process.

The Péclet number (*Pe*) can also be used to reveal the competition between the advective transport process and the diffusive transport process. When $Pe \rightarrow 0$, it means that the convection is weak and the diffusion is dominant; When $Pe \approx 1$, it means that the convection and the diffusion contribute equally; When $Pe \gg 1$, it means that the convection is dominant. The calculated *Pe* for single-pass and dual-pass configuration is 0.47 and 0.95, respectively, when the applied flow rate is 3 mL/min and the assumed tortuosity of 3. The calculated *Pe* reveals that the boron transport is conjointly determined by convection flow and boron diffusion in both two flow-through configurations.

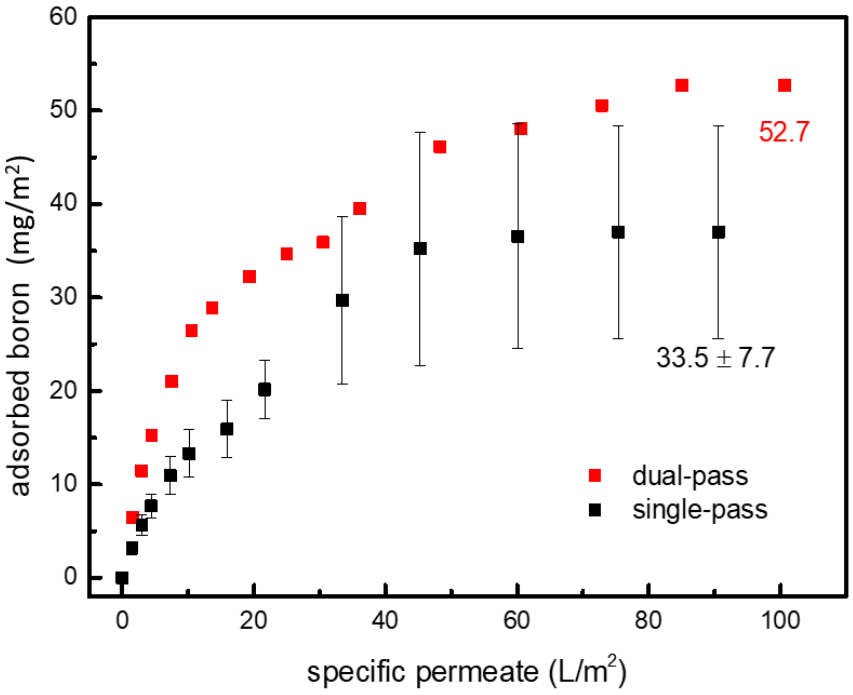

Fig. 4.45 The boron accumulation during flow-through adsorption via single-pass and dual-pass methods.

The accumulated boron uptake during the flow-through adsorption can be found in Fig. 4.45. The boron removal via the dual-pass method shows a higher maximum boron uptake capacity of 52.7 mg/m^2, where the capacity in the single-pass method is 33.5 ± 7.7

mg/m^2. It should be noticed that the membrane volume in the dual-pass configuration is double as which in the single-pass configuration. However, the final boron uptake capacity in the dual-pass configuration was only enhanced by a factor of 1.57 instead of 2. It means that the membrane adsorber in dual-pass configuration is less efficient in dual-pass configuration regarding the boron binding capacity per membrane volume. Two syringe modules are used in the dual-pass process; thus, the uneven flow distribution effect is more severe compared to the single-pass process.

Based on the foregoing discussion and different calculations, a better boron uptake can be achieved by: 1) increasing the boron feed residence time in the membrane adsorber; 2) improving flow distribution by adapting better membrane module design; 3) improving boron mass transport by improving bulk convection. However, it should be noticed that the operating flux will impact the boron feed residence time and bulk convection simultaneously, where increase bulk convection would lead to low residence time at the giving laminar flow scenario in the membrane. This trade-off can be resolved by enhancing operation flow rate and extent flowing path, such as applying membrane stacks and using a higher tortuosity membrane.

4.3.4.5 Regeneration process

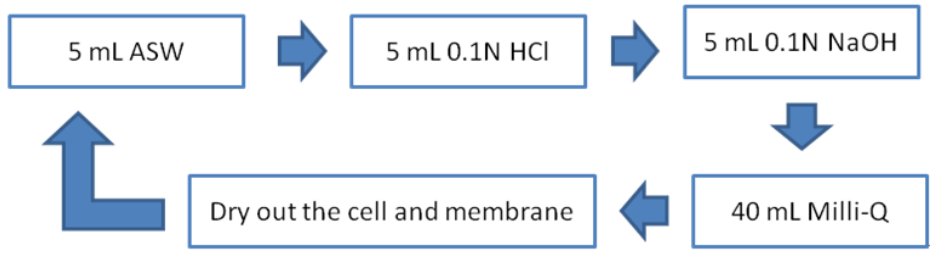

Fig. 4.46 Schematic presentation of the regeneration cycle.

The regeneration of membrane 14-2-2 is done via the single-pass method, and Fig. 4.46 presents the overall regeneration procedures, where the membrane with an effective area of 3.46 cm^2 experiences 5 rounds of flow through adsorption and 4 rounds of regeneration. Boron uptake of each adsorption cycle is presented in Fig. 4.47. The 14-2-2 membrane only achieves ~75% of the total boron uptake capacity after the first regeneration procedures.

Afterward, the modified membrane gives a constant boron uptake in the following three adsorption cycles indicating good stability under 0.1 N HCl and 0.1 N NaOH treatment. The good stability of the modified membrane possibly arises from 1) the good mechanical stability of the hydrogel coating due to the adequate washing step before using the membrane; 2) good chemical stability due to the acidic and basic tolerated amide groups in the hydrogel matrix. However, the modified membrane still has 25 wt% of irreversible adsorption.

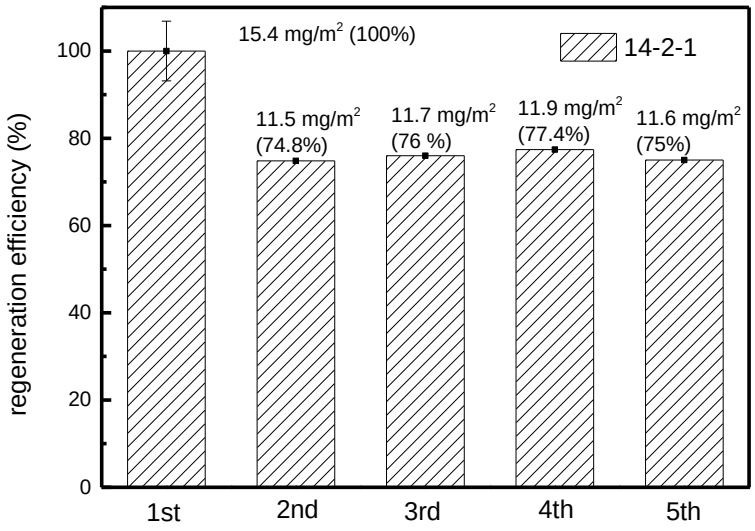

Fig. 4.47 Regeneration efficiency of 14-2-2 membrane.

4.3.5 Interim summary for Section 4.3

The hydrogel grafting degree has been improved by using integrated initiation system in terms of hydrogel loading and modification controllability. The boron binding and the water permeability can be tailored by altering monomer solution conditions and using a different base membrane. Regarding optimization, a two-stage parameter optimization has been applied where the DOE and ANOVA are used to pre-screen the parameters by study the main effect and significance of each parameter. It shows that the monomer concentration plays a dominant impact on boron uptake and permeability. Afterward, the single-factor experiment is applied based on the outcome from DOE as the parameter fine-screening, and the final optimal monomer solution condition is 14-2-2 with a TEMED/APS ratio of 1.

The adsorption isothermal and kinetics have been analysed to study the boron adsorption mechanism and mass-transport condition. The 14-2-2 membrane fits well with the Langmuir isotherm model and the Pseudo-second-order model.

Moreover, the 14-2-2 membrane shows higher and faster boron uptake in the recirculation method in comparison with the static adsorption method. The faster boron uptake can be explained by the sufficient mass transport in the recirculation flow-through method. And the higher boron uptake at the early adsorption stage can also be explained by better mass transport. However, the 14-2-2 membrane could uptake more boron (2.5-3.0 mg/m^2) in the recirculation method compared to static equilibrium, and the reason still unknown.

Regarding the boron uptake performance in flow-through adsorption, single-pass and dual-pass configurations are used. It shows higher boron removal in the dual-pass configuration. However, the zero breakthrough point is still missing in both of these two configurations. The unobservable zero breakthrough point is mainly due to the uneven flow condition in the membrane syringe modules. The residence time and *Pe* number in single-pass and dual-pass configurations have been studied. It shows that convection flow fraction and bulk diffusion fraction contribute equally to the boron mass transport process.

With respect to the membrane adsorber regeneration under single-pass configuration, the 14-2-2 membrane shows around 25% adsorption capacity drop after the first generation and then stays constant in the following 4 regeneration cycles, indicating a good mechanical and chemical stability of boron affinity coating. However, for the boron adsorption capacity of this membrane still remains space to improve to cater to the practical application.

4.4 Other modification approaches that show good potential in boron removal

Several trials have been proceeded to achieve a better trade-off of boron uptake against permeability during the whole working period. Here only selectively present some preliminary data of two modifications, which shows good potential for the projected application.

4.4.1 UF membrane modification via integrated initiation system

In this modification strategy, the GAEMA coating has been grafted in the support layer of the PES-100 UF membrane by using monomer solution of 5-2-2 or 10-2-2 (cf. Section 3.3.2.3). A comparable boron uptake can be achieved but using less amount of chemicals (cf. Table 4.35), i.e., lower monomer and cross-linker concentration, showing an economic advantage.

Table 4.35 The membrane performance of the modified UF membrane (PES-100) by integrated initiation system.

Note	Monomer condition	TEMED/APS	PBD	P. (LMH bar)	Boron uptake (mg/m^2)	Flux drop (%)
Pristine PES-100	-	-	-	510	-	-
premodified	-	-	PBD-74	190 ± 17	-	63
	5-2-2	0.5	PBD-74	60 ± 10	8.3	88
	5-2-2	1	PBD-74	85 ± 30	4.5	83
	10-2-2	1	PBD-74	7 ± 1	-	99
premodified	-	-	PBD-300	140 ± 5	-	-
	5-2-2	0.5	PBD-300	65 ± 13	4.1	87
	5-2-2	1	PBD-300	20 ± 3	13.6	96
	10-2-2	1	PBD-300	9 ± 2	16.4	98

Interestingly the PES-100 membrane (nominal MWCO is 100 kDa) premodified by PBD-300 has lower permeability (140 ± 5 LMH bar) than the PES-100 premodified by PBD-74 (190 ± 17 LMH bar). When infiltration PBD-74 or PBD-300, the PBD-74 would penetrate to the pores of the selective layer, while the PBD-300 would be rejected by the selective layer via size exclusion effect due to its larger molecular weight. For another, the intermolecular charge repulsion arising from the protonated tertiary amine moieties in both PBD-300 and PBD-74, preventing the multilayer adsorption. Namely the PBD-300 and PBD-74 would prefer to form single layer adsorption on the membrane surface. Under this context, one hypothesis is proposed: infiltration of PBD-300 would lead to pore coverage, while only internal pore blocking occurs in the PBD-74 infiltration step. And the pore coverage is

responsible for the lower permeability when the membrane premodified via infiltration of PBD-300.

For another, when the PBD-74 penetrates and adsorbs in the pores of the selective layer, the GAEMA coating could form in the pores leading to pore blocking dramatically. However, no obvious difference can be found when the PES-100 membrane modified by PBD-300 or PBD-74, and only the monomer solution condition plays a dominant effect on permeability. It has been demonstrated in Section 4.2 that the pore size is one of the crucial factors affecting the grafting degree. The pore size in the selective layer is around 20-30 nm in the PES-100 membrane. Such a small pore size will give a highly confined environment to restrict chain propagation leading to a limited functionalization degree in the pores of the selective layer.

Compared with the modified MicroPES-6F membrane (cf. Section 4.3) at analogous modification procedures, the modified PES-100 membrane shows comparable boron uptake but less chemicals consumption. It means that the modification performed on the UF membrane can achieve a more sufficient utilization of chemicals due to the larger specific area in the PES-100 membrane.

4.4.2 MF modification via three-step modification

4.4.2.1 Concept

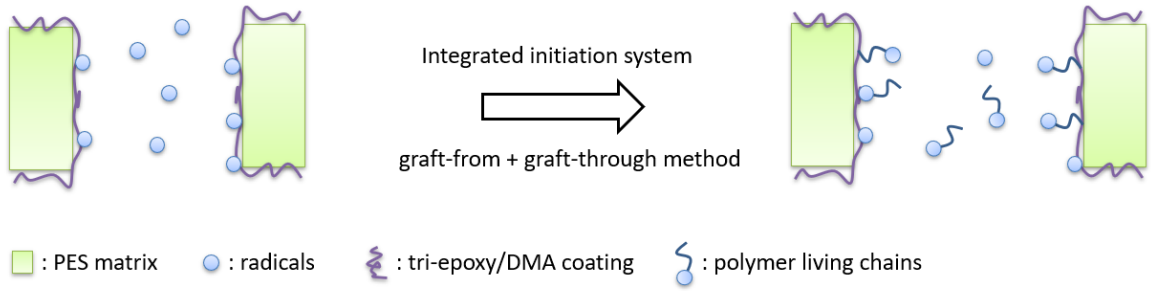

Fig. 4.48 Schematic presentation of the principle of surface-initiated polymerization and the integrated initiation system on tri-epoxy/DMA modified membrane.

Similar to the idea of surface initiation polymerization system, the membrane surface was designed to be pre-modified with a layer containing adequate tertiary amine moieties to accelerate the decomposition of APS for the subsequent hydrogel grafting (cf. Fig. 4.48 and Section 3.3.2)). In the premodification step, the membrane first adsorbs tri-epoxy compounds, and then the adsorbed tri-epoxy was cross-linked by DMA, giving a tertiary amine included coating at the membrane surface as shown in Fig. 4.49. This coating can attach firmly to the membrane surface due to the partially penetrating of tri-epoxy compound in the PES matrix. Also, it has π-π interaction between the aromatic part fraction of coating and PES matrix, both interactions ensuring mechanical robustness [130].

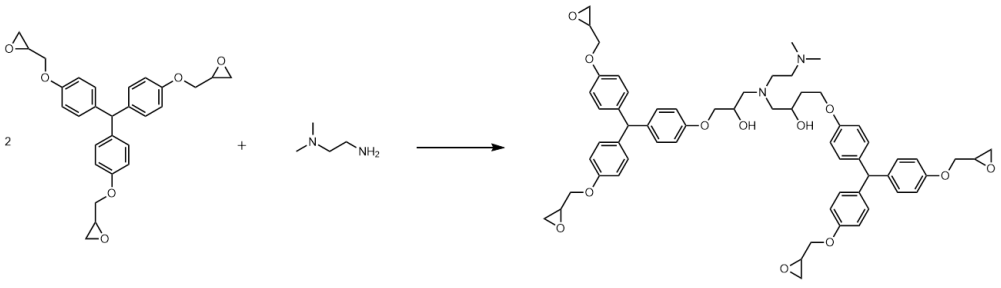

Fig. 4.49 The cross-linking between tri-epoxy compound and DMA.

4.4.2.2 Characterization of the modified membrane

The pre-modified membrane was first characterized by the ATR-FTIR spectrum to reveal the surface chemistry variation during the premodification step (cf. Fig. 4.50). For the washed pristine PES-100 membrane, there is no apparent absorption at the wave numbers of 910 cm^{-1}, 2800-2900 $cm^{-1,}$ and 3200 cm^{-1}. When the membrane adsorbs tri-epoxy groups, the peaks at 910 cm^{-1} and 2800-2900 cm^{-1} appear, which belong to the C-O-C vibration for epoxy moieties, and the C-H vibration in aromatic moieties, respectively. The IR transmission at these two wave numbers gives clear evidence of successful adsorption of tri-epoxy compound.

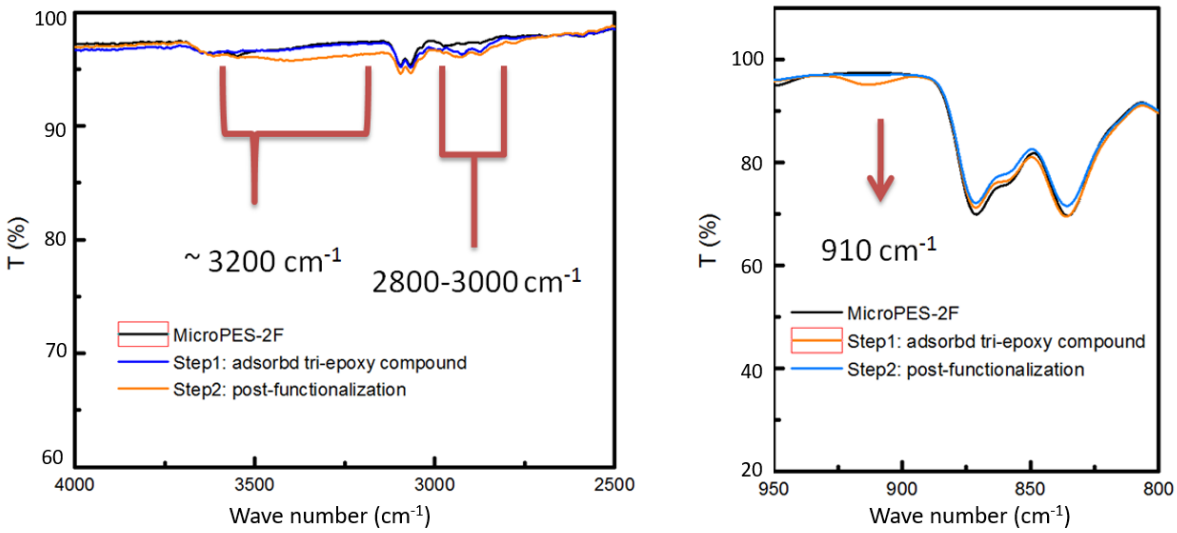

Fig. 4.50 ATR-FTIR spectrum of the pristine membrane (black curve), tri-epoxy modified membrane (blue curve), and tri-epoxy/DMA modified membrane (orange curve).

In the second step of the premodification protocol, the tri-epoxy included PES-100 was immersed into DMA solution for 48 h to post-functionalize membrane with tertiary amine group via the ring open reaction between epoxy and primary amine. And after this post-functionalization, the characteristic peaks for the adsorbed tri-epoxy compound, the C-O-C vibration, disappears, and new board adsorption at 3200 cm^{-1} shows up, which corresponds to -O-H vibration (cf. Table 4.36). However, the appearance of -O-H vibration can be caused by either the hydrolysis of epoxy groups or the hydroxyl group coming from the ring open reaction. Thus, a further characterization needs to be done, such as the

investigation of change of surface charge.

Table 4.36 The IR absorption variation over each premodification step.

Wave number	910 cm^{-1}	2800-2900 cm^{-1}	~3200 cm^{-1}
	C-O-C	Aromatic C-H	-O-H
MicroPES	-	-	-
tri-epoxy modified	√	√	-
tri-epoxy/DMA modified	-	√	√

Fig. 4.51 presents the surface zeta potential variation along with the modification proceeded. The pristine PES-100 membrane shows a negatively charged surface within the pH window from 3 to 11, and the surface remains negatively charged after adsorbing tri-epoxy groups. However, a phenomenon of surface charge reversion can be observed when the membrane experienced DMA treatment. The surface charge shifts to positive when pH < 4 due to the grafted tertiary amine groups. Moreover, after pumping the monomer solution through the premodified membrane under the same operation protocol as mentioned in Section 3.3.2.4., the IEP shift to around 7, which is in line with the IEP of glycopolymer. The shifting of IEP indicates a successful grafting of GAEMA hydrogel. This modification strategy is feasible based on the IR characterization and surface zeta potential investigation.

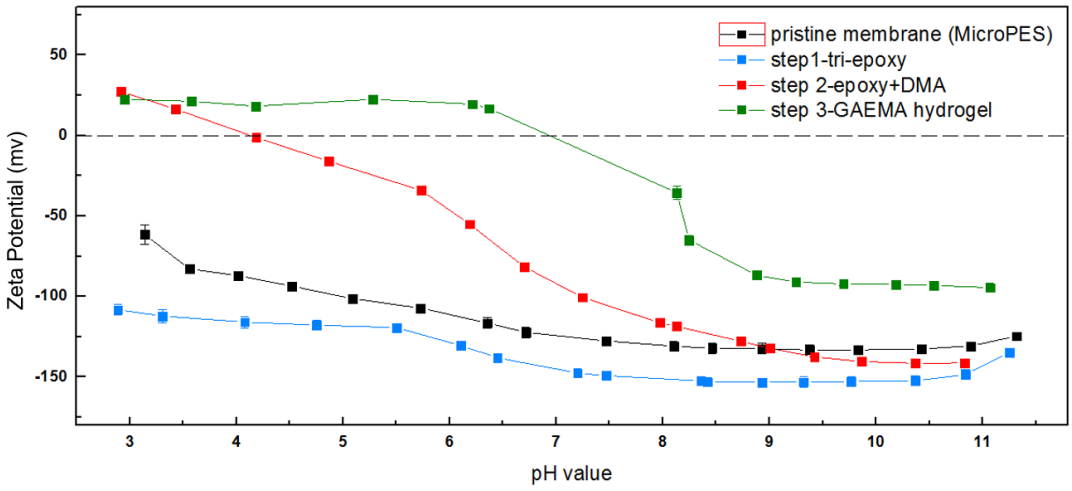

Fig. 4.51 Zeta potential of the pristine membrane (black curve), tri-epoxy modified membrane (blue curve), tri-epoxy/DMA modified membrane (red curve), and GAEMA coated membrane (green curve).

4.4.2.3 Membrane performance

Table 4.37 Membrane performance of modified membrane by using PBD-74 or tri-epoxy/DMA in premodification.

premodification	Monomer condition	membrane	TEMED/APS	P. (LMH bar)	Boron uptake (mg/m^2)
tri-epoxy/DMA	15-5-2	MicroPES-2F	0	1900	5.2
tri-epoxy/DMA	15-1-2	MicroPES-6F	0.5	3200	13.8
PBD-74	15-5-2	MicroPES-2F	0	1000 ± 200	2.1
PBD-74	15-1-2	MicroPES-6F	0.5	8900 ± 2000	6.7

Table 4.37 gives the information related to the filtration and boron uptake performance for the membrane premodified by tri-epoxy/DMA and PBD-74. After coating formation, the tri-epoxy/DMA modified MicroPES-2F shows higher final permeability (1900 LMH bar) and boron uptake (5.2 mg/m^2) in comparison with PBD-74 modified membrane (1000 ± 200 LMH bar and 2.1 mg/m^2). For the integrated initiation system, the tri-epoxy/DMA modified MicroPES-6F also shows higher boron uptake (13.8 mg/m2) after coating formation compared to PBD-74 modified MicroPES-6F. These results indicate an improved hydrogel functionality when the membrane was premodified via adapting tri-epoxy/DMA protocol.

Table 4.38 The -CH_2-$N(CH_3)_2$ loading in PBD-74 and tri-epoxy/DMA modified membrane.

Premodification	Membrane	V-loading (mg/cm^3)	Mass of DMA (mg/cm^3)	Mass of -CH_2-$N(CH_3)_2$ (mg/cm^3)
tri-epoxy adsorption	MicroPES-2F	25	-	-
tri-epoxy/DMA	MicroPES-2F	36	11	7.3
PBD-74	MicroPES-2F	9.2	-	1.2

To further reveal the possible reason for the more effective coating formation in tri-epoxy/DMA modified membrane, the tertiary amine loading is determined. Table 4.38 presents the mass gain after tri-epoxy/DMA and PBD-74 premodification on MicroPES-2F. The tri-epoxy/DMA modified MicroPES-2F carries 11 mg/cm^3 of DMA moieties, which is equivalent to 7.3 mg/cm^3 of tertiary amine groups at the membrane surface. The PBD-74 modified MicroPES-2F membrane only carries 9.2 mg/cm^3 of PBD-74, which is equivalent to 1.2 mg/cm^3 of tertiary amine moieties at the surface. It has been discussed previously that the amount of surface tertiary amine determines the surface free radical concentration, and more free radical concentration is favourable to improve hydrogel loading. The tri-epoxy/DMA modified MicroPES-2F carries more than 6 times of tertiary amine groups compared with the PBD-74 modified MicroPES-2F. And this could be the main reason why the tri-epoxy/DMA modified membrane can achieve a higher hydrogel functionalization degree, further leading to more boron uptake.

4.5 Estimation of cost by applyling membrane adsorber

4.5.1 Cost estimation

The previous modification approaches are all performed on flat sheet membranes, assuming that the modification can be successfully transfered to the spiral wound modules under the analogous procedures. Hereof, the cost of boron removal via two modified membrane/modules, PEI-5Acl/PES-50 (cf. Section 4.1), and single-pass 14-2-2/MF (cf. Section 4.3) have been estimated in terms of modification cost and the reagent cost for regeneration, and the calculation flow chats can be found in Section 3.8.

4.5.1.1 Modification cost

Table 4.39 The estimated modification cost per m^2 membrane (euro/m^2).

Membrane type	Modification solution	$\mathbf{COST_{mem}}$ (euro/m^2)
PEI-5Acl/PES-50	0.3 g/L PES + 9 wt% glycidol	23
single-pass 14-2-2/MF	14-2-2 GAEMA solution	41

All the calculation steps are in detail presented in Appendix B. The modification cost can be related to the modification cost per membrane area (euro/m^2), modification cost per treated seawater capacity (million gallons per day, MGD), and modification cost per treated seawater volume (euro/m^3). The modification cost per membrane will be first discussed, and the calculated results can be found in Table 4.39. In order to modify the spiral wound module, the modification solution should be filled in the module. Thus the modification solution usage depends on membrane module void fraction ($\emptyset_{spiralwound}$, cf. Table B1), which can be calculated based on the spacer thickness (assumed as 30 mils) and the membrane thickness (~ 110 μm). Furthermore, the volume of chemical usage ($V_{chemical\ usage}$, cf. Table B1) to modified specific membrane (e.g., 1 m^2) can be later deducted. Finally, the modification cost per m^2 membrane can be obtained when imputing the chemical price. The cost of PEI-5Acl/PES-50 (23 euro/m^2) shows economic advantage comparing to the single-pass 14-2-2/MF (41 euro/m^2). That is basically due to the huge price advantage of PEI and glycidol in comparison with the self-prepared GAEMA (cf.

Table B2).

Table 4.40 The estimated modification cost per treated seawater capacity (euro/MGD) and volume (cent euro/m^3).

Membrane type	j_{op} (LMH)	Membrane service life (years)	$\mathbf{COST_{MGD}}$ (euro/MGD)	$\mathbf{COST_{m^3}}$ (cent euro/m^3)
PEI-5Acl/PES-50	50	5	40	1.06
single-pass 14-2-2/MF	390	5	9	0.25

Based on the modification cost per m^2 membrane, the modification cost per treated seawater capacity (MGD) and volume (m^3) can be further deduced (cf. Table 4.40). For a capacity of 1 MGD (3785 m^3/day), the modification material consumption depends on flux and duration of the modified membrane (membrane service life). Higher flux and longer membrane service life enable to reduce modification cost. The membrane service life was assumed as 5 years, and the operation flux of modified UF and MF membrane has been set as 50 and 390 LMH, respectively. Table 4.40 presents the calculated modification cost for 1 MGD. Furthermore, the modification cost to treat 1 m^3 is calculated as well. A higher operation flux leads to higher throughput; therefore, the modified MF membrane (14-2-2/MF) gives a significantly lower modification cost comparing to the modified UF (PEI-5Acl/PES-50)

4.5.1.2 Reagent cost in regeneration

In order to estimate the reagent cost, several assumptions are proposed in Appendix B2. Briefly, the estimation is under the context of: 1) seawater treatment throughput of 1 m^3/h (1000 L/h); 2) the modified membrane have a perfect break-through behaviour; 3) performing the regeneration at 50% break-through points; 4) 4 MV is required in each regeneration; 5) 0.05 M H_2SO_4 and 0.1 M NaOH are chosen as acidic elution reagent and neutralization reagent, respectively. The reagent cost depends on two aspects: 1) the require elution volume in regeneration steps ($V_{regeneration}$); 2) the chemical price. The calculated reagent cost of each membrane is summarized in Table 4.41.

Table 4.41 The estimated reagent cost for membrane regeneration under specific operation conditions.

Membrane type	50 % Breakthrough (L/m^2)	Operating permeability (LMB bar)	$V_{regeneration}$ (L)	Reagent cost (cent Euro/m^3)
PEI-5Acl/PES-50	2.1	50	203	52-84
single-pass 14-2-2/MF	1.5	390	290	74-121

The estimated reagent cost is 52-84 cent € for PEI-5Acl/PES-50, and 74-121 cent € for single-pass 14-2-2/MF. It shows that the membrane with delayed breakthrough would consume less volume for cleaning reagent, i.e., lower $V_{regeneration}$.

4.5.2 Comparison with other established boron removal methods

The total cost of boron removal via single-pass 14-2-2/MF has been summarized in Table 4.42, as well as the boron removal cost for two others established methods. The implementation, materials, energy, reagent, and maintenance are the five main expenditures that should be considered when doing cost estimation [11]. This project aims to integrate boron adsorption with the filtration process in the pre-treatment step for SWRO. As such, no extra cost on implementation, energy, or maintenance is required in the single-pass 14-2-2/MF. For the traditional boron removal by ion-exchange method, the main contributions in total cost are the ion-exchange resin usage (material cost). For the boron removal via 2nd pass RO, energy and reagent consumption account for the main portion in total boron removal cost. Therefore, boron removal via single-pass 14-2-2/MF shows significant economic advantage in aspects of implementation, materials, and energy consumption. However, the total cost of single-pass 14-2-2/MF is 13 times higher than ion-exchange and 2nd pass RO in the frame of the adapted cost estimation scenario. Such high capital cost for the boron removal in single-pass 14-2-2/MF is due to the enormous consumption of reagents in the regeneration step. It is well known that a fast breakthrough would lead to high regeneration frequency under the given seawater treatment capacity. And the breakthrough behaviour depends on operation condition, boron binding isotherm and kinetic, mass transport condition, and module design. The main reason for the modified membrane in this work is known as the relatively lower boron binding capacity per membrane adsorber volume or area compared to the traditional ion-exchange resin in

the bead-based fixed-bed adsorption. Secondly, the uneven flux distribution and boron mass transfer condition are responsible for the fast breakthrough.

Table 4.42 Cost comparison of different boron removal methods.

Cost for	**Ion exchange at post-treatment (cent euro/m^3)**	**2nd pass RO (cent euro/m^3)**	**14-2-2/MF (cent euro/m^3)**
Implementation	0.62	0.7	-
Material	1.52 - 8.9	0.52 - 1.42	0.25
Energy	0.33 - 0.96	1.46 – 5.59	-
Reagents (for regeneration)	0.23 - 0.55	0.12 – 4.88	48-79
Maintenance	0.019	0.02	-
Total	3.85 - 11.05	2.82 – 12.61	74.25 - 121.25
Total (mid-value)	7.45	7.72	97.75

4.5.3 Toward reducing reagent usage in regeneration steps

A conservative cost estimation based on the available results shows a tremendous reagents consumption in membrane regeneration when using 14-2-2/MF membrane for boron removal. However, there is clear potential to further reduce the reagent cost, and the solution is straightforward: delaying the boron breakthrough or reducing chemical usage. On the basis of the available results and the foregoing discussion, several approaches are proposed here to cut the reagent expense:

a) Further increasing boron binding capacity by improving tertiary amine loading in the premodification step, which could further increase hydrogel functionalization. In the best case, it can delay boron breakthrough by a factor of 2, i.e., cut the reagent cost by a factor of 2.

b) Optimizing the pH values for regeneration toward less acidic and basic solution used. The literature data indicate that there is limited complexation between boric acid and polyols compounds when pH < 3 [143]. The acid and base concentration used in the cost estimation is 0.05M H_2SO_4 and 0.1 M NaOH. Therefore, in a conservative case of using pH = 2 acidic solution for boron desorption and pH = 12 for neutralization can reduce reagent cost by a factor of 10!

c) Due to the buffering effect of seawater, the neutralization steps can be done conjointly by seawater flushing and basic solution, thus able to reduce the NaOH dosage by a factor of 2. Therefore, the overall reagent cost can be reduced by a factor of 1.5.

d) The fluctuant price of 98% H_2SO_4 and 50% NaOH depends on the market and supplier. In the best case, selecting a suitable chemical supplier can reduce 5-10 % of the chemical cost.

e) It has a more effective regeneration process in membrane adsorber because of more efficient mass transfer in the porous membranes than fixed-bed adsorption. A more efficient regeneration process may lead to less elution volume used during the regeneration step, for example, flash saturated membrane by 2 MV instead of 4 MV (this

is required for resin particle bed), thus will cut reagent cost by a factor of 2.

f) The residence time of feed solution in the membrane is of crucial importance on breakthrough behaviour. As shown in Table 4.41, the double residence time may lead to triple lagging of breakthrough points. Performing modification on a thicker membrane, such as MFG-2 PSF (Alf Laval, 298 µm) or Accurel PP (3M, 198 µm), can proportionally delay the breakthrough. On the other hand, with the precondition of sufficient mass transfer and the specific throughput, optimizing operation flux could also delay the breakthrough. Overall, improving the feed solution's residence time distribution in the membrane adsorber could reduce the reagent cost by a factor of 2.

g) Optimized integration of membrane adsorber into the entire treatment chain; one option is to combine the regeneration step with the membrane chemical cleaning. And the cost-saving extent strongly depends on the cleaning frequency, which refers to the specific application scenario.

By now, the established modified membrane shows high reagents cost compared with the established ion-exchange method and 2nd pass RO method. However, it has clear potential to cut reagents expense by means of optimizing operation condition, modification procedures, altering membrane structure, and so on.

5. Conclusion

5.1 Modification approaches

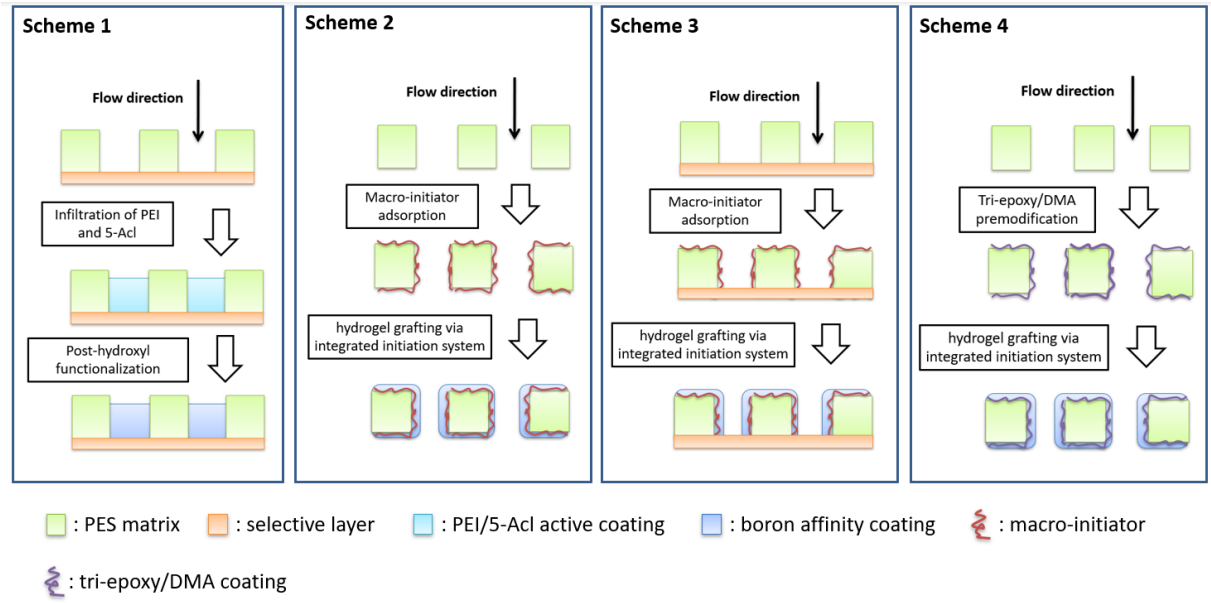

Fig. 5.1 Schematic presentation of four modification approaches used in this work.

The commercial UF or MF fleet sheet membrane or capillary membrane has been functionalized by a boron affinity coating via different modification protocols. The surface functionalization can be accomplished via a surface initiation polymerization, an integrated initiation system, or a post-functionalization on the preformed active coating. To summarize, four schemes are proposed to prepare UF or MF membrane adsorber (Fig. 5.1)

In Scheme 1, the asymmetric support layer of PES-50 was modified by infiltration of PEI/5-Acl, forming an active cross-linked PEI coating of which is ready for subsequent post-functionalization by glycidol (cf. Section 4.1). The modified membrane has been characterized by ATR-FTIR, SEM, etc., demonstrating the success of this modification approach. In the support layer, the grafted boron affinity coating unevenly accumulates at the selective layer due to the rejection of PEI during the infiltration step. In addition, it has been proofed that the coating would partially plug in the pores of the selective layer diminishing the pore size, leading to flux decline and lower MWCO.

In Scheme 2, the MicroPES-2F and MicroPES-6F membrane were firstly premodified by the

macroinitiators, PBD-74 or PBD-300. Afterward, a coating can be formed by recirculating monomer solution containing a designed amount of GAEMA, MBA, APS, and TEMED (cf. Section 4.3). The adsorbed macroinitiator PBD has been verified to enable to accelerate the decomposition of APS, making sure the free radical generation at the membrane surface. Moreover, bulk initiation was introduced by adding TEMED into the bulk monomer solution to assist hydrogel grafting, accomplish a better functionalization degree. This integrated initiation system outperforms the alone-surface-initiated system in terms of higher grafting degree and better controllability. Besides, it has been demonstrated that the larger pore size is preferable due to the less confine environment for hydrogel growing. On the other hand, the mass of PBD saturated adsorption can be altered by tailoring the Mw of PBD, and more PBD is preferable to achieve a higher functionalization degree.

In Scheme 3, the support layer of PES-100 was firstly pre-modified by macroinitiator PBD, and then a GAEMA coating can be grafted into the support layer of the pre-modified membrane when infiltrating monomer solution, which contains a designed amount of GAEMA, MBA, APS, and TEMED (cf. Section 4.4.1). In this modification approach, it can achieve similar boron uptake performance but consume less chemicals than the similar modification performed in the MF membrane. Such superiority is considered as the benefit of the higher specific area for the UF membrane.

In Scheme 4, a tri-epoxy compound was firstly adsorbed by MicroPES-6F and MicroPES-2F membrane, and then the adsorbed tri-epoxy layer was cross-linked by DMA, forming a tertiary amine included layer at the membrane surface. The GAEMA coating can be grafted onto the tri-epoxy/DMA modified membrane via an integrated initiation system (cf. Section 4.4.2). Due to the high adsorption mass of tri-epoxy and the high reactivity between epoxy groups and the primary amine, the surface of the tri-epoxy/DMA modified membrane carries 6-times more tertiary amine moieties compared to the macroinitiator modified surface. The high tertiary amine loading leads to more free radicals generated at the membrane surface for higher hydrogel grafting. However, the organic solvent used in this modification is unfriendly to membrane module and tubing, thus restrict the further attempt to upscale this approach.

5.2 Membrane performance

This work aims to prepare membrane adsorber integrating boron uptake with the filtration process. Thus, the performance of modified membranes is evaluated by two criterions, boron uptake and water permeability. A diagram of plotting boron uptake against permeability of overall modified membranes is shown in Fig. 5.2, and obviously, it has a clear trade-off between boron uptake and water permeability.

The functionalized PES-50 via Scheme 1 gives a permeability of 40-60 LMH bar. The adsorption isotherm and kinetic study demonstrate a boron binding capacity of 9.5-10.7 mg/m^2 for the modified PES-50 membrane. In the flow-through adsorption experiment, it presents a steep boron breakthrough curve, which can be blamed for the poor boron binding capacity of modified PES-50. In addition, the modified PES-50 presents different binding capacities in bath adsorption and flow through adsorption, and this is the result of different mass transfer condition. A better mass transfer condition is favourable for improving boron diffusion inside the coating, leading to more binding of boric acid and the internal binding sites of the affinity coating. On the other hand, the modification condition can be successfully transferred to the Multibore® capillary module, and the modified Multibore® module shows analogous boron uptake and permeability.

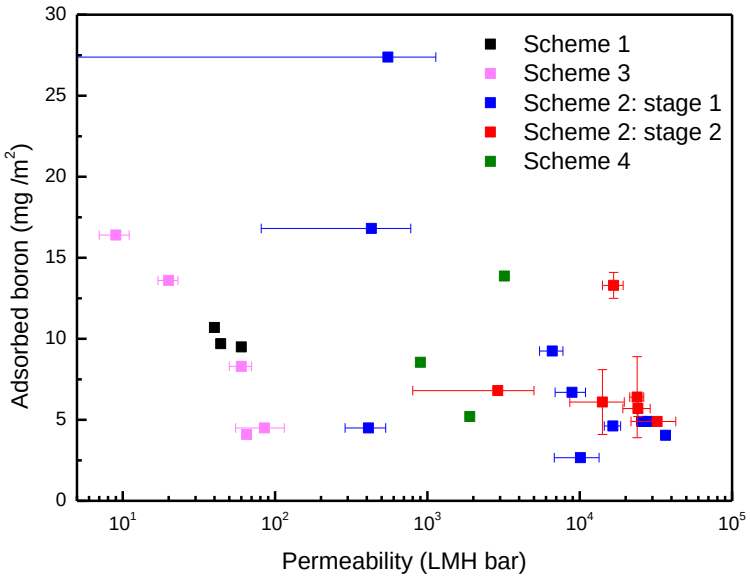

Fig. 5.2 Permeability and boron uptake of the overall modified membranes in this work.

In scheme 2, the modification was performed on a commercial MF membrane. Altering the modification parameter, monomer condition, and macroinitiator size would lead to various grafting degrees. A systematic data analysis via DOE and ANOVA gives a clear overview to reveal the influence of input factors on output membrane performance. It clearly shows that the enhancement of monomer concentration and cross-linking degree would lead to more boron uptake with a certain level of permeability loss. Besides, the more free radical in the bulk concentration (higher TEMED amount) can improve boron uptake with less flux drop. The DOE and ANOVA results demonstrate that the monomer concentration plays a dominant impact compared with other factors. Moreover, on the ground of DOE analysis, by fine-turning the modification parameters, the membrane modified by adapting the monomer condition of 14-2-2 can reach a better trade-off, giving a permeability of 16,700 LMH bar and a boron uptake of 17.5 mg/m^2 in ASW. The mass transfer condition has been investigated via the Fourier module, and the calculated result leads to a conclusion that the poor mass transfer condition at the early adsorption stage of bath adsorption can impede boron binding. Moreover, the residence time of the feed solution has a crucial impact on breakthrough behaviour. The *Pe* number has also been calculated, revealing that the convection flow and boron diffusion contribute equally to the boron

mass transport in the membrane pores. Regarding coating duration, the 14-2-2 membrane is chemically and mechanically stable and presents high stability after regenerations.

The membrane modified via Scheme 3 and 4 shows comparable membrane performance. In comparison with PBD-74 modified MicroPES-2F, a higher functionalization degree can be achieved on tri-epoxy/DMA MicroPES-2F (scheme 4) under an analogous modification procedure. This superior performance is due to the high tertiary amine moieties loading at the surface of tri-epoxy/DMA MicroPES-2F. The UF membrane modified via Scheme 3 can reach similar boron uptake as the MF membrane modified via scheme 2 but consume less chemicals, which can be explained by the larger specific area in the UF membrane. Overall, the research on the membrane modified by Scheme 3 and 4 gives a new vision of tailoring proper membrane adsorber with a better trade-off of boron uptake against permeability.

5.3 Boron removal cost

On the ground of the available results, the cost of boron removal via PEI-5Acl/PES-50 (Scheme 1), and single-pass 14-2-2/MF (scheme 2), have been estimated in aspects of implementation, materials (modification cost), energy, reagent for regeneration, and maintenance. In comparison with two other established boron removal methods, ion-exchange and 2nd pass RO, the prepared membrane adsorber shows significant economic advantage in terms of implementation, materials (modification cost), energy, and maintenance. Regarding the reagent cost in membrane adsorber regeneration, the modified membrane would consume huge amount of reagent in the given operation scenario. The overall reagent cost depends on regeneration frequency and reagent concentration. The boron binding capacity, mass transfer condition, and residence time of feed boron solution determine the cost of regeneration conjointly. In order to cut the reagent cost, the most straightforward approach is to regenerate membrane adsorber with a less concentrated chemical. The alternative approach is to diminish regeneration frequency, which can be improved by enhancing membrane boron binding capacity, optimizing operation conditions, or fine turning the membrane structure.

6. Outlook

Commercial UF and MF membranes have been successfully modified via different modification approaches to integrate boron binding property. The current result indicates that it still has considerable space to improve membrane functionalization degree, functionalization homogeneity, boron binding capacity, and regeneration efficiency.

Regarding the functionalization degree and homogeneity, it can be improved upon the following aspects. Firstly, the membrane with a larger pore size would provide a less confined environment for surface-initiated polymerization. However, the selection of based membrane is based on the required flux in the projected application scenario. On the other hand, homogenous surface chemistry across the membrane structure is favourable that to afford homogenous premodification (i.e., adsorption of macroinitiator), leading to an even distribution of functional coating. Moreover, the adsorption mass of co-initiator (tertiary amine moieties) is of crucial importance to enhance free radical concentration for the higher grafting degree. And it can be achieved by enhancing interaction between macro-initiator and membrane surface, or alternatively, diminishing the molecular size of co-initiator, which would lead to more adsorption of the co-initiator group.

The most straightforward approach is to increase functionalization degree and homogeneity, as foregoing discussed, to improve boron binding capacity. In addition, boron binding capacity is also relating to the coating chemistry and structure. A functional coating containing proton acceptor moieties would facilitate boron binding. Thus an alternative improvement can be achieved by copolymerizing GAEMA with 2-Aminoethyl methacrylate hydrochloride (AEMA). Regarding the coating structure, a low cross-linked network is considered to have more accessible boron binding sites compared with the denser network.

With respect to the regeneration process, decreasing the regeneration frequency is thought to be one of the straightforward methods to cut down the regeneration expense. At the required capacity and throughput for seawater treatment, lower regeneration frequency can be achieved by increasing membrane boron binding capacity. Additionally, higher packing density in the membrane module would also give positive feedback to the

breakthrough behaviour. Hereof, hollow fiber membrane or capillary membrane is more suitable to fabricate membrane adsorber. For the mass transport process, since the rate-controlling step of boron adsorption by membrane adsorber is the interaction between boron and binding site, a thicker membrane is more attractive due to its longer mass transfer path result in longer contact time in the adsorption process. Optimizing the operation conditions is another point that should be carefully considered to improve the mass transport conditions of the adsorbate.

The porous membrane adsorber is known for its unavoidable drawback of the less binding site per area than the bead-based adsorbent. But the membrane adsorber shows a significant advantage of the efficient mass transport process. Thus, the membrane adsorber is very suitable for removing the substance of which the rate-controlling step in adsorption is the mass transfer process. Besides, the established modification approaches in this work can be widely adapted to various monomers, making it possible to transfer these surface modification techniques to other specific applications, such as bio-based purification.

References

[1] N. Nadav, Boron removal from seawater reverse osmosis permeate utilizing selective ion exchange resin, Desalination 124 (1999) 131–135.

[2] WHO/HSE/WSH/09.01/2., Boron in drinking water, background document for development of WHO guidelines for drinking water quality, 2009.

[3] Australian Water Association, Australian and New Zealand Guidelines for Fresh and Marine Water Quality, 2000.

[4] J. Redondo, M. Busch, J.-P. de Witte, Boron removal from seawater using FILMTECTM high rejection SWRO membranes, Desalination 156 (2003) 229–238.

[5] N. Kabay, M. Bryjak, S. Schlosser, M. Kitis, S. Avlonitis, Z. Matejka, I. Al-Mutaz, M. Yuksel, Adsorption-membrane filtration (AMF) hybrid process for boron removal from seawater: an overview, Desalination 223 (2008) 38–48.

[6] V. Freger, H. Shemer, A. Sagiv, R. Semiat, Boron Removal Using Membranes, in: Boron Separation Processes, Elsevier, 2015, pp. 199–217.

[7] A.C.-T. Chiang, J.C.-T. Lin, D.R. Wijayanti, D.-J. Lee, Boron removal with UTC-series reverse osmosis filtration, Journal of the Taiwan Institute of Chemical Engineers 44 (2013) 317–321.

[8] F. Münk, Comparative study for seawater desalination by ED, NF and RO membranes quality analysis of product water, MS Thesis. 2008.

[9] E. Goli, T. Hiemstra, W.H. van Riemsdijk, R. Rahnemaie, M.J. Malakouti, Diffusion of neutral and ionic species in charged membranes: boric acid, arsenite, and water, Analytical chemistry 82 (2010) 8438–8445.

[10] E. Güler, N. Kabay, M. Yüksel, N. Yiğit, M. Kitiş, M. Bryjak, Integrated solution for boron removal from seawater using RO process and sorption-membrane filtration hybrid method, Journal of Membrane Science 375 (2011) 249–257.

[11] M.F. Chillón Arias, L. Valero i Bru, D. Prats Rico, P. Varó Galvañ, Approximate cost of the elimination of boron in desalinated water by reverse osmosis and ion exchange resins, Desalination 273 (2011) 421–427.

[12] M. Nair, D. Kumar, Water desalination and challenges: The Middle East perspective: a review, Desalination and Water Treatment 51 (2013) 2030–2040.

[13] A.F. Corral, U. Yenal, R. Strickle, D. Yan, E. Holler, C. Hill, W.P. Ela, R.G. Arnold, Comparison of slow sand filtration and microfiltration as pretreatments for inland desalination via reverse osmosis, Desalination 334 (2014) 1–9.

[14] D. Vial, G. Doussau, The use of microfiltration membranes for seawater pre-treatment

prior to reverse osmosis membranes, Desalination 153 (2003) 141–147.

[15] N. Voutchkov, Considerations for selection of seawater filtration pretreatment system, Desalination 261 (2010) 354–364.

[16] J. Zhang, L. Chen, H. Zeng, X. Yan, X. Song, H. Yang, C. Ye, Pilot testing of outside-in MF and UF modules used for cooling tower blowdown pretreatment of power plants, Desalination 214 (2007) 287–298.

[17] K.T. Chua, M. Hawlader, A. Malek, Pretreatment of seawater: Results of pilot trials in Singapore, Desalination 159 (2003) 225–243.

[18] N. Ingri, G. Lagerström, M. Frydman, L.G. Sillén, Equilibrium Studies of Polyanions. II. Polyborates in $NaClO_4$ Medium, Acta Chemica Scandinavica 11 (1957) 1034–1058.

[19] N. Ingri, L.G. Sillén, D. Timm, K. Motzfeldt, O. Theander, H. Flood, High-speed Computers as Supplement to Graphical Methods. II. Some Computer Programs for Studies of Complex Formation Equilibria, Acta Chemica Scandinavica 16 (1962) 173–191.

[20] K. Hinz, M. Altmaier, X. Gaona, T. Rabung, D. Schild, M. Richmann, D.T. Reed, E.V. Alekseev, H. Geckeis, Interaction of Nd(iii) and Cm(iii) with borate in dilute to concentrated alkaline NaCl, $MgCl_2$ and $CaCl_2$ solutions: solubility and TRLFS studies, New Journal of Chemistry 39 (2015) 849–859.

[21] M. Tsuda, I. Shirotani, S. Minomura, Y. Terayama, The Effect of Pressure on the Dissociation of Weak Acids in Aqueous Buffers, Bulletin of the Chemical Society of Japan 49 (1976) 2952–2955.

[22] Y. Marcus, Thermodynamics of solvation of ions. Part 6.—The standard partial molar volumes of aqueous ions at 298.15 K, Journal of the Chemical Society, Faraday Transactions 89 (1993) 713–718.

[23] M. Landi, T. Margaritopoulou, I.E. Papadakis, F. Araniti, Boron toxicity in higher plants: an update, Planta 250 (2019) 1011–1032.

[24] N Kabay, M Bryjak, N Hilal, Boron Separation Processes, Elsevier, 2015.

[25] K. Yoshimura, Y. Miyazaki, F. Ota, S. Matsuoka, H. Sakashita, Complexation of boric acid with the N-methyl-D-glucamine group in solution and in crosslinked polymer, Journal of the Chemical Society, Faraday Transactions 94 (1998) 683–689.

[26] J. Schott, J. Kretzschmar, M. Acker, S. Eidner, M.U. Kumke, B. Drobot, A. Barkleit, S. Taut, V. Brendler, T. Stumpf, Formation of a Eu(III) borate solid species from a weak Eu(III) borate complex in aqueous solution, Dalton transactions 43 (2014) 11516–11528.

[27] N Ingri, G Lagerstrom, M Frydman, Equilibrium studies of polyanions. Acta Chemica Scandinavica (1957) 1034–1058.

[28] C.G. Salentine, High-field boron-11 NMR of alkali borates. Aqueous polyborate equilibria,

Inorganic Chemistry 22 (1983) 3920–3924.

[29] A. Bick, G. Oron, Post-treatment design of seawater reverse osmosis plants: boron removal technology selection for potable water production and environmental control, Desalination 178 (2005) 233–246.

[30] Lenntech, Purolite-S108, https://www.lenntech.com/Data-sheets/Purolite-S108-L.pdf.

[31] Lenntech, https://www.lenntech.com/Data-sheets/Mitsubishi-DIAION-Cataloque.pdf.

[32] Dupont, AmberSep™ IRA743, https://www.dupont.com/products/ambersepira743.html.

[33] M. Badruk, N. Kabay, M. Demirciogle, H. Mordogan, U. Ipekoglu, Removal of Boron from Wastewater of Geothermal Power Plant by Selective Ion-Exchange Resins. I. Batch Sorption–Elution Studies, Separation Science and Technology 34 (1999) 2553–2569.

[34] N. Kabay, I. Yılmaz, S. Yamac, S. Samatya, M. Yuksel, U. Yuksel, M. Arda, M. Sağlam, T. Iwanaga, K. Hirowatari, Removal and recovery of boron from geothermal wastewater by selective ion exchange resins. I. Laboratory tests, Reactive and Functional Polymers 60 (2004) 163–170.

[35] T.E. Köse, H. Demiral, N. Öztürk, Adsorption of boron from aqueous solutions using activated carbon prepared from olive bagasse, Desalination and Water Treatment 29 (2011) 110–118.

[36] M.D. Joshi, G. Chalumot, Y. Kim, J.L. Anderson, Synthesis of glucaminium-based ionic liquids and their application in the removal of boron from water, Chemical communications 48 (2012) 1410–1412.

[37] N. Hilal, G.J. Kim, C. Somerfield, Boron removal from saline water: A comprehensive review, Desalination 273 (2011) 23–35.

[38] E.H. Ezechi, M.H. Isa, S.R.B.M. Kutty, Boron in Produced Water: Challenges and Improvements: A Comprehensive Review, Journal of Applied Sciences 12 (2012) 402–415.

[39] E. Loizou, P.N. Kanari, G. Kyriacou, M. Aletrari, Boron determination in a multi element national water monitoring program: the absence of legal limits, Journal für Verbraucherschutz und Lebensmittelsicherheit 5 (2010) 459–463.

[40] M. Rodríguez Pastor, A. Ferrándiz Ruiz, M.F. Chillón, D. Prats Rico, Influence of pH in the elimination of boron by means of reverse osmosis, Desalination 140 (2001) 145–152.

[41] K.L. Tu, L.D. Nghiem, A.R. Chivas, Coupling effects of feed solution pH and ionic strength on the rejection of boron by NF/RO membranes, Chemical Engineering Journal 168 (2011) 700–706.

[42] D. Hasson, H. Shemer, I. Brook, I. Zaslavschi, R. Semiat, C. Bartels, M. Wilf, Scaling propensity of seawater in RO boron removal processes, Journal of Membrane Science 384 (2011) 198–204.

[43] M.H. Oo, S.L. Ong, Boron removal and zeta potential of RO membranes: impact of pH and salinity, Desalination and Water Treatment 39 (2012) 83–87.

[44] K.L. Tu, L.D. Nghiem, A.R. Chivas, Boron removal by reverse osmosis membranes in seawater desalination applications, Separation and Purification Technology 75 (2010) 87–101.

[45] M. Bodzek, The removal of boron from the aquatic environment–state of the art, Desalination and Water Treatment 57 (2016) 1107–1131.

[46] G.M. Geise, H.-S. Lee, D.J. Miller, B.D. Freeman, J.E. McGrath, D.R. Paul, Water purification by membranes: The role of polymer science, Journal of Polymer Science Part B: Polymer Physics 48 (2010) 1685–1718.

[47] M.H. Oo, S.L. Ong, Implication of zeta potential at different salinities on boron removal by RO membranes, Journal of Membrane Science 352 (2010) 1–6.

[48] K.L. Tu, A.R. Chivas, L.D. Nghiem, Effects of membrane fouling and scaling on boron rejection by nanofiltration and reverse osmosis membranes, Desalination 279 (2011) 269–277.

[49] K.L. Tu, A.R. Chivas, L.D. Nghiem, Enhanced boron rejection by NF/RO membranes by complexation with polyols: Measurement and mechanisms, Desalination 310 (2013) 115–121.

[50] S. Samatya, S.A. Tuncel, N. Kabay, Boron removal from RO permeate of geothermal water by monodisperse poly(vinylbenzyl chloride-co-divinylbenzene) beads containing N-methyl-d-glucamine, Desalination 364 (2015) 75–81.

[51] J.G. Neo, S. Japip, L. Luo, T.-S. Chung, M. Weber, C. Maletzko, Hydroxyl-terminated poly(ethyleneimine) polymer enhanced ultrafiltration for boron removal, Separation and Purification Technology 222 (2019) 214–220.

[52] J. Jeon, B. Park, Y. Yoon, S. Kim, An optimal design approach of forward osmosis and reverse osmosis hybrid process for seawater desalination, Desalination and Water Treatment 57 (2016) 26612–26620.

[53] N. Kabay P. Köseoğlu, D. Yapıcı, Ü. Yüksel, M. Yüksel, Coupling ion exchange with ultrafiltration for boron removal from geothermal water-investigation of process parameters and recycle tests, Desalination 316 (2013) 17–22.

[54] N. Kabay, P. Köseoğlu, E. Yavuz, Ü. Yüksel, M. Yüksel, An innovative integrated system for boron removal from geothermal water using RO process and ion exchange-ultrafiltration hybrid method, Desalination 316 (2013) 1–7.

[55] P. Dydo, I. Nemś, M. Turek, Boron removal and its concentration by reverse osmosis in the presence of polyol compounds, Separation and Purification Technology 89 (2012) 171–180.

[56] J. Liu, L. Xie, Z. Wang, J. Yuan, Complexation-Enhanced Boron Removal in a Dual-Stage Nanofiltration Seawater Desalination Process, Separation Science and Technology 48 (2013) 1648–1656.

[57] Ç. Dilek, H.Ö. Özbelge, N. Biçak, L. Yılmaz, Removal of boron from aqueous solutions by continuous polymer-enhanced ultrafiltration with polyvinyl alcohol, Separation Science and Technology 37 (2002) 1257–1271.

[58] A. Yürüm, A. Taralp, N. Bıçak, H.Ö. Özbelge, L. Yılmaz, High performance ligands for the removal of aqueous boron species by continuous polymer enhanced ultrafiltration, Desalination 320 (2013) 33–39.

[59] Y.P. Tang, S. Yuwen, T.S. Chung, M. Weber, C. Staudt, C. Maletzko, Synthesis of hyperbranched polymers towards efficient boron reclamation via a hybrid ultrafiltration process, Journal of Membrane Science 510 (2016) 112–121.

[60] P. Dydo, M. Turek, Boron transport and removal using ion-exchange membranes: A critical review, Desalination 310 (2013) 2–8.

[61] A. Boubakri, S.A.-T. Bouguecha, I. Dhaouadi, A. Hafiane, Effect of operating parameters on boron removal from seawater using membrane distillation process, Desalination 373 (2015) 86–93.

[62] X. Wen, F. Li, X. Zhao, Removal of nuclides and boron from highly saline radioactive wastewater by direct contact membrane distillation, Desalination 394 (2016) 101–107.

[63] X. Jin, C.Y. Tang, Y. Gu, Q. She, S. Qi, Boric acid permeation in forward osmosis membrane processes: modeling, experiments, and implications, Environmental science & technology 45 (2011) 2323–2330.

[64] Y.-J. Choi, S. Lee, J. Koo, T.-M. Hwang, Theoretical and experimental investigation of boron rejection by forward osmosis membrane, Desalination and Water Treatment 57 (2016) 24615–24625.

[65] H. Nagasawa, A. Iizuka, A. Yamasaki, Y. Yanagisawa, Utilization of Bipolar Membrane Electrodialysis for the Removal of Boron from Aqueous Solution, Industrial & Engineering Chemistry 50 (2011) 6325–6330.

[66] C. Kim, S. Lee, H.K. Shon, M. Elimelech, S. Hong, Boron transport in forward osmosis: Measurements, mechanisms, and comparison with reverse osmosis, Journal of Membrane Science 419-420 (2012) 42–48.

[67] W. Fam, S. Phuntsho, J.H. Lee, J. Cho, H.K. Shon, Boron transport through polyamide-based thin film composite forward osmosis membranes, Desalination 340 (2014) 11–17.

[68] Blanca Salgado, Juan Manuel Ortega, Jasna Blazheska,Joan Sanz &Verónica García-Molina, High-permeability FILMTEC™ SEAMAXX™ reverse osmosis elements: a success story in the Canary Islands, Desalination and Water Treatment 55 (2014) 3003–3011.

[69] L. Luo, Z. Zhou, T.-S. Chung, M. Weber, C. Staudt, C. Maletzko, Experiments and Modeling of Boric Acid Permeation through Double-Skinned Forward Osmosis Membranes, Environmental Science & Technology 50 (2016) 7696–7705.

[70] D. Hou, J. Wang, X. Sun, Z. Luan, C. Zhao, X. Ren, Boron removal from aqueous solution by direct contact membrane distillation, Journal of Hazardous Materials 177 (2010) 613–619.

[71] M. Faigon, D. Hefer, Boron rejection in SWRO at high pH conditions versus cascade design, Desalination 223 (2008) 10–16.

[72] D. Möckel, E. Staude, M.D. Guiver, Static protein adsorption, ultrafiltration behavior and cleanability of hydrophilized polysulfone membranes, Journal of Membrane Science 158 (1999) 63–75.

[73] E. Drioli, L. Giorno, Comprehensive Membrane Science and Engineering, Elsevier, 2017.

[74] M. Ulbricht, 1.5 State-of-the-Art and Perspectives of Organic Materials for Membrane Preparation, in: Comprehensive Membrane Science and Engineering, Elsevier, 2017, pp. 85–119.

[75] K.C. Khulbe, C. Feng, T. Matsuura, The art of surface modification of synthetic polymeric membranes, Journal of Applied Polymer Science 115 (2010) 855–895.

[76]B. van der Bruggen, Chemical modification of polyethersulfone nanofiltration membranes: A review, Journal of Applied Polymer Science 114 (2009) 630–642.

[77] X. Lin, R. Huang, M. Ulbricht, Novel magneto-responsive membrane for remote control switchable molecular sieving, Journal of Materials Chemistry. B 4 (2016) 867–879.

[78] M. Quilitzsch, R. Osmond, M. Krug, M. Heijnen, M. Ulbricht, Macro-initiator mediated surface selective functionalization of ultrafiltration membranes with anti-fouling hydrogel layers applicable to ready-to-use capillary membrane modules, Journal of Membrane Science 518 (2016) 328–337.

[79] P. Marchetti, M.F. Jimenez Solomon, G. Szekely, A.G. Livingston, Molecular separation with organic solvent nanofiltration: a critical review, Chemical Reviews 114 (2014) 10735–10806.

[80] V. Orr, L. Zhong, M. Moo-Young, C.P. Chou, Recent advances in bioprocessing application of membrane chromatography, Biotechnology Advances 31 (2013) 450–465.

[81] C. Zhao, J. Xue, F. Ran, S. Sun, Modification of polyethersulfone membranes – A review of methods, Progress in Materials Science 58 (2013) 76–150.

[82] A.K. Dutta, G. Belfort, Interactions between polycationic and polyanionic layers: Changes in rigidity, charge and adsorption kinetics, Sensors and Actuators B: Chemical 136 (2009) 60–65.

[83] G. Decher, Fuzzy Nanoassemblies: Toward Layered Polymeric Multicomposites, Science

277 (1997) 1232–1237.

[84] H. Guo, M. Ulbricht, Surface modification of polypropylene microfiltration membrane via entrapment of an amphiphilic alkyl oligoethyleneglycolether, Journal of Membrane Science 349 (2010) 312–320.

[85] M. Ulbricht, Advanced functional polymer membranes, Polymer 47 (2006) 2217–2262.

[86] E.M. van Wagner, A.C. Sagle, M.M. Sharma, Y.-H. La, B.D. Freeman, Surface modification of commercial polyamide desalination membranes using poly(ethylene glycol) diglycidyl ether to enhance membrane fouling resistance, Journal of Membrane Science 367 (2011) 273–287.

[87] Q. Yang, M. Strathmann, A. Rumpf, G. Schaule, M. Ulbricht, Grafted glycopolymer-based receptor mimics on polymer support for selective adhesion of bacteria, ACS Applied Materials & Interfaces 2 (2010) 3555–3562.

[88] D. Yin, M. Ulbricht, Antibody-imprinted membrane adsorber via two-step surface grafting, Biomacromolecules 14 (2013) 4489–4496.

[89] D. Yin, M. Ulbricht, Protein-selective adsorbers by molecular imprinting via a novel two-step surface grafting method, Journal of Materials Chemistry. B 1 (2013) 3209–3219.

[90] Q. Yang, N. Adrus, F. Tomicki, M. Ulbricht, Composites of functional polymeric hydrogels and porous membranes, Journal of Materials Chemistry 21 (2011) 2783–2811.

[91] C.-M. Chan, T.-M. Ko, H. Hiraoka, Polymer surface modification by plasmas and photons, Surface Science Reports 24 (1996) 1–54.

[92] M.S. Islam, S. Hernández, H. Wan, L. Ormsbee, D. Bhattacharyya, Role of membrane pore polymerization conditions for pH responsive behavior, catalytic metal nanoparticle synthesis, and PCB degradation, Journal of Membrane Science 555 (2018) 348–361.

[93] D. He, H. Susanto, M. Ulbricht, Photo-irradiation for preparation, modification and stimulation of polymeric membranes, Progress in Polymer Science 34 (2009) 62–98.

[94] Y. Yu, H. Yuk, G.A. Parada, Y. Wu, X. Liu, C.S. Nabzdyk, K. Youcef-Toumi, J. Zang, X. Zhao, Multifunctional "Hydrogel Skins" on Diverse Polymers with Arbitrary Shapes, Advanced materials 31 (2019) e1807101.

[95] X. de Feng, X.Q. Guo, K.Y. Qiu, Study of the initiation mechanism of the vinyl polymerization with the system persulfate/N,N,N’,N’-tetramethylethylenediamine, Die Makromolekulare Chemie 189 (1988) 77–83.

[96] N.L. Le, M. Ulbricht, S.P. Nunes, How Do Polyethylene Glycol and Poly(sulfobetaine) Hydrogel Layers on Ultrafiltration Membranes Minimize Fouling and Stay Stable in Cleaning Chemicals?, Industrial & Engineering Chemistry 56 (2017) 6785–6795.

[97] Improving membrane chromatography performance at manufacturing scales,

Biotechnology & Bioengineering 109 (2012) fmvi-fmvi.

[98] R. GHOSH, T. WONG, Effect of module design on the efficiency of membrane chromatographic separation processes, Journal of Membrane Science 281 (2006) 532–540.

[99] K.C. Khulbe, T. Matsuura, Removal of heavy metals and pollutants by membrane adsorption techniques, Appl Water Sci 8 (2018).

[100] P. Francis, E. von Lieres, C.A. Haynes, Zonal rate model for stacked membrane chromatography. I: characterizing solute dispersion under flow-through conditions, Journal of chromatography. A 1218 (2011) 5071–5078.

[101] R. Field, Fundamentals of Fouling, in: K.-V. Peinemann, S. Pereira Nunes (Eds.), Membrane Technology, Wiley-VCH Verlag GmbH & Co. KGaA, Weinheim, Germany, 2010, pp. 1–23.

[102] E.M. Tracey, R.H. Davis, Protein Fouling of Track-Etched Polycarbonate Microfiltration Membranes, Journal of Colloid and Interface Science 167 (1994) 104–116.

[103] The dispersion of matter in turbulent flow through a pipe, Proceedings of the Royal Society of London A 223 (1954) 446–468.

[104] Dispersion of soluble matter in solvent flowing slowly through a tube, Proceedings of the Royal Society of London A 219 (1953) 186–203.

[105] J. Meng, J. Yuan, Y. Kang, Y. Zhang, Q. Du, Surface glycosylation of polysulfone membrane towards a novel complexing membrane for boron removal, Journal of Colloid and Interface Science 368 (2012) 197–207.

[106] M. Palencia, M. Vera, B.L. Rivas, Modification of ultrafiltration membranes via interpenetrating polymer networks for removal of boron from aqueous solution, Journal of Membrane Science 466 (2014) 192–199.

[107] Q. Shi, J.-Q. Meng, R.-S. Xu, X.-L. Du, Y.-F. Zhang, Synthesis of hydrophilic polysulfone membranes having antifouling and boron adsorption properties via blending with an amphiphilic graft glycopolymer, Journal of Membrane Science 444 (2013) 50–59.

[108] Y.-T. Wei, Y.-M. Zheng, J.P. Chen, Functionalization of regenerated cellulose membrane via surface initiated atom transfer radical polymerization for boron removal from aqueous solution, Langmuir 27 (2011) 6018–6025.

[109] Z. Wang, P. Wang, J. Cao, Y. Zhang, B. Cheng, J. Meng, A novel mixed matrix membrane allowing for flow-through removal of boron, Chemical Engineering Journal 308 (2017) 557–567.

[110] X. Du, J. Meng, R. Xu, Q. Shi, Y. Zhang, Polyol-grafted polysulfone membranes for boron removal: Effects of the ligand structure, Journal of Membrane Science 476 (2015) 205–

215.

[111] T.V. Nguyen, Preparation of Artificial Sea Water (ASW) for Culturing Marine Bacteria, Unpublished, 2018.

[112] R. Horikawa, H. Sunayama, Y. Kitayama, E. Takano, T. Takeuchi, A Programmable Signaling Molecular Recognition Nanocavity Prepared by Molecular Imprinting and Post-Imprinting Modifications, Angewandte Chemie International Edition 55 (2016) 13023–13027.

[113] J. Hoffmann, U. Kazmaier, A straightforward approach towards cyclic photoactivatable tubulysin derivatives, Angewandte Chemie International Edition 53 (2014) 11356–11360.

[114] H. Wang, J. Zhuang, S. Thayumanavan, Functionalizable Amine-based Polymer Nanoparticles, ACS Macro Letters 2 (2013) 948–951.

[115] X. Jiang, M. Ahmed, Z. Deng, R. Narain, Biotinylated glyco-functionalized quantum dots: synthesis, characterization, and cytotoxicity studies, Bioconjugate Chemistry 20 (2009) 994–1001.

[116] G. Liu, H. Shi, Y. Cui, J. Tong, Y. Zhao, D. Wang, Y. Cai, Toward rapid aqueous RAFT polymerization of primary amine functional monomer under visible light irradiation at 25 °C, Polymer Chemistry 4 (2013) 1176–1182.

[117] Q. Liu, W. Li, H. Wang, B.-M.Z. Newby, F. Cheng, L. Liu, Amino Acid-Based Zwitterionic Polymer Surfaces Highly Resist Long-Term Bacterial Adhesion, Langmuir the ACS Journal of Surfaces and Colloids 32 (2016) 7866–7874.

[118] K.-C. Huang, R.A. Couttenye, G.E. Hoag, Kinetics of heat-assisted persulfate oxidation of methyl tert-butyl ether (MTBE), Chemosphere 49 (2002) 413–420.

[119] R. Silverstein, F.X. Webster, D.J. Kiemle, D.L. Bryce, Spectrometric identification of organic compounds, John Wiley and Sons, Inc, Hoboken, NJ, 2015.

[120] C.H. Giles, T.H. MacEwan, S.N. Nakhwa, D. Smith, 786. Studies in adsorption. Part XI. A system of classification of solution adsorption isotherms, and its use in diagnosis of adsorption mechanisms and in measurement of specific surface areas of solids, Journal of the Chemical Society (1960) 3973.

[121] S. Karahan, M. Yurdakoç, Y. Seki, K. Yurdakoç, Removal of boron from aqueous solution by clays and modified clays, Journal of Colloid and Interface Science 293 (2006) 36–42.

[122] N. Geffen, R. Semiat, M.S. Eisen, Y. Balazs, I. Katz, C.G. Dosoretz, Boron removal from water by complexation to polyol compounds, Journal of Membrane Science 286 (2006) 45–51.

[123] M.-K. Kim, K.H. Eom, J.-H. Lim, J.-K. Lee, J.D. Lee, Y.S. Won, Simple boron removal from seawater by using polyols as complexing agents: A computational mechanistic study, The Korean Journal of Chemical Engineering 32 (2015) 2330–2334.

[124] M. Yurdakoç, Y. Seki, S. Karahan, K. Yurdakoç, Kinetic and thermodynamic studies of boron removal by Siral 5, Siral 40, and Siral 80, Journal of Colloid and Interface Science 286 (2005) 440–446.

[125] B. Kronberg, K. Holmberg, B. Lindman, Surface Chemistry of Surfactants and Polymers, John Wiley & Sons, Ltd, Chichester, UK, 2014.

[126] D. Welch, M.P. Lettinga, M. Ripoll, Z. Dogic, G.A. Vliegenthart, Trains, tails and loops of partially adsorbed semi-flexible filaments, Soft Matter 11 (2015) 7507–7514.

[127] J.B. Schlenoff, S.T. Dubas, Mechanism of Polyelectrolyte Multilayer Growth: Charge Overcompensation and Distribution, Macromolecules 34 (2001) 592–598.

[128] M. Schönhoff, Layered polyelectrolyte complexes: physics of formation and molecular properties, Journal of Physics: Condensed Matter 15 (2003) R1781–R1808.

[129] N. Polikarpov, V. Potolytsyna, E. Bessonova, S. Tripp, D. Appelhans, B. Voit, L. Kartsova, Dendritic glycopolymers as dynamic and covalent coating in capillary electrophoresis: view on protein separation processes and detection of nanogram-scaled albumin in biological samples, Journal of Chromatography. A 1378 (2015) 65–73.

[130] Y. Wang, R. Narain, Y. Liu, Study of bacterial adhesion on different glycopolymer surfaces by quartz crystal microbalance with dissipation, Langmuir 30 (2014) 7377–7387.

[131] X. Gao, W. Feng, S. Zhu, H. Sheardown, J.L. Brash, Kinetic Modeling of Surface-Initiated Atom Transfer Radical Polymerization, Macromolecular Reaction Engineering 4 (2010) 235–250.

[132] E. Mastan, L. Xi, S. Zhu, What Limits the Chain Growth from Flat Surfaces in Surface-Initiated ATRP: Propagation, Termination or Both?, Macromolecular Theory and Simulations 24 (2015) 89–99.

[133] D. Zhou, X. Gao, W. Wang, S. Zhu, Termination of Surface Radicals and Kinetic Modeling of ATRP Grafting from Flat Surfaces by Addition of Deactivator, Macromolecules 45 (2012) 1198–1207.

[134] J.O. Zoppe, N.C. Ataman, P. Mocny, J. Wang, J. Moraes, H.-A. Klok, Surface-Initiated Controlled Radical Polymerization: State-of-the-Art, Opportunities, and Challenges in Surface and Interface Engineering with Polymer Brushes, Chemical Reviews 117 (2017) 1105–1318.

[135] R. Wang, S.A. Egorov, A. Milchev, K. Binder, Stretching of Free Chains Confined in Concave Brush-Coated Nanocylinders, Macromolecules 45 (2012) 2580–2587.

[136] P. Pasetto, H. Blas, F. Audouin, C. Boissière, C. Sanchez, M. Save, B. Charleux, Mechanistic Insight into Surface-Initiated Polymerization of Methyl Methacrylate and Styrene via ATRP from Ordered Mesoporous Silica Particles, Macromolecules 42 (2009) 5983–5995.

[137] H. Liu, Y.-L. Zhu, J. Zhang, Z.-Y. Lu, Z.-Y. Sun, Influence of Grafting Surface Curvature on Chain Polydispersity and Molecular Weight in Concave Surface-Initiated Polymerization, ACS Macro Letters 1 (2012) 1249–1253.

[138] M. Tagliazucchi, O. Azzaroni, I. Szleifer, Responsive polymers end-tethered in solid-state nanochannels: when nanoconfinement really matters, Journal of the American Chemical Society 132 (2010) 12404–12411.

[139] T.G. Thompson, R.U. Bonnar, The buffer capacity of sea water, Industrial Engineering Chemistry and Analytical Edition 3 (1931) 393–395.

[140] J.E. Mackin, The free-solution diffusion coefficient of boron: influence of dissolved organic matter, Marine Chemistry 20 (1986) 131–140.

[141] E.L. Cussler, Diffusion: Mass transfer in fluid systems, 3rd ed., Cambridge University Press, Cambridge, 2009.

[142] H. Patel, Fixed-bed column adsorption study: a comprehensive review, Applied Water Science 9 (2019).

[143] P. Dydo, Transport model for boric acid, monoborate and borate complexes across thin-film composite reverse osmosis membrane, Desalination 311 (2013) 69–79.

Appendix A: Supporting Information

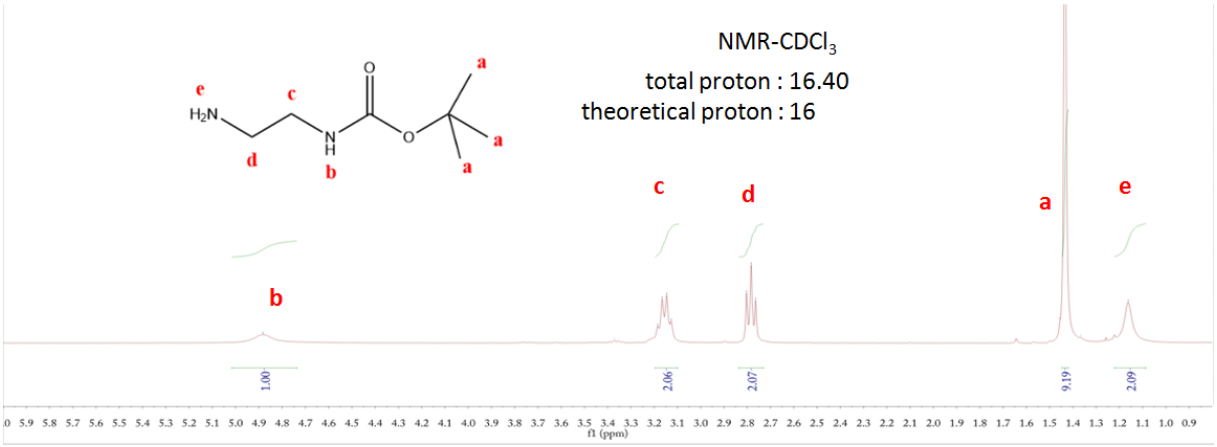

Fig. A1. NMR spectra of synthesized Boc-EDA.

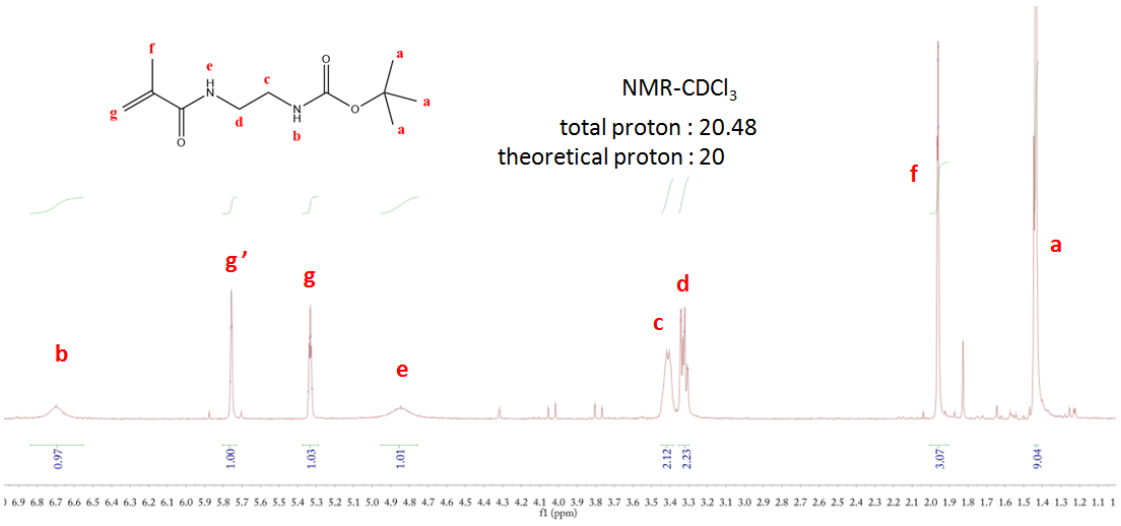

Fig. A2. NMR spectra of synthesized Boc-AEMA.

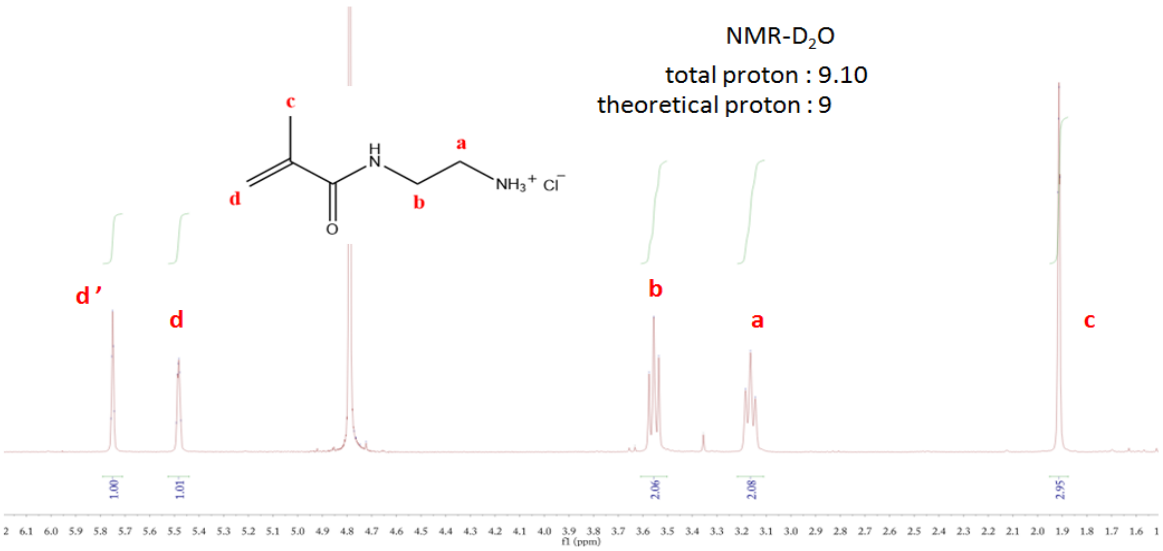

Fig. A3. NMR spectra of synthesized AEMA.

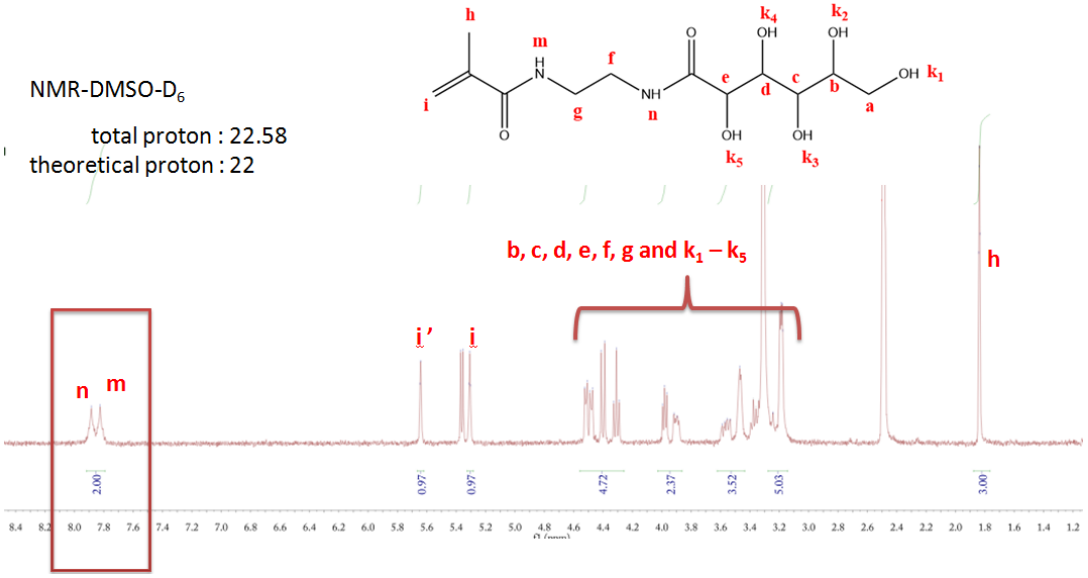

Fig. A4. NMR spectra of synthesized GAEMA

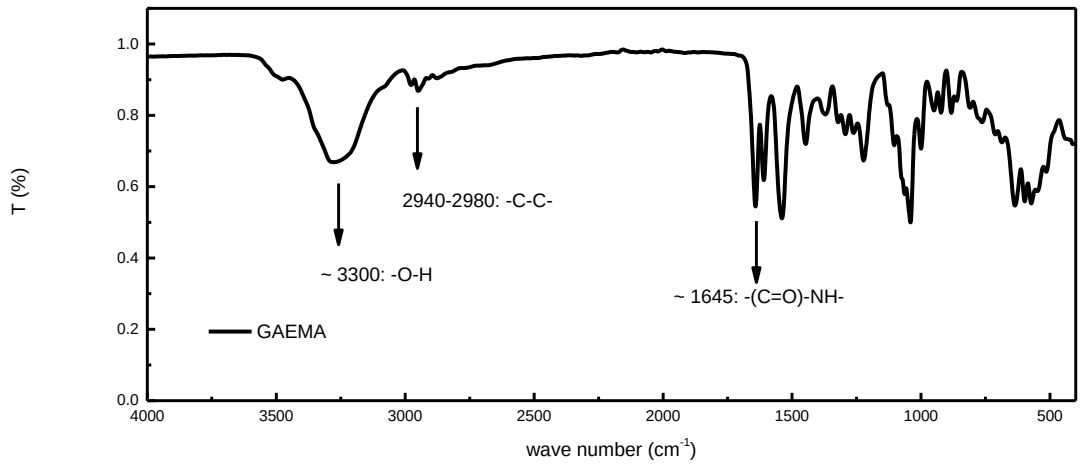

Fig. A5. NMR spectra of synthesized GAEMA.

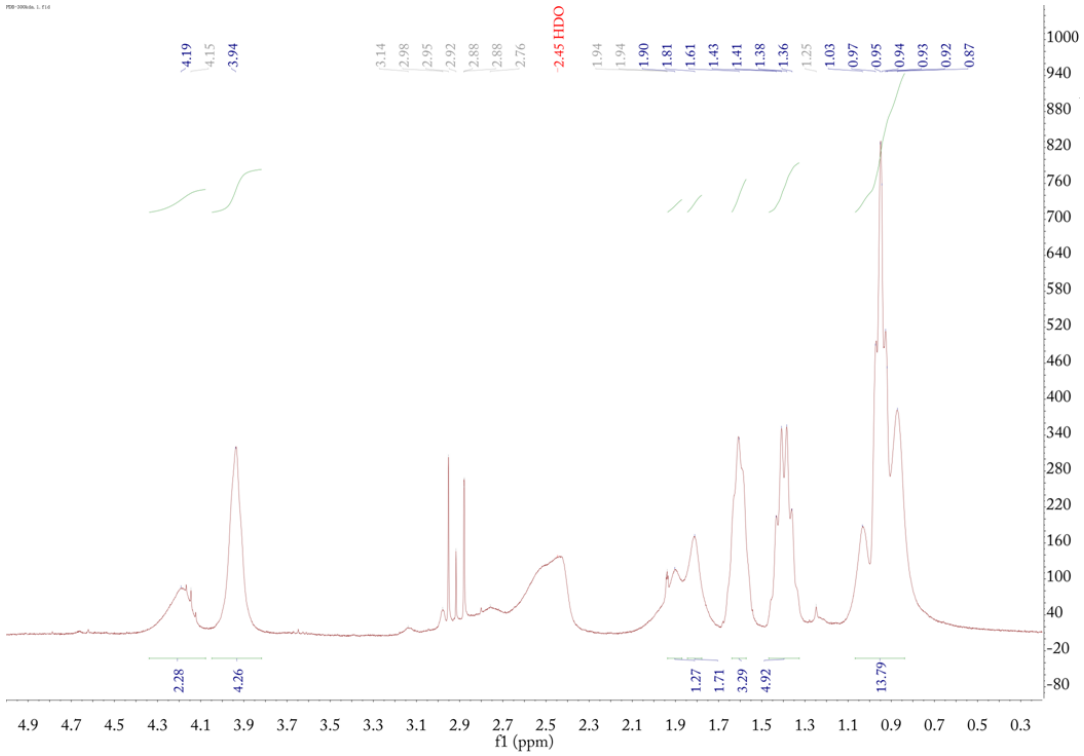

Fig. A6. NMR spectra of synthesized macroinitiator, where the peaks at 4.19 ppm and 3.94 ppm belong to BMA segment and DMAEMA segment, respectively. The molar ratio of BMA to DMAEMA is 2 to 1.

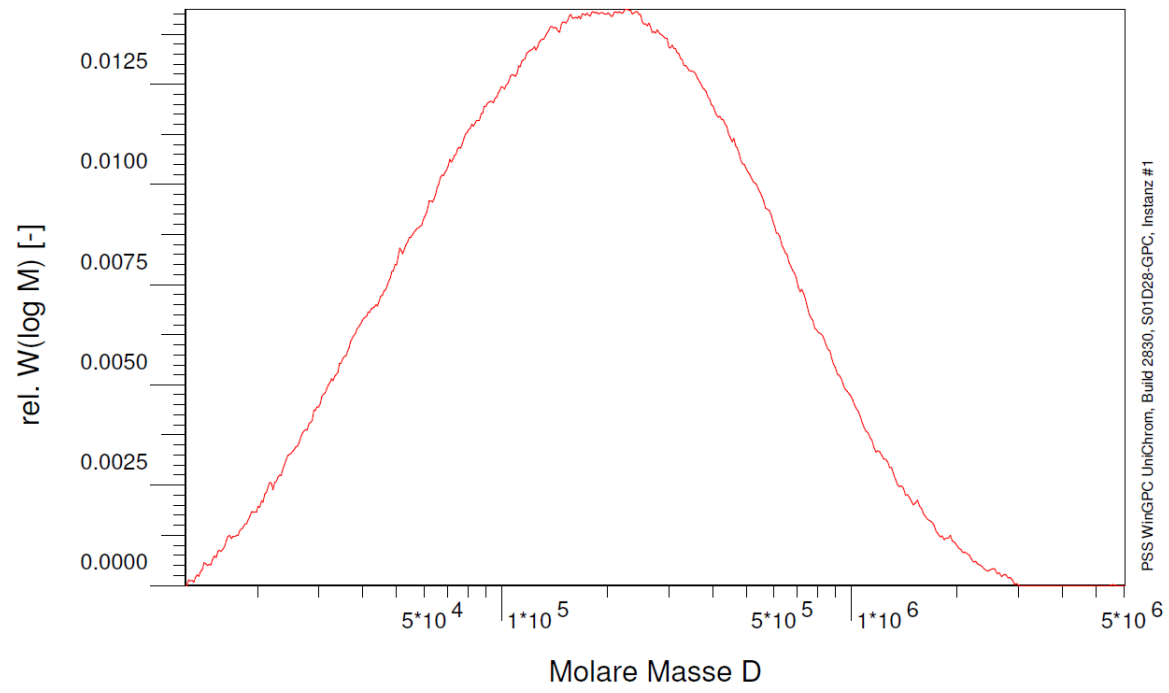

Fig. A7 GPC result of PBD-300, the calculated Mw, Mn and Mz is 300 kDa, 108 kDa, 231 kDa, respectively. The polydispersity of PBD-300 is 2.79.

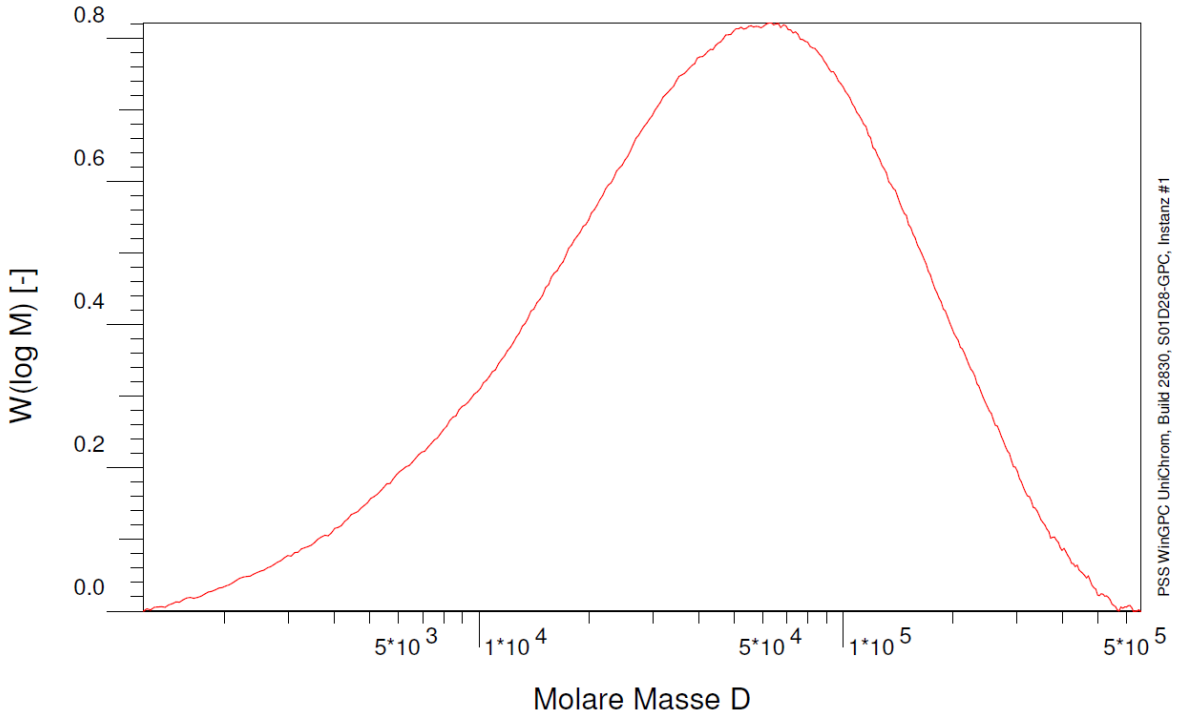

Fig. A8. GPC result of PBD-74, the calculated Mw, Mn and Mz is 74 kDa, 22 kDa, 150 kDa, respectively. The polydispersity of PBD-300 is 3.3.

Table A1. Gelation test of different monomer condition.

Hydrogel	Monomer [mg/ml]	MBA [mg/ml]	APS [mg/ml]	APS/TEMED	gelation
5_1	50	0.5	2	2.25	N*
5_2	50	1	2	2.25	N*
5_5	50	2.5	2	2.25	N*
10_1	100	1	2	2.25	N*
10_2	100	2	2	2.25	N*
10_5	100	5	2	2.25	G**
15_0.1	150	0.15	2	2.25	-
15_0.5	150	0.75	2	2.25	-
15_1	150	1.5	2	2.25	N*
15_2	150	3	2	2.25	N*
15_5	150	7.5	2	2.25	G**

* N : no gelation.

**G: gelation time can be measured.

Appendix B: Calculation of boron removal cost

B1. Modification cost

B1.1 Membrane volume fraction in spiral wound modules

$$\emptyset_{spiral\ wound} = \frac{l_{mem}}{l_{spacer} + l_{mem}} \quad (B.1)$$

Where $\emptyset_{spiralwound}$ refers to membrane volume fraction in the spiral wound modules; l_{mem} is the membrane thickness (mm); l_{spacer} is the feed spacer thickness which depends on a specific module, and assumes that both feed and permeate spacer have a thickness of 0.7 mm (30 mils). When considering the porosity of spacer (it also consists of a solid fraction, the effective $\emptyset_{fleet-sheet}$ should higher than the calculated values, depending on the specific geometry of the used spacer. However, the most common thickness for the spacer is 0.7 mm (30 mils), and this thickness will be used in the following calculation and the final $\emptyset_{spiralwound}$ of each membrane is shown in Table B1.

Table B1 The calculated $\emptyset_{spiral\ wound}$, a and $V_{chemical\ usage}$ of boron removal method.

Membrane type	Thickness (μm)	$\emptyset_{spiralwound}$ (%)	a (mm^{-1})	$V_{chemical\ usage}$ (L)
PEI-5Acl/PES-50	106	13.2	9.4	0.81
single-pass14-2-2/MF	109	13.5	9.2	0.81

* in the dual-pass method, the boron solution is transported through two modified 14-2-2 membranes. Thus, assume that the boron transport path is 218 μm, i.e. set the membrane thickness of 218 μm.

B1.2 Volume of modification solution

Assuming that all of the modifications can be transfer to the spiral wound modules. Thus the required modification solution depends on the module volume:

$$a = \frac{S_{filtration}}{V_{membrane}} = \frac{1}{l_{mem}} \tag{B.2}$$

$$V_{moudle} = \frac{S_{filtration}}{a \ * \ \emptyset_{spiral\ wound}} = V_{chemical\ usage} \tag{B.3}$$

where a is the ratio of filtration area to membrane volume; l_{spacer} is the membrane thickness (mm); $S_{filtration}$ refers to total filtration area, here set as 1 m^2; $V_{membrane}$ refers to membrane volume (m^3); $\emptyset_{spiralwound}$ refers to membrane volume fraction; V_{mudule} refers to the volume of the spiral wound module; $V_{chemical\ usage}$ refers to the volume of the spiral wound module. The calculated a and V_{moudle} for each membrane can be found in Table B1. It needs about 0.81 L of modification solution to modify 1 m^2 membrane, i.e., the modification solution volume is 0.81 L/m^2.

B1.3 The modification cost per m^2 membrane

The modification cost per m^2 membrane can be calculated according to:

$$\mathrm{COST_{mem}} = V_{chemical\ usage} \ * Cost_{chemicals} \tag{B.4}$$

Where $Cost_{chemicals}$ is the chemical price taken from Aldrich-Sigma (cf. Table B2). According to the modification method in Section 4.1, the 3.46 cm^2 membrane was premodified by infiltrating 30 mL of 0.3 g/L PEI solution. Afterward, the premodified membrane is later treated with 5 mL of 9 wt% of glycidol solution. Thus the PEI usage to modify the PEI-5-UF is 86L/m^2, and glycidol solution usage of the modification depends on the $V_{multibore}$, which is 0.81 L/m^2. For 14-2-2/MF membrane, the monomer accounts for the main expense (cf. Table B2). Therefore, only consider the consuming of monomer solution with the monomer concentration of 14 wt%. In addition, assuming that 90% of which can be recycled, thus the materials cost to fabricate 1 m^2 of 14-2-2/MF membrane can be final calculated (cf. Table B3).

Table B2. Price of chemicals used in the modification which are taken from Aldrich-Sigma.

Chemicals	Euro/kg	Purity
Urea	18	99%
Isopropanol	2.8	99%
Macroinitiator	67	> 99% *
Monomer	3600	> 99 % *
PEI-750	150	50 %
Glycidol	276	99 %

* the macroinitiator and monomer is self-prepared. The price is calculated based on the price of the substrates from Aldrich-Sigma. The yield of each synthesis step is considered.

B1.4 The modification cost of per MGD (3785 m^3/day)

For a capacity of 1 MGD, the usage of material depends on flux and duration of membrane. And the modification cost per MGD would be:

$$\mathrm{COST_{MGD}} = \frac{V_{seawater} * \mathrm{COST_{mem}}}{j_{op} * 24 * d} \qquad (B.5)$$

where $\mathrm{COST_{mem}}$ refers to modification cost per m^2 of membrane; $V_{seawater}$ refers to the volume of seawater needed to be treated, which set as 1 MGD (3785 m^3/day) here; j_{op} refers to operation flux which is 50 LMH and 390 LMH for the modified UF and MF membrane, respectively; d refers to the membrane service life in days, here the service life of membrane is set as 365*5 (5 years). The calculated modification cost per MGD can be found in Table B3.

Table B3 The estimated modification cost per treated seawater capacity (euro/MGD) and volume (cent euro/m^3).

Membrane type	j_{op} (LMH)	Required membrane area (m^2)	$\mathbf{COST_{mem}}$ (euro/m^2)	$\mathbf{COST_{MGD}}$ (euro/MGD)
PEI-5Acl/PES-50	50	3154	23	40
single-pass 14-2-2/MF	390	404	41	9
dual-pass 14-2-2/MF	390	404	46	10

B2. Regeneration cost

B2.1 The break-through point at C/C_0 = 0.5

a) The desired break-through point (C/C_0) in membrane adsorption stage (for maximum dynamic capacity):

$$\frac{C}{C_0} = \frac{C_{Boron}}{C_0\left(1 - R_{RO\ stage}\right)} \qquad (B.6)$$

Where C_0 is the initial boron concentration in seawater, which is 5 mg/L; C is the maximum boron concentration after membrane adsorption stage, i.e., pre-treatment stage, (mg/L); C_{Boron} is the required boron concentration in the final permeate, i.e., after the RO stage, which is 0.5 mg/L; $R_{RO\ stage}$ is the boron rejection for the one-pass RO stage, which is assumed to be 80% (it depends on the specific membrane). And the calculated required C/C_0 for membrane adsorption stage is 0.5.

b) When using C/C_0 = 0.5, the specific permeate volume through the modified membrane can be calculated according to the breakthrough curve in the flow-through adsorption experiment (cf. Table. B4).

Table B4 Information of operation flux, thickness, and boron uptake of each boron removal method.

Membrane type	Operating flux (LMH	Thickness (μm)	Boron uptake (mg/m^2)	50 % Breakthrough point (L/m^2)
PEI-5Acl/PES-50	50	106	9.7	2.1
single-pass 14-2-2/MF	390	109	17.5	1.5

B2.2 The required reagent volume for regeneration to treat 1 m^3/h of seawater

Assuming that: a) 1 m^3/h (1000 L/h) of seawater need to be treated at a flux of 50 LMH for modified UF membrane, and 390 LMH for modified MF membrane; b) the modified membrane has perfect break-through behaviour (without dispersion) to the desired boron concentration; c) the boron removal rate of 50% (C/C_0 = 0.5) is achieved; d) the elution volume in the regeneration step is the same as for resin beds, i.e., 4 membrane volumes (4MV) are needed. Finally, the chemicals consumption to treat 1 m^3 seawater can be calculated according to:

$$V_{one-regeneration} = \frac{4 * S_{membrane}}{a} = \frac{4 * V_{seawater}}{a * j_{mem}} \quad (B.7)$$

$$V_{regeneration} = \frac{j_{mem} * V_{one-regeneration}}{50\%\ breakthough\ point} \quad (B.8)$$

Where $V_{one-regeneration}$ is the required reagents volume for one regeneration (L); $S_{membrane}$ is required membrane area to achieve 1 m^3/h capacity at specific operation flux (m^2); $V_{seawater}$ is the volume of seawater need to be treated, which is 1 m^3/h; j_{mem} is the operation flux for modified UF and MF membrane, 50 and 390 LMH, respectively; a is the ratio of membrane area to membrane volume; $V_{regeneration}$ is required regeneration reagents volume for 1 m^3/h throughput; $50\%\ breakthough\ point$ is the required breakthrough points to achieve C/C_0 = 0.5, which is 2.1 L/m^2 for PEI-5Acl/PES50 and 1.5 L/m^2 for single-pass 14-2-2/MF, respectively; The final calculated results for each membrane can be found in Table B5.

Table B5 The operation flux, a, and calculated regeneration volume ($V_{regeneration}$) of each boron removal method.

Membrane type	**50 % Breakthrough (L/m^2)**	**Operating flux (LMH bar)**	**a (mm^{-1})**	**$V_{regeneration}$ (L)**
PEI-5Acl/PES-50	2.1	50	9.4	203
single-pass 14-2-2/MF	1.5	390	9.2	290

B2.3 The reagent cost to treat 1 m3/h of seawater

Table B6 The market price of 98% H_2SO_4 and 50% NaOH.

Chemicals	Euro/t	Euro/L
98% H_2SO_4	250 - 320	0.22 - 0.59
50% NaOH	120 - 240	0.37 - 0.48

The regeneration contains two steps: boron elution by acidic solution (0.05 M - 0.5 M H_2SO_4) and neutralization step by basic solution (0.05 M - 0.5 M NaOH). Thus, the chemical usage strongly depends on the selected regeneration regents. According to the regeneration protocol in section 4.3.4.5, the membrane can be regenerated by 0.1 M of HCl (equivalent to 0.05 H_2SO_4) and 0.1 M NaOH. Hereof, 0.05 M H_2SO_4 and 0.1 M NaOH were taken as elution reagent and neutralization reagent, respectively. The reagent has been converted to 98% H_2SO_4 (18 M H_2SO_4) and 50% NaOH (19 M NaOH). The market price of 98% H_2SO_4 and 50% NaOH are shown in Table B6, according to Alibaba.com. Finally, the calculated reagent cost for regeneration can be found in Table B7.

Table B7 The calculated reagent cost of each boron removal method.

Membrane type	$V_{regeneration}$ (L)	98% H_2SO_4 (cent Euro)	50% NaOH (cent Euro)	Total (cent Euro)
PEI-5Acl/PES-50	203	12-33	39-51	52-84
single-pass 14-2-2/MF	290	18-48	56-73	74-121

Appendix C: Abbreviations

5-Acl	Dipentaerythritol penta-/hexa-acrylate
AEM	Anion-exchange membrane
AEMA	N-(2-aminoethyl) methacrylamide hydrochloride
AIBN	2,2'-Azobis(2-methylpropionitrile)
ANOVA	Analysis of variance
APS	Ammonium persulphate
ASW	Artificial seawater
ATR	Attenuated total reflection
BMA	Butyl methacrylate
Boc-AEMA	N-2-[(tert-butoxycarbonyl)amino] ethyl methacrylamide
Boc-EDA	Synthesis of N-(tert-butoxycarbonyl)-1,2-diaminoethane
BSR	Boron selective resin
BV	Bed volume
CA	Contact angle
CEM	Cation exchange membrane
DCM	Dichloromethane
DD	Donnan dialysis
DMAEMA	2-(Dimethylamino)ethyl methacrylate
DMF	N,N-dimethylformamide
DOE	Design of experiment
EA	Ethyl acetate
ED	Electrodialysis
EDA	Ethylenediamine
EU	European Union
F0	Fourier number
FAS	Ferrous ammonium sulfate
FO	Forward osmosis
GA	Gluconolactone
GAEMA	2-gluconamidoethyl methacrylamide

GMA	Glycidyl methacrylate
GMHP	3-(N-glycidol-N-methyl) amino-2-hydroxypropyl methacrylate
GPC	Gel permeation chromatography
GPD	Gallon per day
HAEM	2-(bis(2,3-dihydroxypropyl)amino) ethyl methacrylate
HEMA	2-hydroxyethyl methacrylat
HPMA	2,3-dihydroxypropyl methacrylate
HQ	Hydroquinone
IEP	Isoelectric point
Kn	Knudsen number
KOW	n-Octanol/Water Partition Coefficient
MA	Methacrylic acid
MBA	N,N'-methylene-bis-acrylamide
MF	Microfiltration
MWCO	Molecular weight cut-off
NF	Nanofiltration
NIPS	Non-solvent induced phase separation
NMDG	N-methyl-D-glucamine
PBD	poly(BMA-co-DMAEMA)
PBD-300	poly(BMA-co-DMAEMA), 300 kDa
PBD-74	poly(BMA-co-DMAEMA), 74 kDa
PDI	Polydispersity index
Pe	Péclet number
PEI	Polyethylenimine
PEI-OH	Hydroxyl functionalized PEI
PES	Polyethersulfone
PGMA	poly(glycidyl methacrylate)
Re	Reynolds number
RO	Reverse osmosis
SEM	Scanning electron microscopy

SV	Space velocities
SWRO	Seawater reverse osmosis
TEA	Triethylamine
TEMED	N,N,N',N'-tetramethylethylenediamine
TMP	Trans-membrane pressure
UF	Ultrafiltration
WHO	World Health Organization

Appendix D: List of Tables and Figures

List of Figures

List of Tables